TECHNICAL REPORT STANDARD TITLE PAGE

1. Report No.	2. Government Accession No.	3. Recipient's Catalog No.
FHWA/TX-86/80+350-3		

4. Title and Subtitle	5. Report Date
BEHAVIOR OF ONTARIO-TYPE BRIDGE DECK ON STEEL GIRDERS: NEGATIVE MOMENT REGION AND LOAD CAPACITY	January 1986
	6. Performing Organization Code
7. Author(s)	8. Performing Organization Report No.
C. K. Tsui, N. H. Burns, and R. E. Klingner	Research Report 350-3
9. Performing Organization Name and Address	10. Work Unit No.
Center for Transportation Research The University of Texas at Austin Austin, Texas 78712-1075	11. Contract or Grant No. Research Study 3-5-83-350
	13. Type of Report and Period Covered
12. Sponsoring Agency Name and Address Texas State Department of Highways and Public Transportation; Transportation Planning Division P. O. Box 5051 Austin, Texas 78763	Interim
	14. Sponsoring Agency Code

15. Supplementary Notes

Study conducted in cooperation with the U. S. Department of Transportation, Federal Highway Administration. Research Study Title: "Behavior of Concrete Bridge Decks on Steel Beams—Verification of the Ontario Bridge Deck Design (With and Without Panels)"

16. Abstract

For the experimental phase of this project, the test specimen was a full-size composite bridge, half of which had a cast-in-place deck, and the other half, cast-in-place topping over precast, prestressed panels. Both decks had Ontario-type reinforcement. The test specimen was supported on a 40-ft span. Tiedown forces were applied at the overhang at each end of the bridge, and two tandem loads were applied at midspan. A series of static loads was applied, along with 5 million cycles of fatigue loading. Finally, the specimen was subjected to concentrated load tests involving single and tandem loads.

Analytical predictions using a finite element model were compared with the experimental results from the negative moment tests. Analytical predictions of deck capacity were compared with the experimental results of the concentrated load tests.

Overall, the experimental program showed that the precast, prestressed panel deck was stronger, stiffer and more crack-resistant than the cast-in-place deck.

17. Key Words	18. Distribution Statement
bridge decks, composite, cast-in-place, specimen, prestressed, reinforcement, static load, tandem load, negative moment, finite element model	No restrictions. This document is available to the public through the National Technical Information Service, Springfield, Virginia 22161.

19. Security Classif. (of this report)	20. Security Classif. (of this page)	21. No. of Pages	22. Price
Unclassified	Unclassified	122	

Form DOT F 1700.7 (8-69)

BEHAVIOR OF ONTARIO-TYPE BRIDGE DECK ON STEEL GIRDERS:

NEGATIVE MOMENT REGION AND LOAD CAPACITY

by

C. K. Tsui, N. H. Burns, and R. E. Klingner

Research Report No. 350-3

Research Project 3-5-83-350

"Behavior of Concrete Bridge Decks on Steel Beams - Verification of the Ontario Bridge Deck Design (With and Without Panels)"

Conducted for

Texas

State Department of Highways and Public Transportation

In Cooperation with the
U.S. Department of Transportation
Federal Highway Administration

by

CENTER FOR TRANSPORTATION RESEARCH
BUREAU OF ENGINEERING RESEARCH
THE UNIVERSITY OF TEXAS AT AUSTIN

January 1986

The contents of this report reflect the views of the authors who are responsible for the facts and accuracy of the data presented herein. The contents do not necessarily reflect the official views or policies of the Federal Highway Administration. This report does not constitute a standard, specification, or regulation.

P R E F A C E

Recent research in the U.S. and Canada has suggested that the flexural capacity of bridge decks is increased by in-plane compressive forces, created when the cracked deck is restrained by supports that cannot move laterally. This phenomenon, commonly referred to as "arching action," is the basis for the semi-empirical design provisions of the current Ontario (Canada) Bridge Design Code. That code permits the use of less flexural steel than would be required by current AASHTO Specifications, resulting in bridge decks which are generally more economical and resistant to corrosion.

Previous research on arching action has been carried out mainly using small-scale models with artifical boundary conditions. The overall objective of Research Project 3-5-83-350 was to study the performance of full-scale bridge decks designed taking arching action into account. Using a full-scale model of a realistic prototype highway bridge, both cast-in-place and precast, prestressed panel decks were considered. A previous report for Project 3-5-83-350 discusses the overall behavior of the bridge in a simply supported configuration. The support conditions of the bridge specimen were then modified by moving the supports inward, and tying the end of the bridge to the test floor, creating negative moment regions over each support. This report deals with the negative moment behavior of the deck, and with its ultimate capacity under concentrated loads.

The specific objectives discussed in Report 350-3 are:

1. To study the pre- and post-fatigue behavior of the negative moment region of the cast-in-place and panel decks under service load and overload conditions;

2. To test previously developed analytical models against the observed behavior of the bridge; and

3. To study the ultimate capacity and behavior of the cast-in-place and panel decks under single and double concentrated loads.

SUMMARY

For the experimental phase of this project, the test specimen was a full-size composite bridge, half of which had a cast-in-place deck, and the other half, cast-in-place topping over precast, prestressed panels. Both decks had Ontario-type reinforcement. The test specimen was supported on a 40-ft span. Tiedown forces were applied at the overhang at each end of the bridge, and two tandem loads were applied at midspan. A series of static loads was applied, along with 5 million cycles of fatigue loading. Finally, the specimen was subjected to concentrated load tests involving single and tandem loads.

Analytical predictions using a finite element model were compared with the experimental results from the negative moment tests. Analytical predictions of deck capacity were compared with the experimental results of the concentrated load tests.

The following conclusions were reached:

1. Both halves of the bridge performed satisfactorily at the support regions when subjected to negative moment levels consistent with current AASHTO design loads;

2. Both halves of the bridge performed satisfactorily at the midspan region, under static tandem loads approximately 2.5 times the current AASHTO design level;

3. Bridge behavior was not significantly affected by fatigue loading to approximately service load levels;

4. Finite element analysis predictions agreed well with experimental results;

5. Under both single and tandem concentrated loads, the deck failed in punching shear;

6. A general punching shear model closely predicted the ultimate strength of the deck under both single and tandem concentrated loads;

7. Both the ACI and AASHTO formulas for punching shear capacity were very conservative in estimating the load capacity of the deck; and

8. Overall, the experimental program showed that the precast, prestressed panel deck was stronger, stiffer and more crack-resistant than the cast-in-place deck.

I M P L E M E N T A T I O N

Cast-in-place and precast, prestressed panel bridge decks similar to the one tested in this study, and detailed with Ontario-type reinforcement, can be built in the field. Their field performance should be evaluated by the Texas SDHPT.

To obtain a broader understanding of the behavior of bridge decks before the new deck design is completely incorporated in Texas SDHPT design provision, parametric studies should be conducted involving variables such as the span to thickness ratio of the deck, the effects of line loads, skew bridge behavior, and the stiffness of integral barriers. Work needs to be completed on the effects of arching action on ultimate capacity, and on crack widths and reinforcement stresses at higher load levels.

TABLE OF CONTENTS

TABLE OF CONTENTS (continued)

LIST OF FIGURES

LIST OF FIGURES (continued)

LIST OF FIGURES (continued)

LIST OF FIGURES (continued)

LIST OF TABLES

CHAPTER 1

INTRODUCTION

1.1 General

Slab and girder bridges are a common element in modern highway systems. Considerable research has been done to better understand the behavior and load-carrying capacity of bridge decks. Recent research in the U.S. and Canada has suggested that the flexural capacity of bridge decks may be increased by the presence of in-plane compressive forces, created when the deck is restrained by supports that cannot move laterally. This is referred to as "arching action", and is the basis for the semi-empirical design provisions of the current Ontario (Canada) Bridge Design Code (1). That code requires a considerably smaller amount of flexural steel than do the current AASHTO Specifications (2).

In view of the possible economic advantages, the Texas SDHPT and FHWA have begun to investigate the performance of bridge decks reinforced in accordance with the Ontario design code.

1.2 Research Program

The entire Ontario deck research program to date has consisted of 3 phases:

1) Phase 1, dealing with the overall behavior of a simply supported bridge deck (3);

2) Phase 2, conducted simultaneously with Phase 1, and dealing with the distribution of girder loads from the above deck (4); and

3) Phase 3, dealing with the negative moment behavior of the deck, and with its ultimate capacity under concentrated loads.

This report discusses Phase 3 only.

1.3 Objectives and Scope

As is discussed in the literature review of Chapter 2, no published research addresses the fatigue behavior of Ontario-type decks at the negative moment region, nor under tandem axial concentrated loads. Because those conditions are often encountered during the service life of bridges, it was therefore believed necessary to study a

bridge deck under these conditions. The specimen used in this study was a full-scale composite highway bridge on steel girders, constructed in the laboratory as part of the other phases of this investigation (1,2). The third phase of the study, discussed here, has the following objectives:

1) To study the pre- and post-fatigue behavior of the negative moment region of the CIP deck under service load and overload conditions;

2) To study the pre- and post-fatigue behavior of the negative moment region of the precast panel deck under service load and overload conditions;

3) To test previously developed analytical models of the CIP deck and precast panel deck against the observed behavior of the bridge;

4) To study the ultimate capacity and behavior of the CIP deck under single and double concentrated loads; and

5) To study the ultimate capacity and behavior of the precast panel deck under single and double concentrated loads.

CHAPTER 2

BACKGROUND

2.1 General

This chapter is intended to give a brief historical review of research into the phenomenon of "arching action" as applied to reinforced concrete elements, and specifically to the ultimate strength of concrete bridge decks. Also, a brief description of the test specimen is included. Further details of Phase 1 of this project are given in Ref. 1, particularly with respect to background information and specimen description.

2.2 Historical Review

The effect of in-plane forces on the load-carrying capacity of reinforced concrete slabs has been an active field of structural engineering research for several decades. In 1956, Ockleston (5) tested a three-story reinforced concrete building in Johannesberg, South africa, and recorded collapse loads three or four times the capacities predicted by yield-line theory. Ockleston (6) also identified this phenomenon as the effect of compressive membrane forces. In 1957, Liebenberg, Robertson and McGraw (7) conducted tests on the old Alliance House in Cape Town, South Africa. Fifty slab panels were tested to destruction prior to the demolition of the building. These test results also confirmed the existence of compressive membrane action, and its beneficial effect on the load-carrying capacity of the floor system. After a study of the behavior of continuous prestressed concrete slabs, Guyon (8) suggested that arching action should be taken into account in designing such slabs to resist concentrated out-of-plane loads. Other experimental verifications of this were also carried out by Christiansen, Frederickse (9,10) and Park (11,12,13,14,15).

To predict the strength of edge-restrained slabs, several approximate analytical techniques were proposed and verified using small-scale models. For instance, Park attempted to analyze two-way rectangular slabs for compressive membrane action using rigid-plastic strips running along the short and long directions of the slab. The slab's ultimate capacity was then obtained from a virtual work equation (14).

In the late 1950's, tests were conducted on single panels by Sozen and Gamble (16,17) at the University of Illinois. When bounded by elements which could develop horizontal reactions, such reinforced concrete panels were found to have flexural capacities considerably in

excess of the load calculatled by Johanson's yield line theory. The additional capacity was attributed primarily to the effect of in-plane forces.

Research in this field originally concentrated on the behavior of building floor systems, and most tests were conducted using small-scale models (18,19,20). At the end of 1975, the Ontario Ministry of Transportation and Communicatins decided to develop a code for desigining highway bridges in that province. A series of tests were undertaken by academic researchers and the Ministry's Research and Development Division. Bridge design loads were reevaluated using survey data of actual truck loadings in Ontario (21,22,23).

Since 1969, many bridges have been tested in the field by the Structural Research Section of the Ontario Ministry of Transportation and Communications (24). The load-carrying capacities of these bridges, and theperformance of their structural components, have been evaluated.

From field tests, it was observed that thin concrete deck slabs supported by beams or girders were generally capable of carrying concentrated wheel loads far in excess of capacity predicted by traditional methods of analysis, even if the deck had considerably deteriorated, or a large percent of the reinforcing steel had been lost due to corrosion.

Under the sponsorship of the Ontario Ministry of Transportation and Communication, a series of studies was conducted at Queen's University, Kingston, Ontario, using 1/8-scale models (25,26,27,28). They used nine 1/8 scale models to study the effect of restraint on deck slab on I-beams with conventional, isotropic and no reinforcements. their study showed that 66 out of 68 specimens they tested failed in punching shear. From these they concluded that theoretically, no reinforcement is required in the deck slab of composite I-beam bridges if only the ultimate strength of the desigred structure is considered. However, in view of AASHTO requirements regarding temperature and shrinkage reinforcement, they recommended 0.2 percent isotropic reinforcement at top and bottom as the maximum required requirement.

This research work was supplemented by field tests of actual bridges (29,30,31). It was concluded that a slab's load-carrying capacity was increased by in-plane restraint.

Based on these findings, an empirical design method was proposed, involving an isotropic reinforcement layout in the deck. Required reinforcement is considerably less than that specified by the AASHTO Code (1). Some bridge decks in Ontario have been designed using the proposed empirical method.

Recent field tests of a trapezoidal box girder bridge in Canada (32), conducted by the Ontario Highway Department, have shown that a bridge deck detailed with the 0.3% isotropic reinforcement performed satisfactorily. Under the mximum wheel load of 100 kips, the maximum observed transverse reinforcing steel stress was 18.64 ksi, and the longitudinal stress, 14.5 ksi. The load-deflection relatinship at the loaded point was very linear up to that load level.

Field tests were also recently conducted in Canada on a composite prestressed concrete girder bridge with a deck detailed in accordance with the empirical method (33). The load-deflection curve at the loaded point was again very linear up to about 100 kips wheel load level. The maximum observed stresses in reinforcement were less than 20 ksi at that load level.

The convenience in construction of such decks, and the savings in the amount of reinforcement required, have attracted the attention of researchers in the United States. The New York Highway Department has recently conducted a study of the strength of highway bridge decks (34). Both the proposed Ontario reinforcing details and those consistent with current AASHTO design procedures were tested, using reduced-scale bridge decks. Tests were conducted on uncracked and cracked slabs. The uncracked-slab test was intended to simulate the behavior of the deck slab under vehicular overload, and to better study steel strains.

Under design loads, the stress in reinforcement was found not to exceed 12 ksi. When loaded to ultimate, all locations bounded by longitudinal girders failed by punching shear. Regardless of the reinforcing pattern used, failure loads always exceeded six times the design wheel load for slabs bound by girders.

Thus, a reduction in reinforcement from 7 to 2 psf would have had no effect on the failure mode, and would not have reduced the strength below a safe level. The tests also demonstrated that in bridge decks of ordinary proportions the service-load stress level was lower than that predicted by existing AASHTO Pdesign procedures and methods based on elastic isotropic thin plate theory.

Even though no published research studies addressed the fatigue behavior of Ontario-type decks in negative moment regions, researchers had suggested that this topic should be studied more carefully before using the Ontario empirical design procedure (34).

2.3 Development of Test Specimen

The design of the bridge specimen for this experimental testing program took into account the known details suggested by the Ontario Highway Department's research. In the Ontario design method, the deck design is reduced to a prescription of the isotropic

reinforcement (35). The Texas-proposed highway bridge deck details (following the Ontario code quite closely) showed two layers of reinforcement in a 7-1/2 in. thick deck slab (36). This slab was to be made composite with the steel girders by means of shear studs. Figures 2.1 and 2.2 show the plan and elevation views of the test specimen, and Fig. 2.3 shows the composite bridge cross section.

Another design consideration for the experimental program was that precast-prestressed concrete deck panels were to be included in some portions of the deck of the test specimen. Figure 2.4 shows the cross section with panels used for the south half of the deck. Previous studies by Buth et al. (37 through 46) and, more recently, Bieschke and Klingner (47), had shown excellent behavior of bridge decks incorporating precast panels. Experience in the field has followed the experimental work, and 4-in. thick panels (see detail, Fig. 2.5) have become standard products in Texas for use in construction of composite deck slabs similar to the one in this experimental program. It was decided that this test slab would need to be full-sized (7-1/2 in. thick) in order to allow use of the standard precast-prestressed panels for half the bridge. Use of the full-size bridge deck, as indicated above, was also designed to take advantage of standard materials and avoid complications due to scaling in the interpretation of test results.

A typical bridge could be simulated with three girders, an interior girder and two exterior ones. Due to the space limitations inherent in full-scale testing, it was decided to use a bridge specimen having only three girders. For the Ontario deck design, a minimum overhang width of about 3 ft was required to satisfy the demands for transferring of in-plane forces from wheel load locations to the adjacent deck. The width between beams was made 7 ft, a representative spacing for many Texas bridges (with and without panels). As is typical, diaphragms were placed at 5 ft from each end support, and at midspan locations.

The deck between steel girders was built with conventiona forms for half the bridge (Fig. 2.3) and with precast-prestressed panels (Fig. 2.4) for the other half. Where panels were used, the reinforcing steel placed in the deck slab consisted of only the top layer of the two-layer reinforcing steel used in the 7-1/2 in. thick cast-in-place portion.

The full-sized deck was connected to three W36x150 girders using standard, 7/8 in. welded studs. The girders were 60 ft long, spanning 40 ft between simple supports. The studs were placed in groups of three per row along the top flange, and their design for composite action in the region of the deck containing precast panels took into account the reduced flange width available. In the southern half of the bridge, in which panels were used (Fig. 2.1), the rows of studs were placed diagonally to allow adequate spacing between the panels. Details of stud placement are shown in Fig. 2.6.

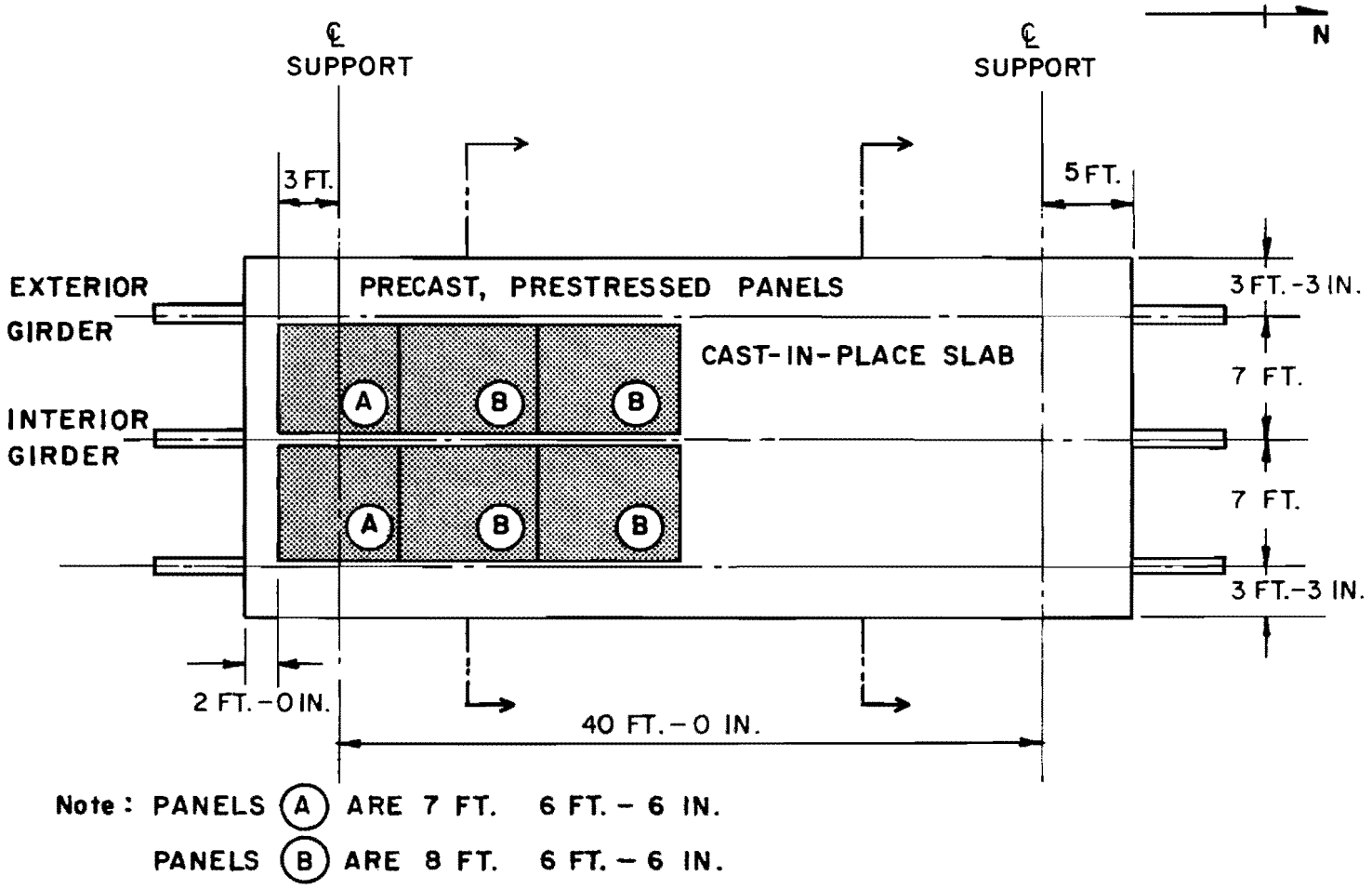

Fig. 2.1 Plan view of laboratory specimen

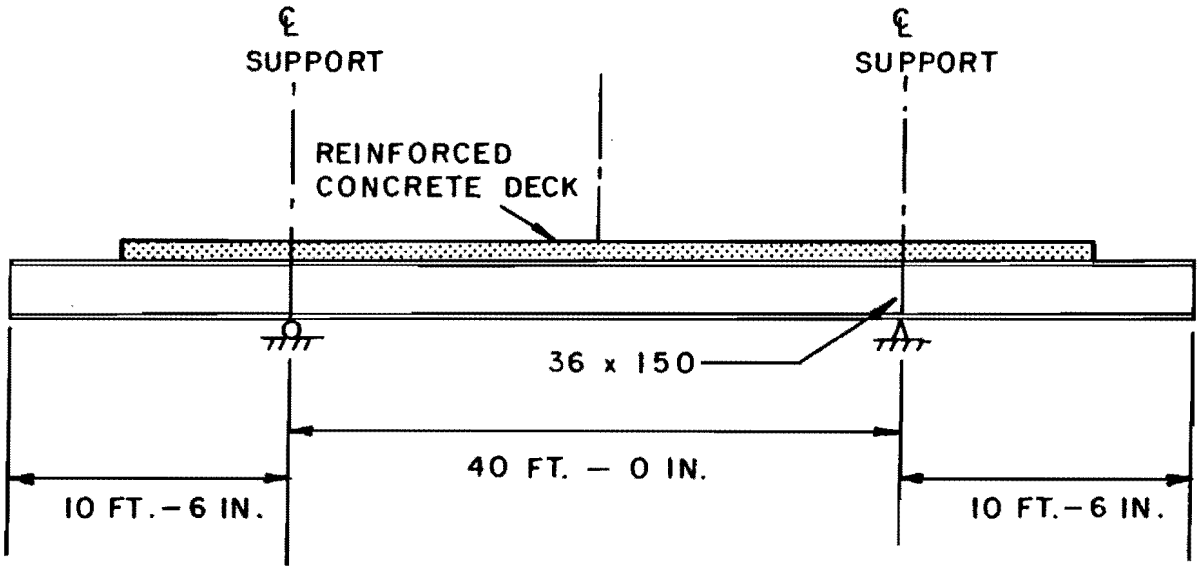

Fig. 2.2 Elevation of laboratory specimen

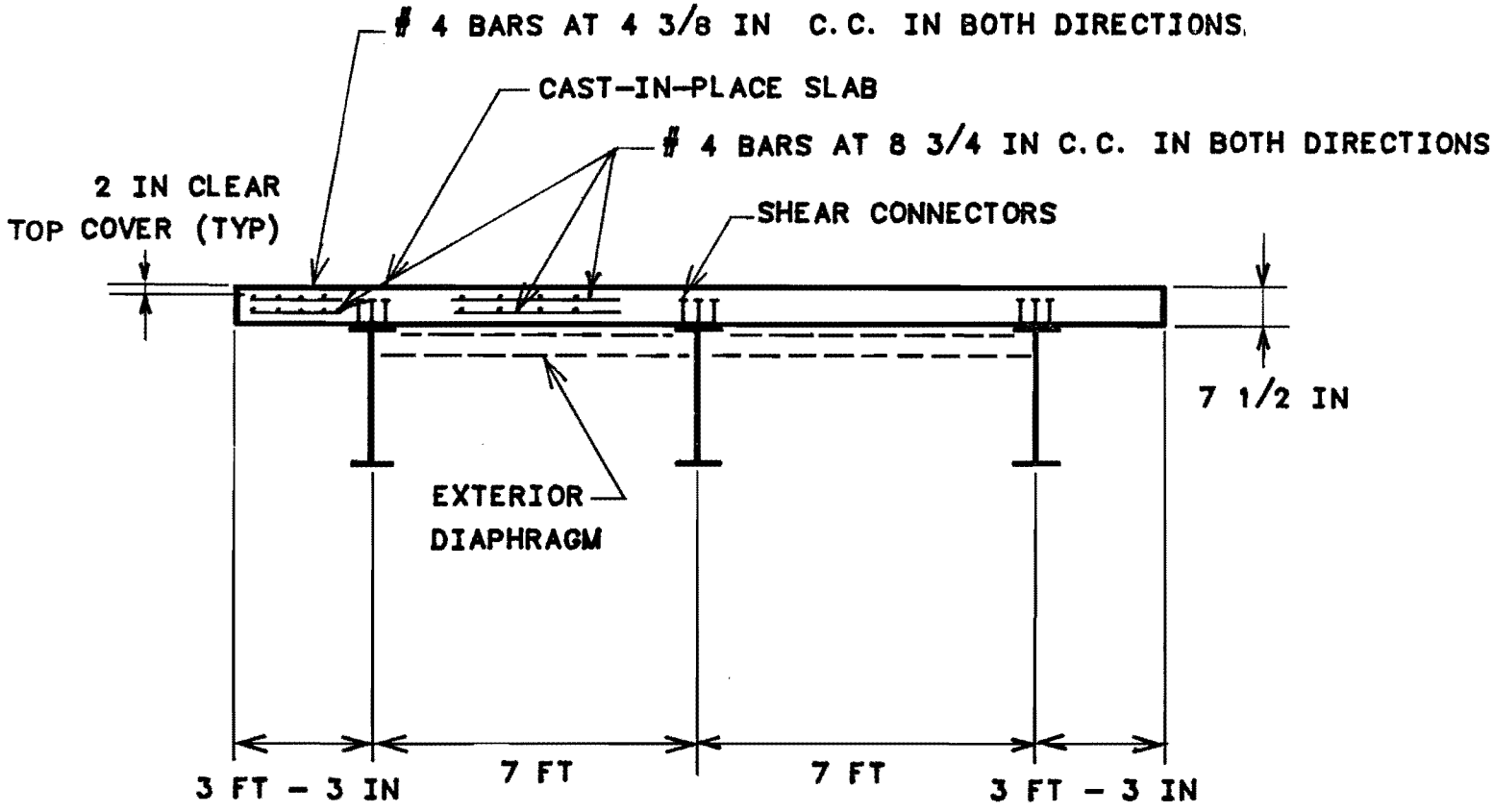

Fig. 2.3 Cross section of laboratory specimen showing cast-in-place deck

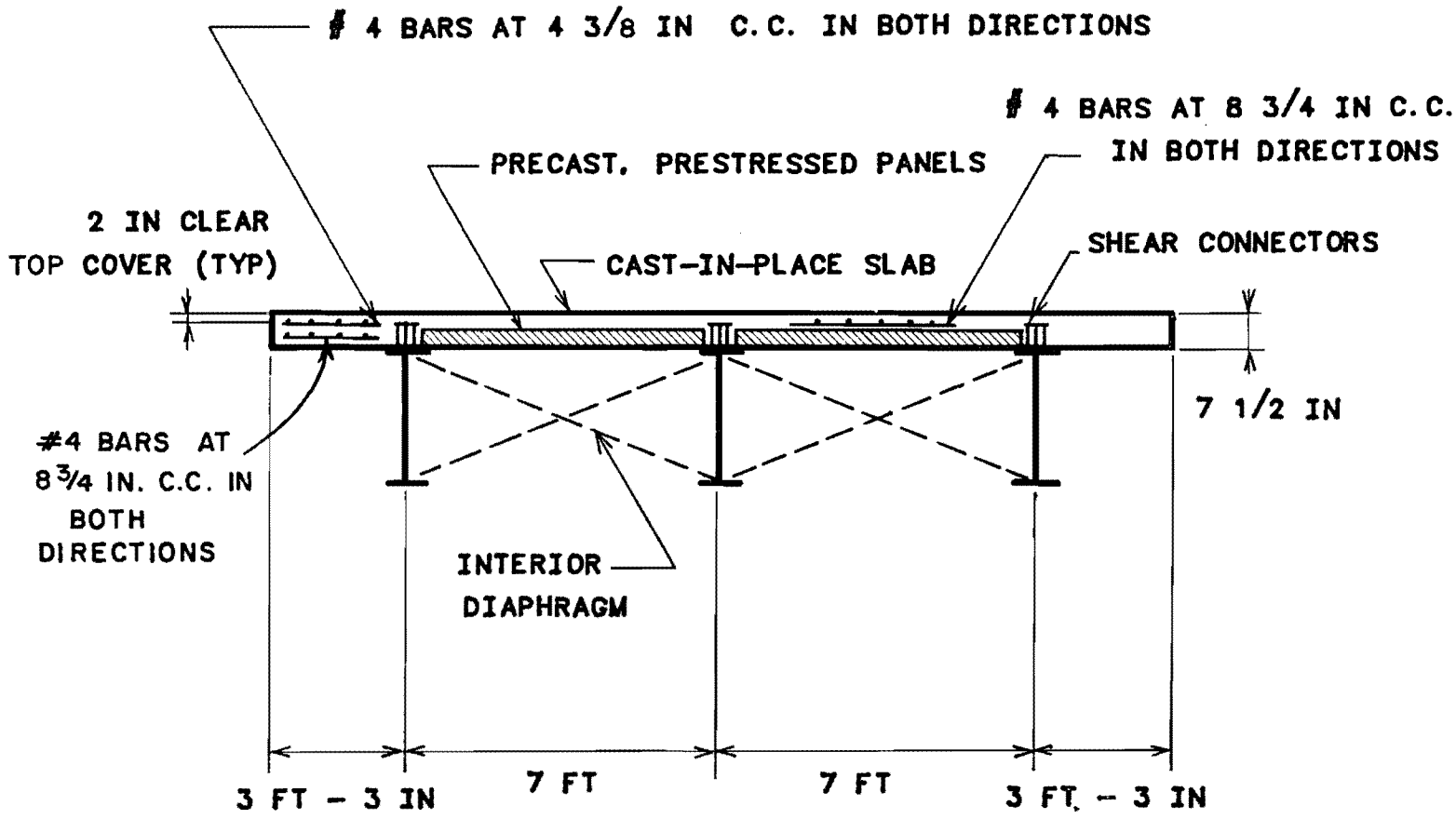

Fig. 2.4 Cross section of laboratory specimen showing precast, prestressed panels

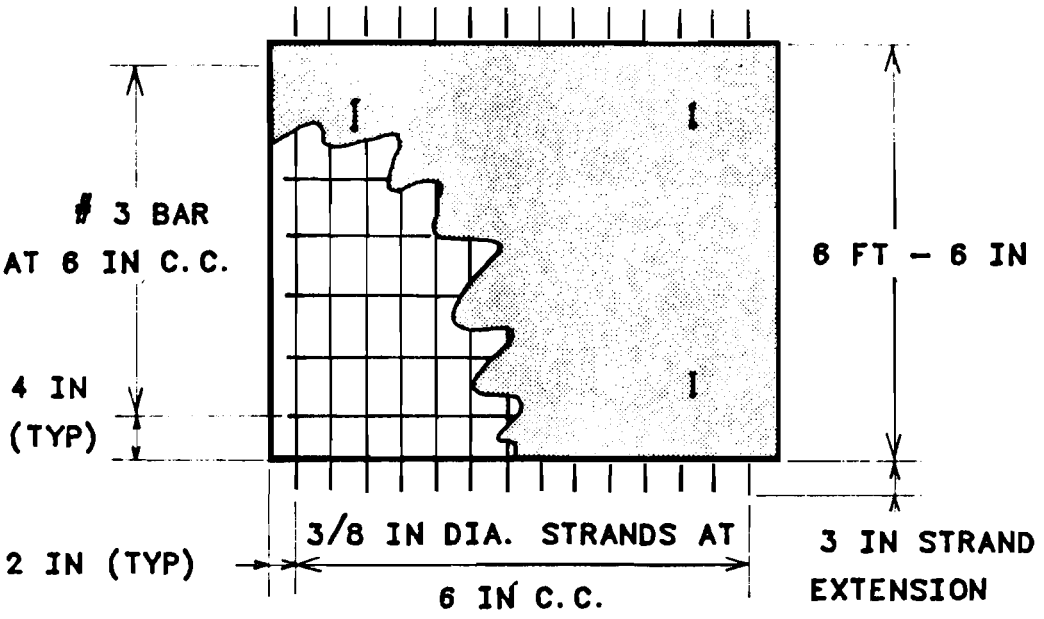

PLAN

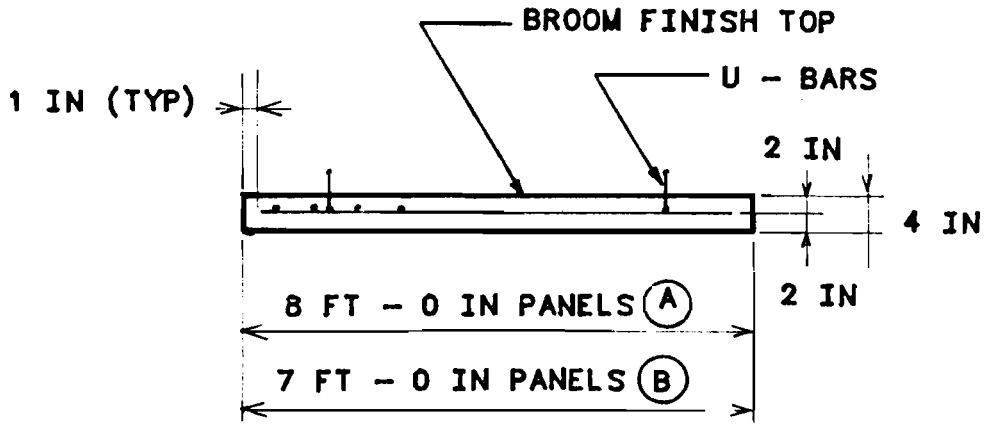

SECTION

Fig. 2.5 Precast, prestressed panels

As shown in Fig. 2.3, the deck was reinforced in accordance with Texas SDHPT details for Ontario-type decks. The cast-in-place deck had two layers of steel (running both ways), supported by chairs from the forms. The overhangs had reinforcement extended from the interior spans, plus some additional steel (Fig. 2.3). They were cast-in-place (full 7-1/2 in. thickness) for the entire length. The material proportions of the cast-in-place concrete and precast panel are detailed in Appendix A.

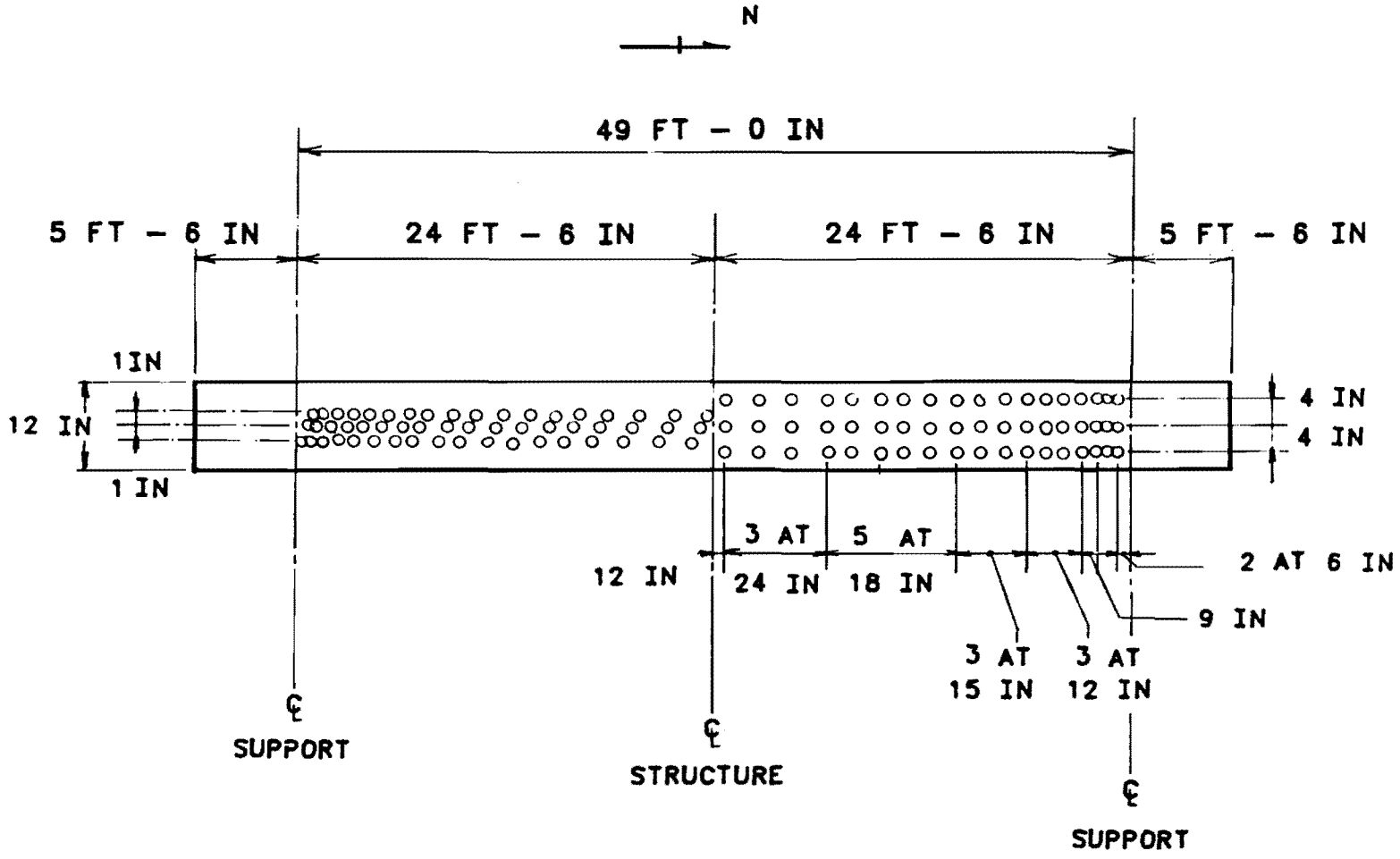

2.6(a) Layout of shear studs on the steel girders

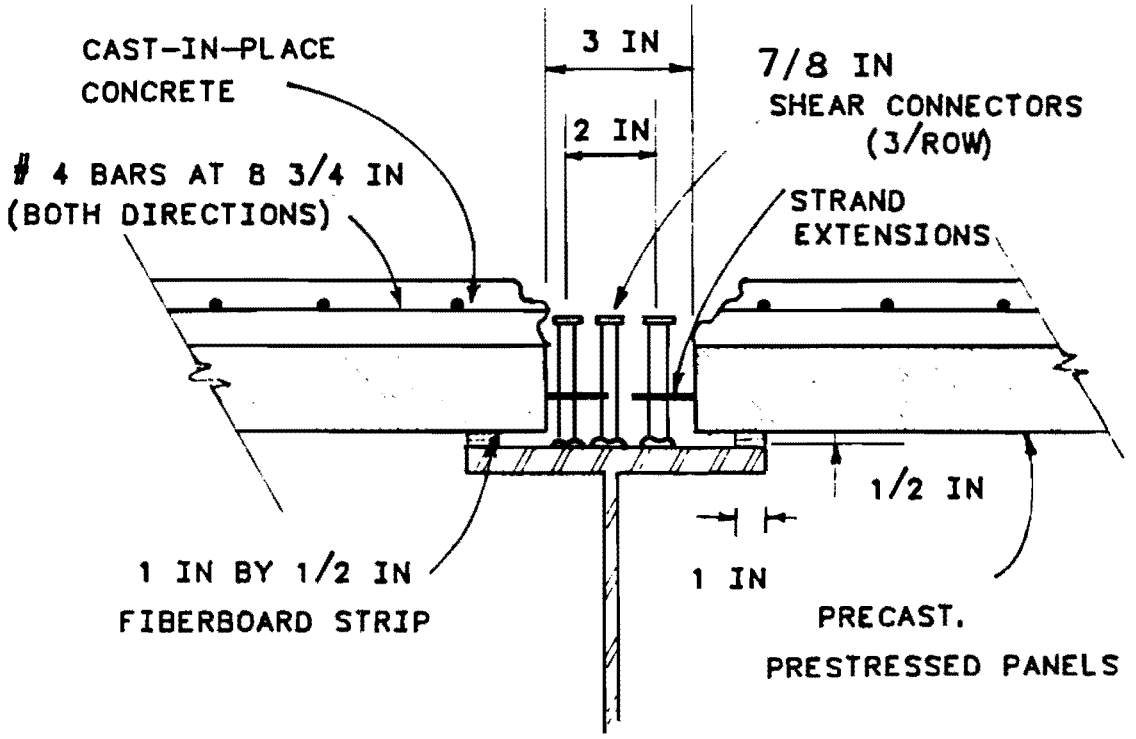

Fig. 2.6(b) Details of connection between girders deck with precast, prestressed panels

CHAPTER 3

NEGATIVE MOMENT TEST

3.1 Development of Test Specimen

As shown in Fig. 3.1, the negative moment test setup was intended to simulate a continuous structure. The structure was chosen because of its typical spans and loading conditions for highway bridges. The structure of Fig. 3.1 was analyzed with the worst loading pattern for interior support moments. The magnitude of the loads (26 kips per actuator) was adopted from the previous test (3). This test load was based on standard AASHTO truck loading of an HS 20 truck of 16 kips as maximum wheel load, multiplied by impact factor of 1.3, and then increased by an additional 25% to be conservative. The wheel load distribution of Fig. 3.5 might also be considered as a 48-kip tandem axle military load. In that case, the applied load of 26 kips per actuator would represent a 12-kip wheel load plus 30% impact (15.6 kips), multiplied by a load factor of about 1.7. The maximum negative moment at the interior support of the structure, also shown in Fig. 3.1, served as a target moment. The test setup was designed to induce this target moment in the bridge over both end supports.

3.2 Test Setup

3.2.1 End Tiedown. Figure 3.2 shows that the test setup actually involved with load added to the beam overhangs at lines perpendicular to the axis of the bridge, and 6 ft away from the line of support (Fig. 3.3). Two C 8 x 18.75 channels were connected back to back by 7/8-in. bolts and placed on the top flange of the girder at each end (Fig. 3.3). On each end, four 1-in. diameter, high-strength Dywidag bars were used to connect the channels to the floor. In order to avoid any fatigue problems in the tiedown bolts to the floor, the tiedown bolts were pretensioned against a 1x1x1 ft steel box, built to allow the tiedown for each bar (Fig. 3.4). The Dywidag bars were connected to the steel boxes, which in turn were tied down to the reaction floor.

3.2.2 Actuator Loads at Mid-Span. The loading points were located 3 ft on either side of the center steel girders and 4 ft apart along the axis of the bridge (Fig. 3.5). The bridge was loaded from below at four locations. As shown in Fig. 3.6 and 3.7, the loading actuators were attached at their bottom ends to the structural test slab underneath the bridge. At their top ends, the actuators loading rods passed through holes in the bridge deck and were held in place by nuts which delivered the load to the concrete deck. Each actuator had a static capacity of about 60 kips and a fatigue capacity of about 35

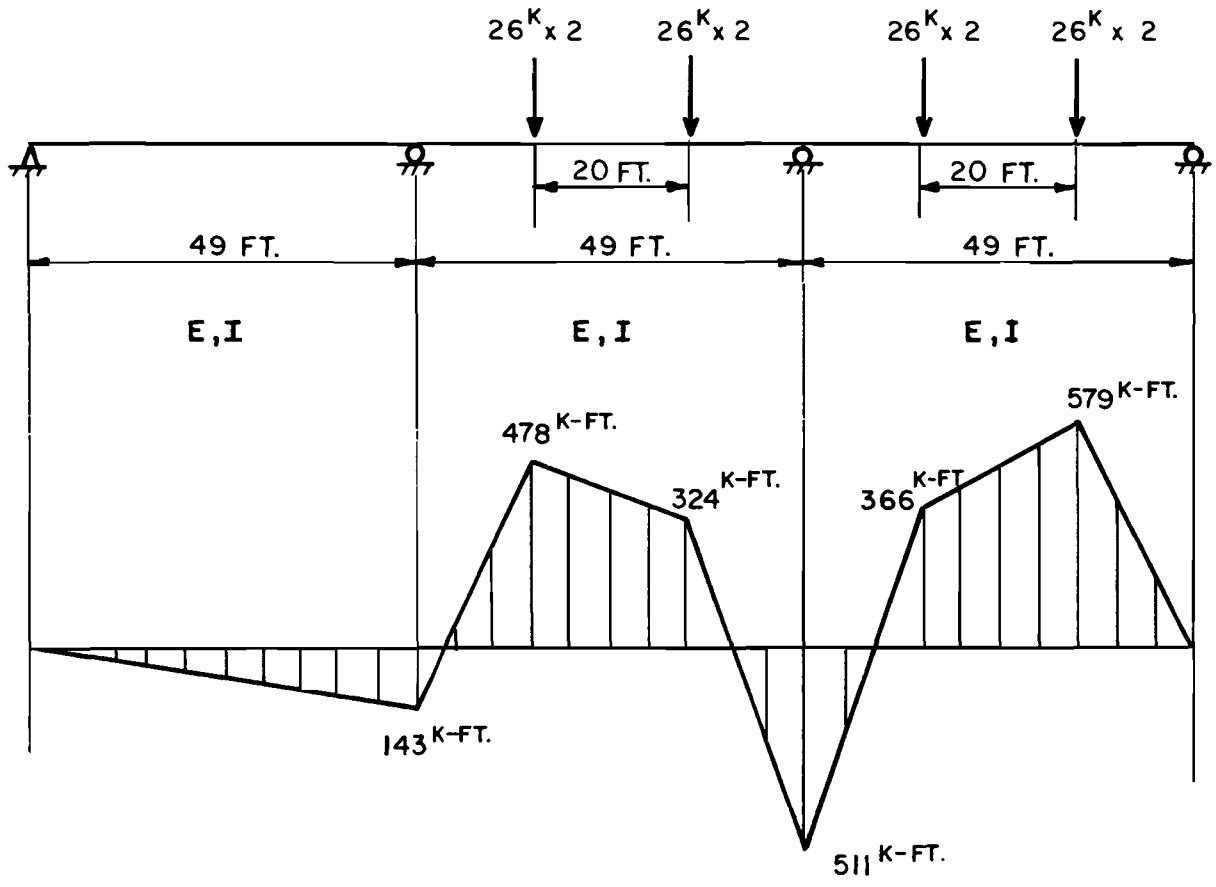

Fig. 3.1 Loading of typical continuous bridge structure showing maximum moment at support

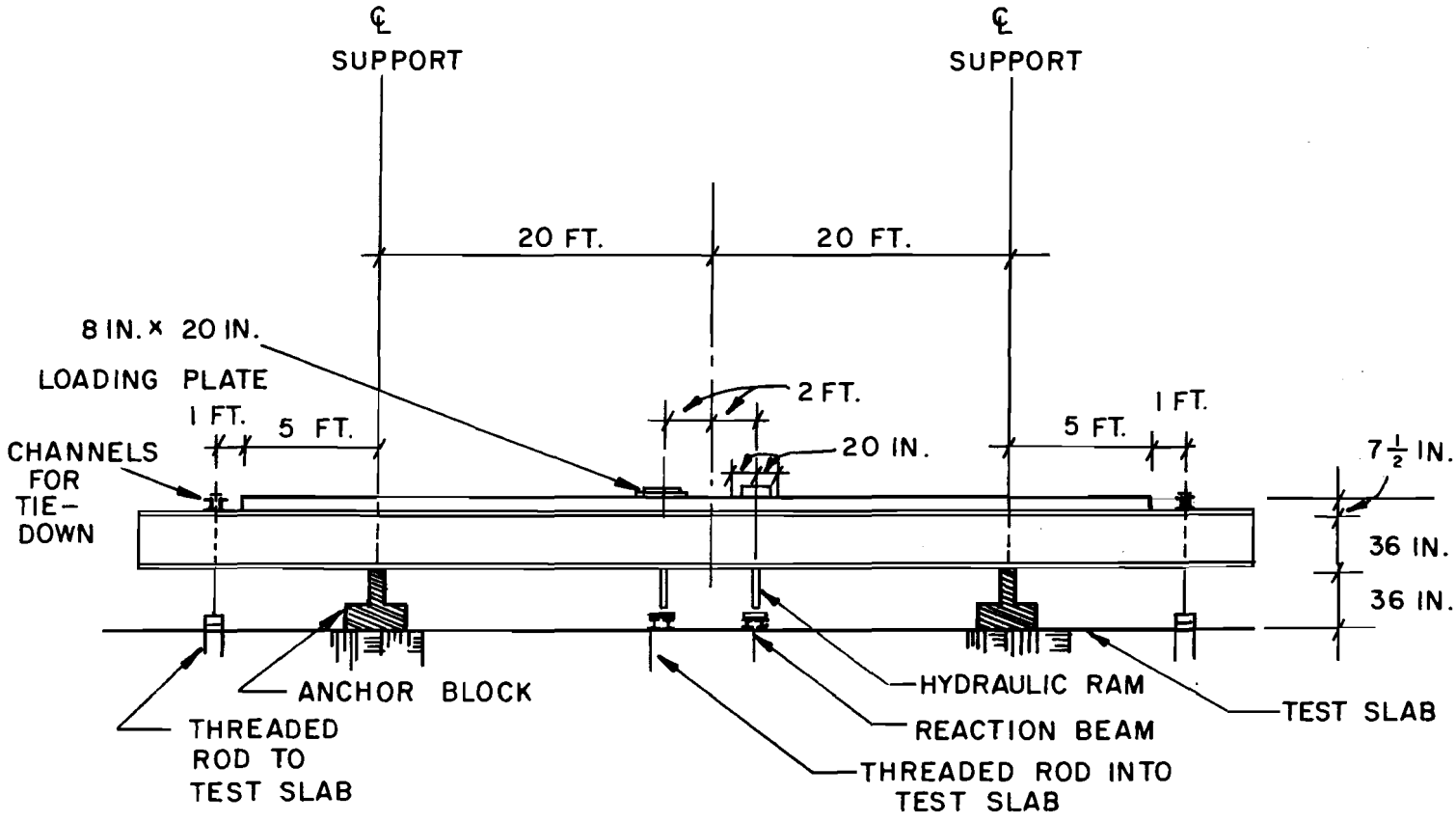

Fig. 3.2 Elevation showing negative moment test setup, supports and loading conditions

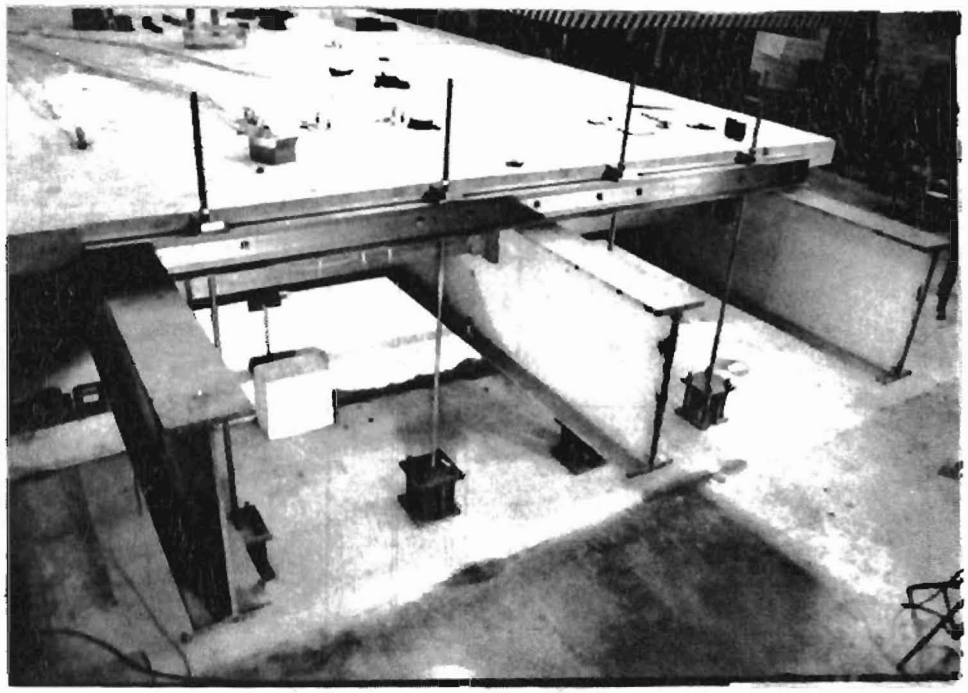

Fig. 3.3 Tiedown of overhang at one end of the laboratory specimen

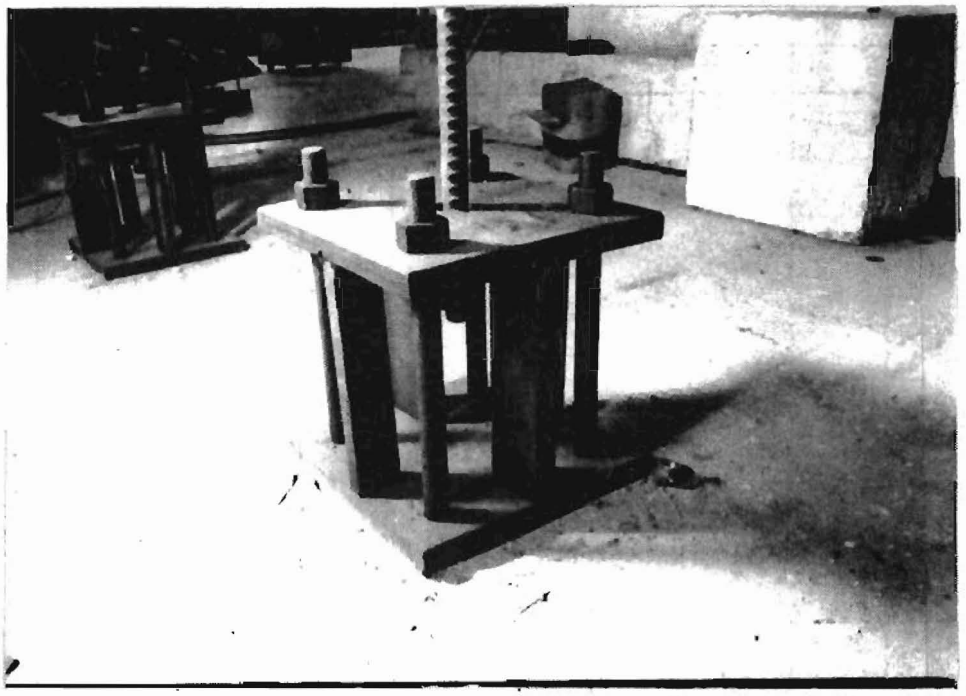

Fig. 3.4 Steel box for tiedown attachment to test floor

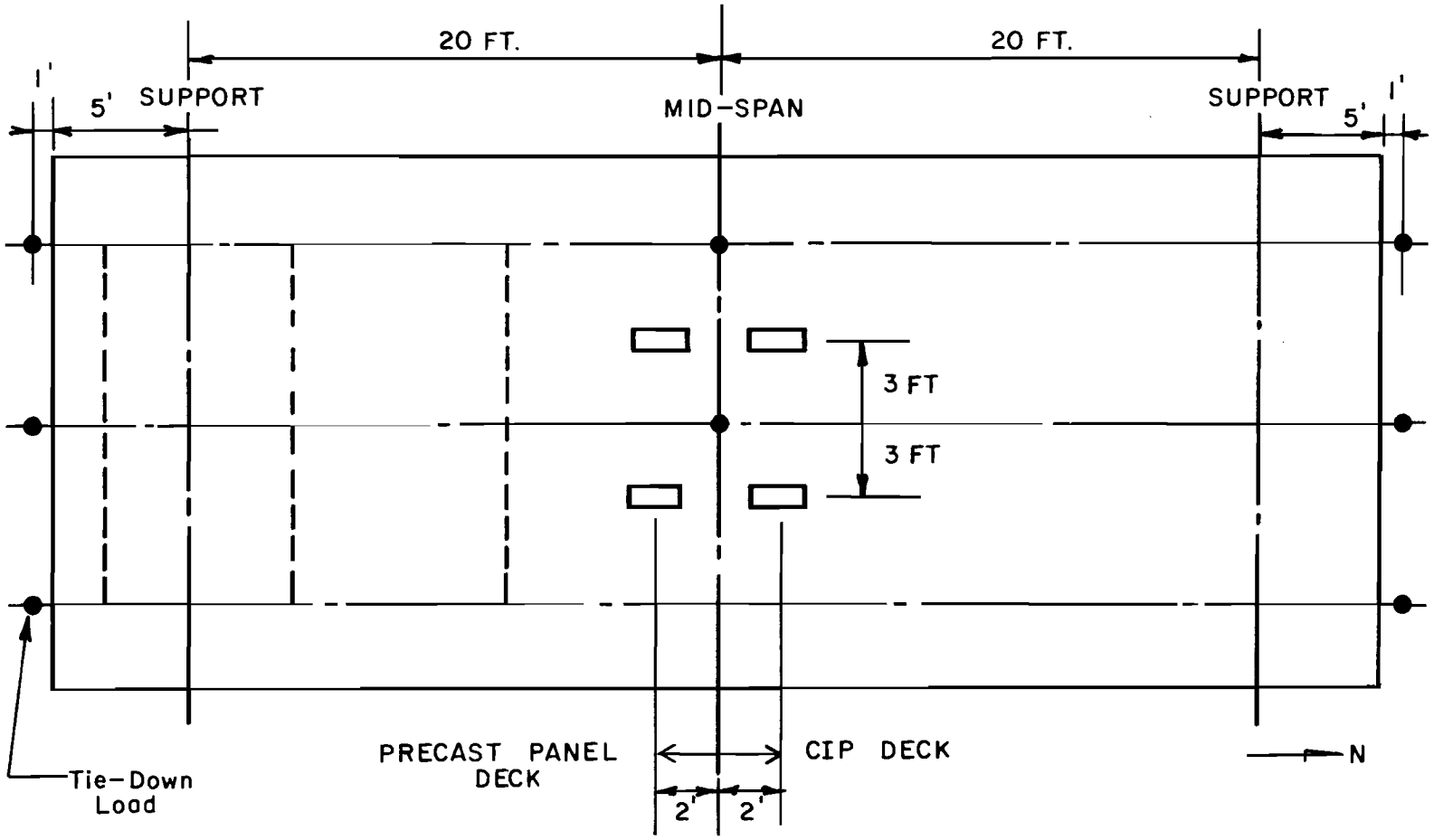

Fig. 3.5 Locations for applied loading and tiedown points

NOTE : ANCHOR BLOCK IS CUT AWAY
TO SHOW THE REACTION BEAM

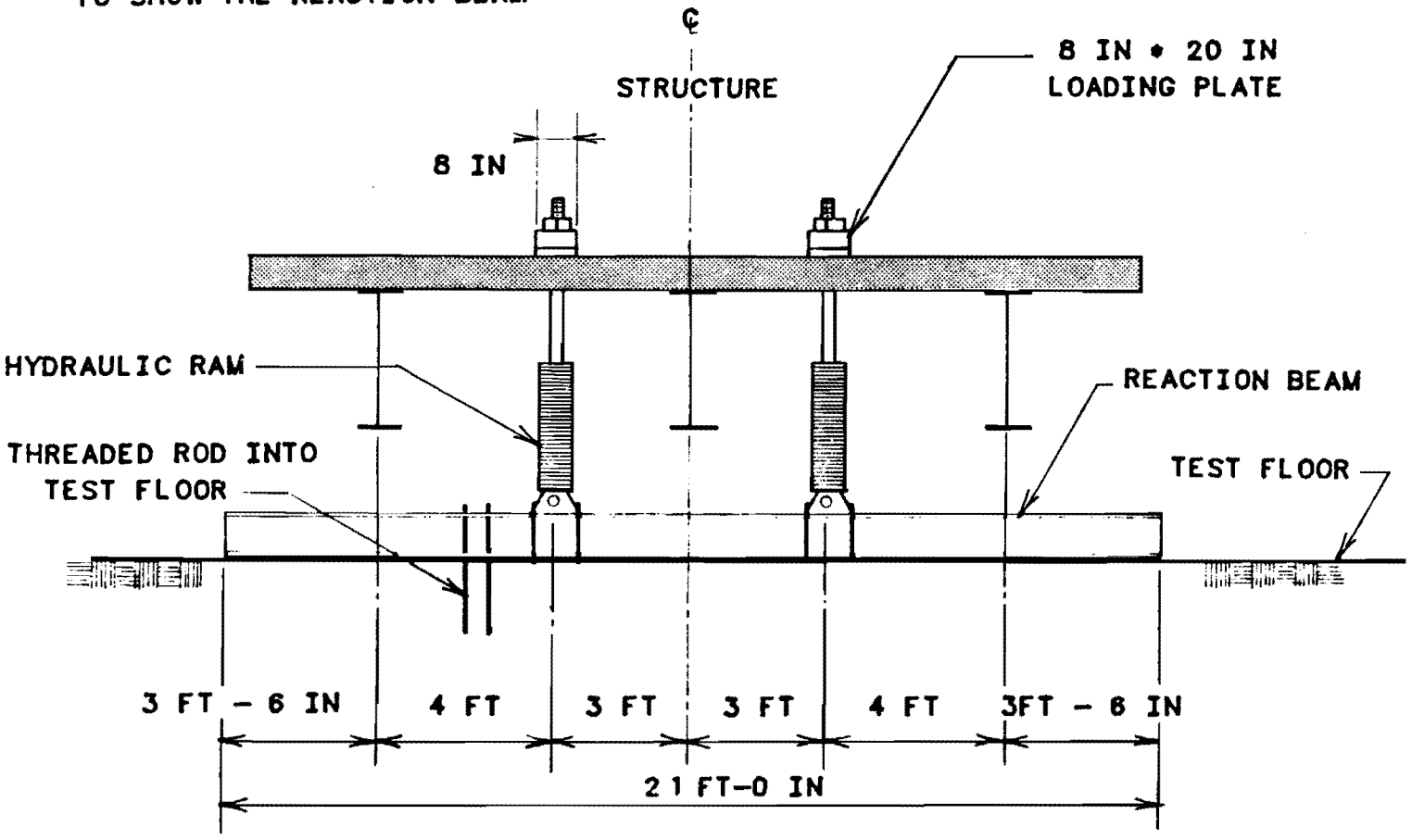

Fig. 3.6 Cross section of loading setup at mid-span region

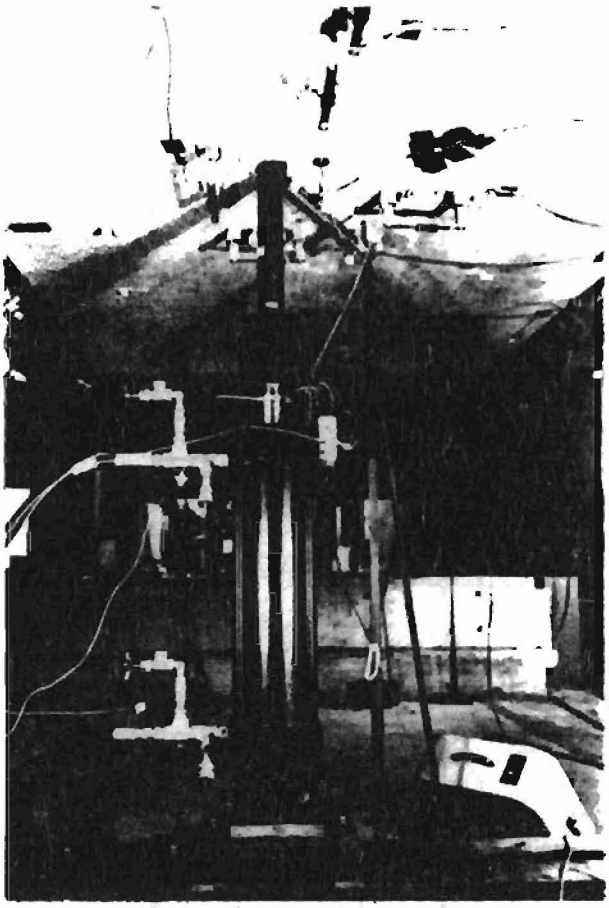

Fig. 3.7 Typical hydraulic actuator

kips. Hydraulic fluid at 3000 psi was supplied by two Shore-Western pumps. The actuators were controlled using a closed-loop feedback system, operating under load control. Load feedback from a fatigue-rated load cell was input to a Shore-Western servocontroller, which compared it to the sinusoidal command signal from a function generator (Fig. 3.8). The resulting error signal operated a single 60-gpm Moog servovalve, which fed all four actuators through a common manifold. The interconnected hydraulic actuators are shown schematically in Fig. 3.9.

3.3 Instrumentation

3.3.1 Loads. The load was monitored by a 200 kip fatigue-rated load cell (Strainset), connected to one of the hydraulic actuators. Loads were also measured using two 5000 psi pressure transducers attached to the high- and low-pressure sides of the other actuators which were connected to a manifold. Both load cell and pressure transducers were calibrated using the laboratory's 600 kip universal load machine and dead weight pressure gage tester. Tests showed that ram friction was low. Because they were interconnected, all rams were assumed to apply equal load. A single load cell was therefore considered sufficient. Also, a load cell was put on each Dywidag tie-down rod to monitor the load on each rod when installed.

3.3.2 Deflections. The vertical deflections of the bridge were measured by 0.001 in. dial gages, placed underneath the bottom flange of the girders at the locations shown in Fig. 3.10.

3.3.3 Strains. As shown in Fig. 3.11, electrical resistance strain gages were mounted on the reinforcement and on the concrete surface. Reinforcement strains were measured using 0.32 in. paper-backed gages (Precision Measurement W-32). Concrete surface strains were measured using 2.5 in. suface mounted strain gages (PL-60). Three-wire hookups were used to provide temperature compensation for all gages. Over the support regions, gages were installed longitudinally to detect the strain of the deck. Strain gages mounted on the top and bottom flanges of the girders showed the longitudinal strains in the girders, and also the strains in the deck near the girders. To avoid loss of gages due to concrete cracking in the negative moment regions of the deck subjected to tensile strains, those regions were instrumented using clip gages.

3.3.4 Cracking of Deck. Cracking from previous tests on the deck were carefully recorded before beginning this phase of testing. Cracks were carefully marked as each load increment applied. During the test, crack propagation was documented, and crack widths were measured by a crack width template whose smallest scale is 0.002 in.

3.3.5 Data Acquisition. A total of 76 channels of instrumentation were used for data acquisition. Data were read and recorded

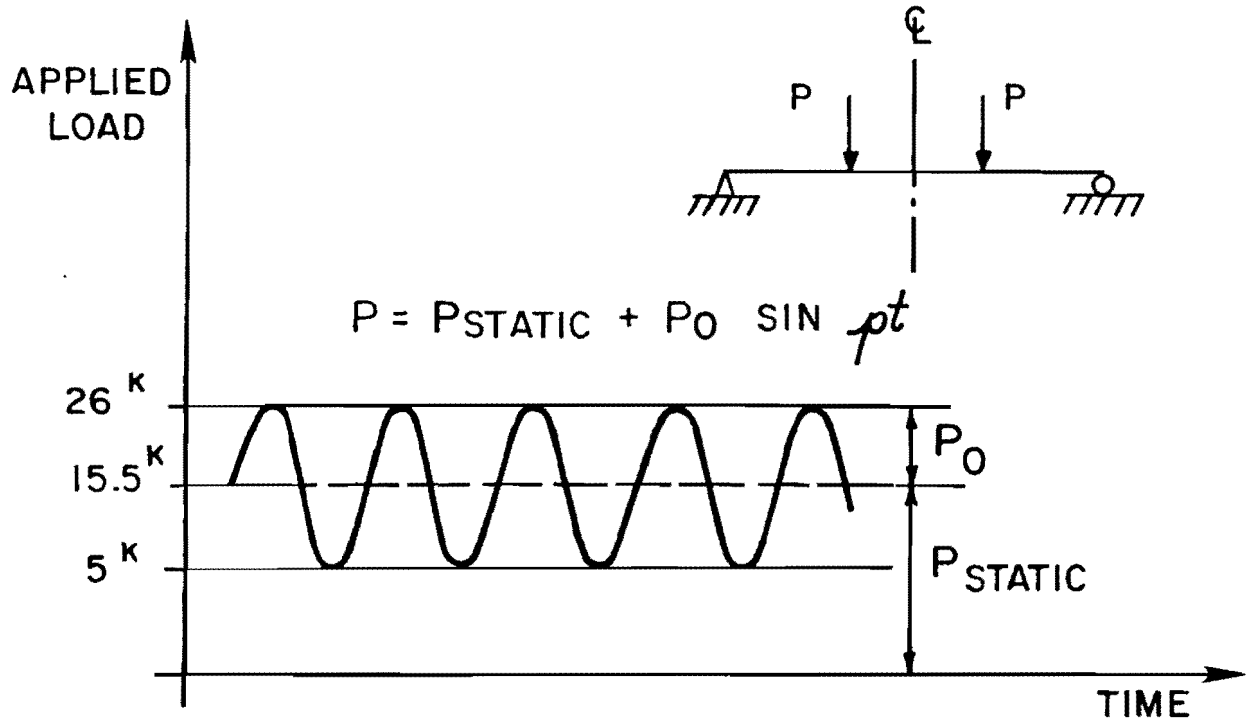

Fig. 3.8 Range of loading during fatigue test

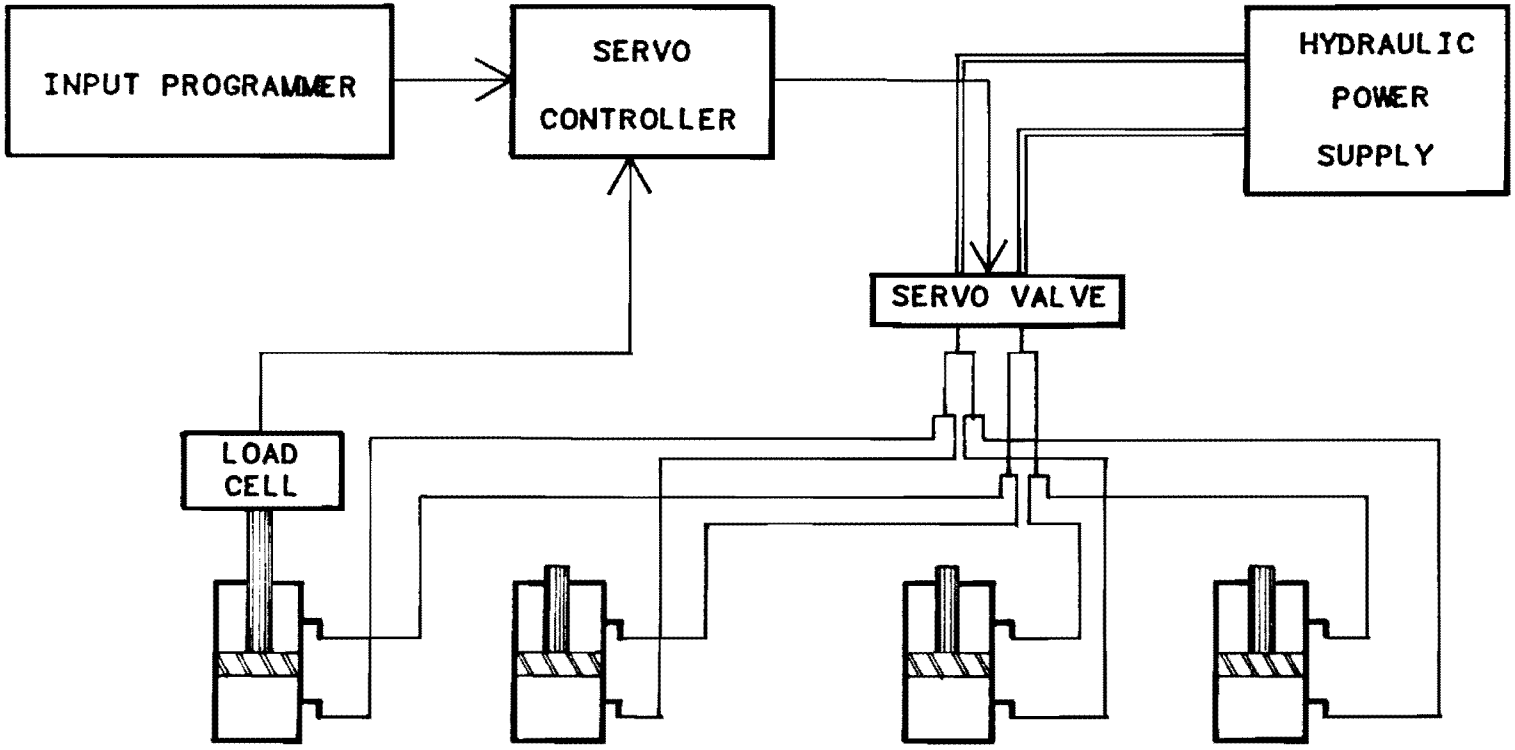

Fig. 3.9 Schematic of loading system

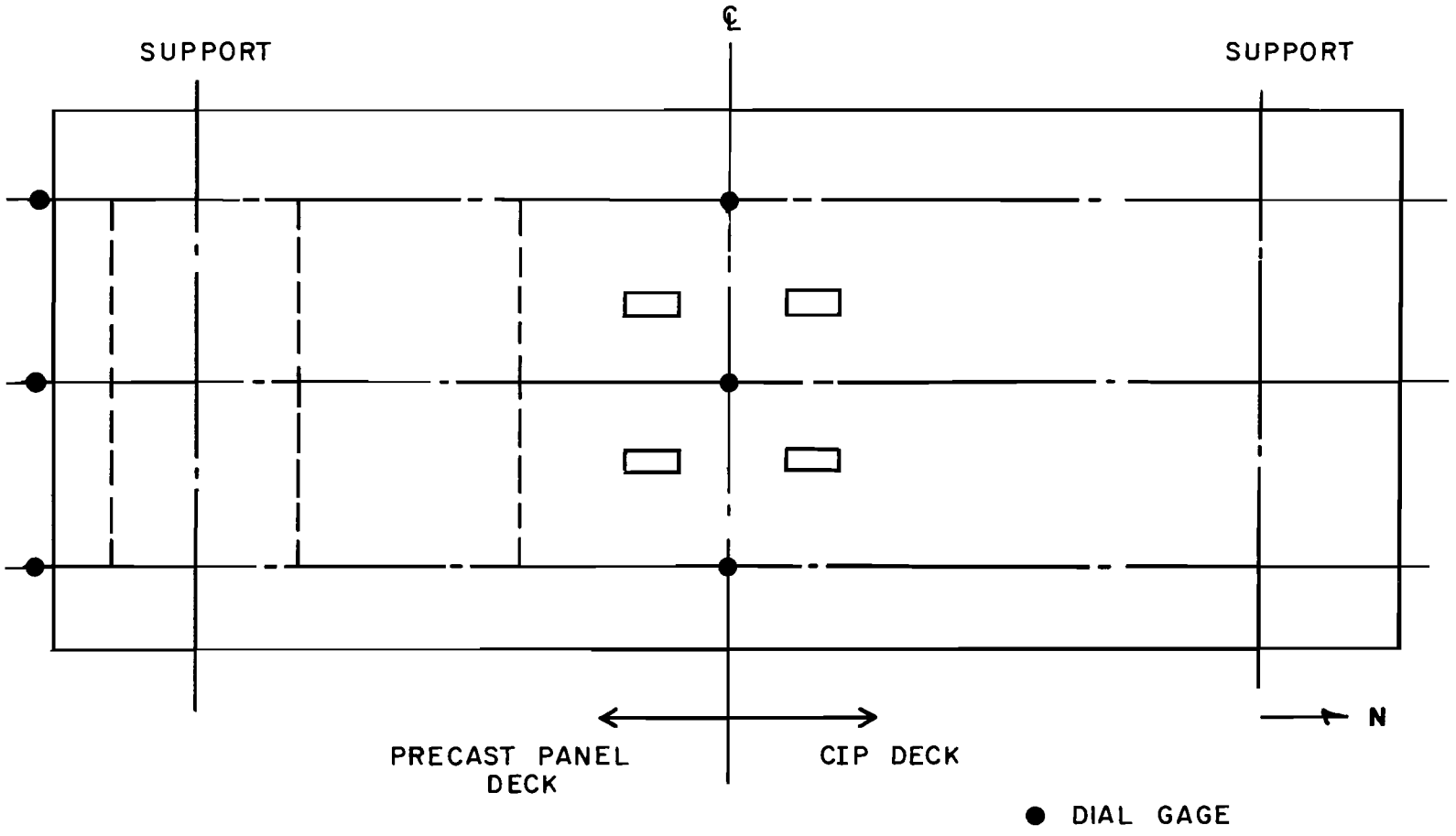

Fig. 3.10 Instrumented locations for deflection measurement

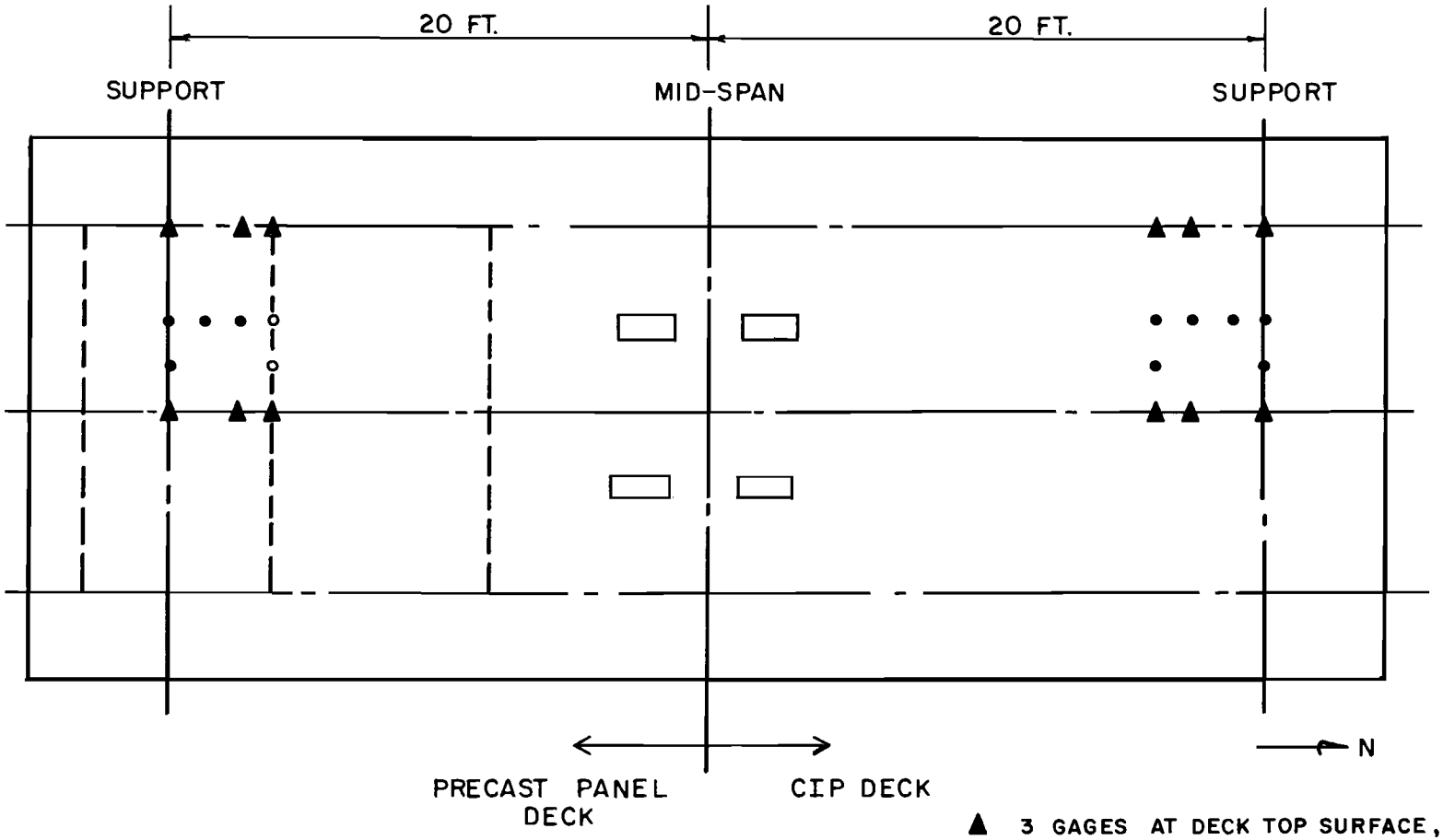

Fig. 3.11 Strain gage locations for deck and girders

electronically by an Acurex digital voltmeter connected to a reed-type scanner, and controlled by a CompuPro microcomputer. Test data for all 76 channels were scanned in less than 10 seconds, avoiding changes in readings due to creep. Digitized data were written immediately onto the microcomputer's diskette, and were also converted to engineering units for immediate review during a test. Data were transferred to the main computer at the University of Texas at Austin campus for further processing.

3.4 Loading Sequence

As shown in Fig. 3.12, this test program involved the following sequence of loading:

1. Preloading to Crack the Deck. The cantilevers were loaded independently at each end by the same tie-down system as described in Subsection 3.2.1, except that the double cross channels (C8x18.75) were replaced by two heavier sections for higher flexural and shear capacity. This procedure was performed to crack the deck along the support line at each end, thereby creating the worst possible bridge deck condition for the subsequent fatigue test at the negative moment regions;

2. The bridge was tested statically to a maximum load of 30 kips on each of the 4 actuators. This load level represented about 1.5 times the service live load of 20.8 kips (including impact factors);

3. The bridge was subjected to 5 million cycles of fatigue loading, varying sinusoidally between 5 and 26 kips on each actuator (Fig. 3.8). The maximum fatigue loading of 26 kips represented the service live load level of 20.8 kips, plus a 25 percent overload for a conservative load test program. After about 2.2 million cycles, the deck was loaded statically to 30 kips on each actuator (an overload condition). The same static tests were performed again at about 4.0 million cycles;

4. After the 5 million cycles, the bridge was tested statically to 55 kips on each actuator. This load level represented about 2.5 times the service live load of 20.8 kips. In every static test, the following data were obtained:

   a) loads applied at one actuator;

   b) strain profiles at various points on the bridge deck;

   c) strain at various points along the steel girders; and

d) crack widths and extensions over the bridge deck.

Deflections were measured only at the final static test after the 5 million cycles of fatigue loading.

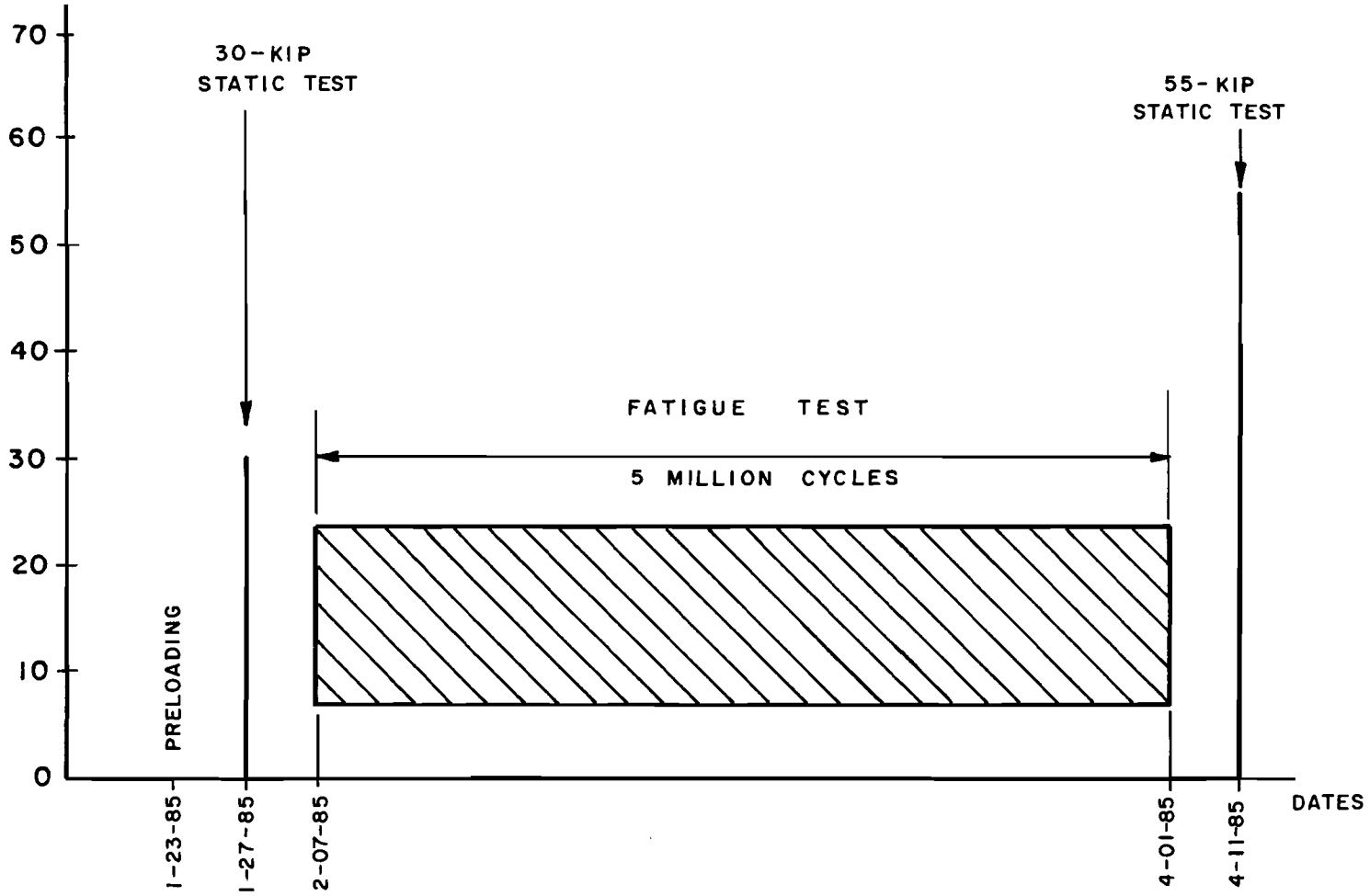

Fig. 3.12 Loading sequence

CHAPTER 4

RESULTS OF NEGATIVE MOMENT TEST

4.1 Description of Test

In this chapter, results and observations from tests of the specimen are presented and discussed. During the test sequence described earlier, the following observations were made:

1. Preloading of the deck: Downward tiedown forces were applied independently at each end of the bridge to create a transverse crack along the support line. Under total tiedown forces of 160 kips at each end, a continuous transverse crack formed across the width of the CIP deck, almost exactly above the support. The cracking load was reasonably close to that predicted by comparing the negative cracking moment of the interior composite girder and the corresponding tie-down forces acting on it. The tie-down force was then increased to 255 kips to ensure that the transverse crack was fully developed. At the panel end, the first crack formed at a total tiedown force of about 200 kips. The load was increased to about 290 kips. However, the crack at the panel was not continuous over the whole width of the bridge. Some parts of the crack were not in line (Fig. 4.1), and one was about 1 ft inside the support line. This may have been due to an existing continuous transverse shrinkage crack at a panel joint, which was only 2 ft from the support. The largest crack width was 0.005 in. at the CIP deck and 0.003 at the panel deck. The difference between the crack width and the cracking load of the CIP deck and the panel deck was due to the prestressing in the panel. Fig. 4.1 shows the cracks on the deck for this test.

2. First static test: A total tie-down force of 60 kips was applied a each end of the bridge, after which the four center rams applied a load which varied from 0 to 30 kips per ram, in 5-kip per ram increments. No new top surface nor bottom suface cracks were found, nor was there any indication of propagation of the existing top surface cracks (Fig. 4.1) from the preloading.

3. Fatigue test: The bridge was then subjected to fatigue testing, using a total tiedown force of 60 kips at each end of the bridge. The center rams supplied the fatigue loads, which varied sinusoidally from 5 to 26 kips per ram. At 500,000 cycles, the weld between the intermediate diaphragms and the East exterior girder was found to have broken. The

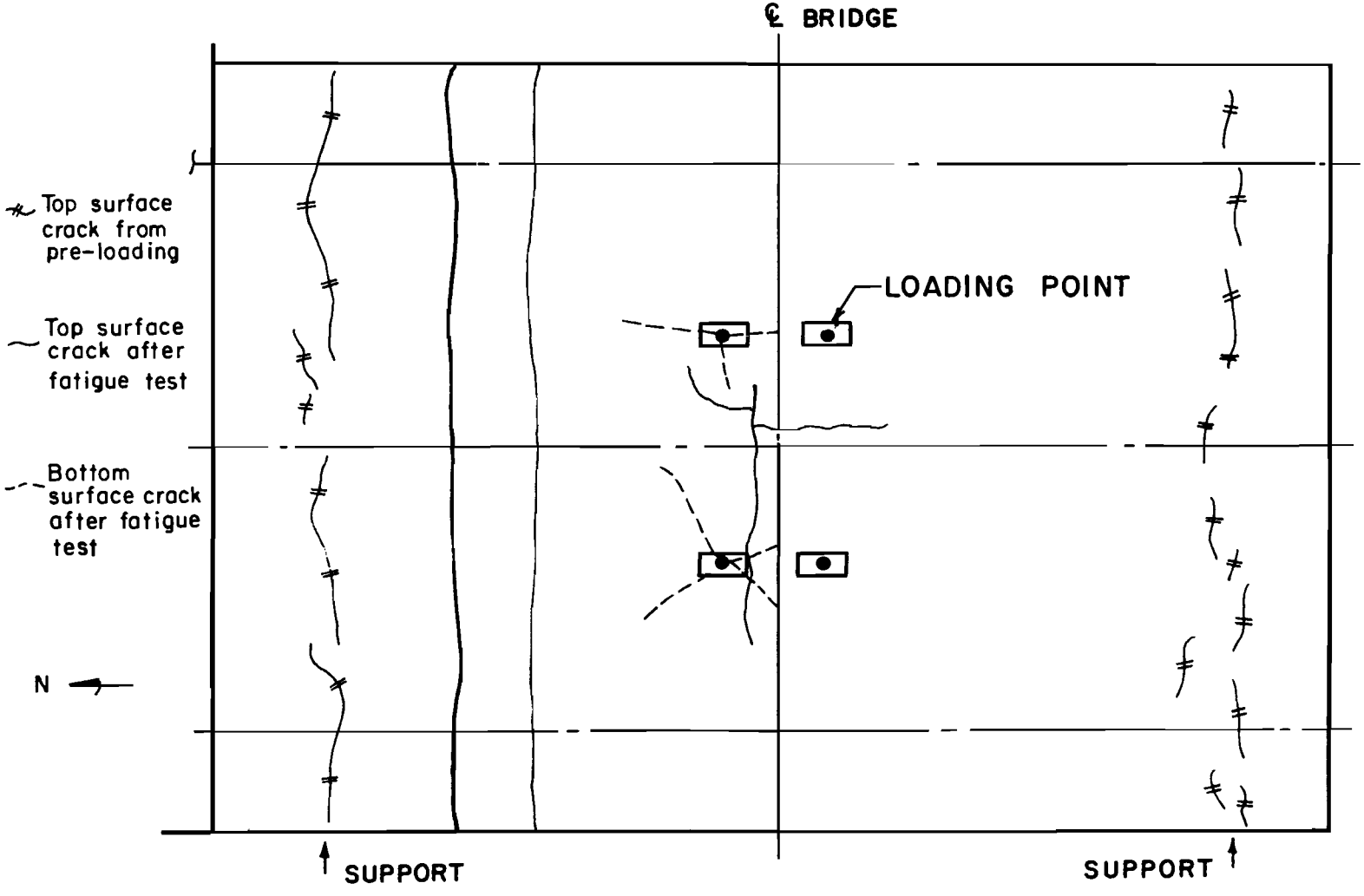

Fig. 4.1 Deck cracking before and after fatigue loading

diaphragm was left broken, simulating an unfavorable situation for the bridge. At 1 million cycles, a few hairline cracks were found around the load points on the CIP deck. At approximately 2.2 and 4.0 million cycles, the bridge was loaded statically to 30 kips per ram to monitor possible deterioration in deck response due to fatigue loading.

4. Final static test: Following the 5 million cycles of fatigue loading, the final static test was carried out. The loading rams applied loads up to 55 kips per ram by the increment of 5 kips per ram. The test was stopped between 55 and 60 kips per ram because of tensile failure of one of the four loading rods. In every static test, the following data were obtained:

   a. load applied at two actuators;

   b. force in each of the tiedown rods;

   c. longitudinal strain at various points on the concrete surface, and also on the embedded reinforcement near the supports;

   d. longitudinal strain at various points on the steel girders near the supports; and

   e. crack widths and extensions on the top and bottom surfaces of the deck.

In addition, the vertical displacements of various points on the steel girders were recorded during the final test.

4.2 Load-Deflection Data

At each load stage during the final static test, readings from 6 dial gages were used to measure the vertical deflections of the steel girders at the overhang and midspan location. Both at the midspan and the overhang, the readings from the two exterior girders were consistently close. Therefore, only data for the interior and one of the exterior girders are discussed below. Typical load-deflection relationships for the interior girder and west exterior girder are presented in Figs. 4.2 and 4.3.

At the midspan, the load-deflection curves for both the interior and exterior girders were linear up to a load of 55 kips per ram, about 3 times the design wheel load of 20.8 kips (including impact). Both the interior and exterior girders deflected upward about 0.05 in. at midspan after the tie-down force was applied. As the

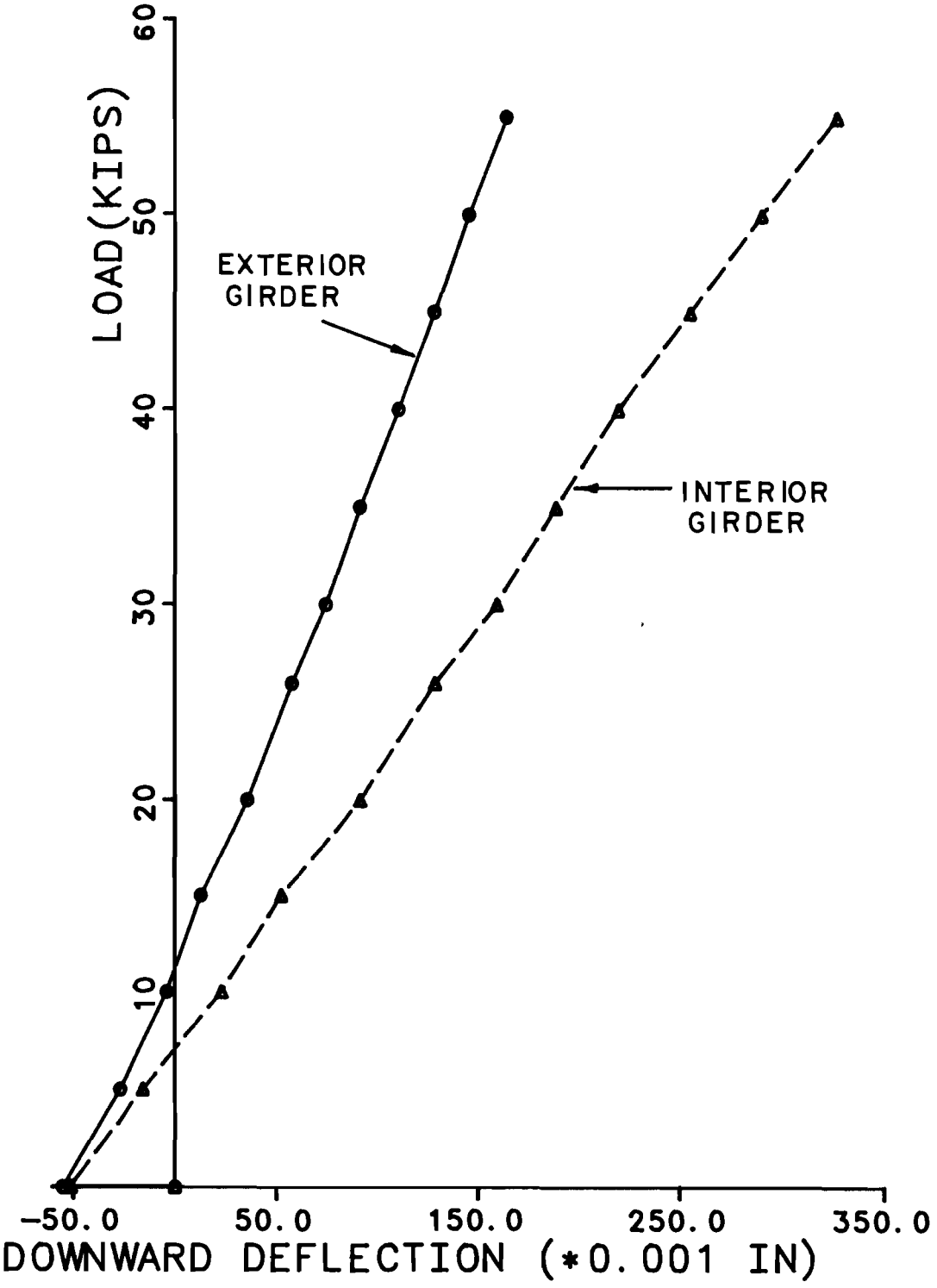

Fig. 4.2 Girder deflections at mid-span from final static test

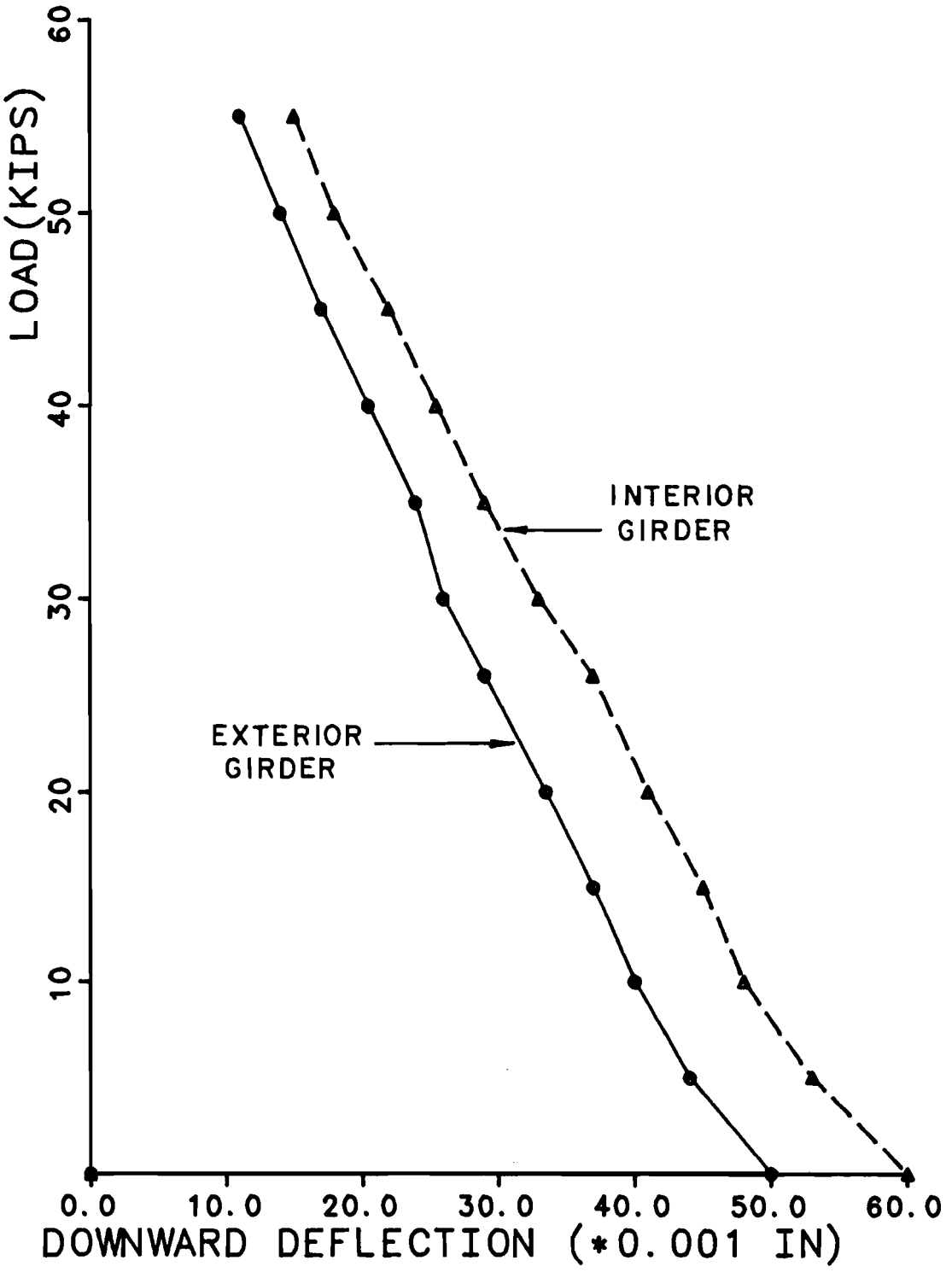

Fig. 4.3 Girder deflections at overhang from final static test.

center rams reached 55 kips per ram, the deflection of the interior girder was about 0.35 in., about twice that of the exterior girder.

At the overhangs, load-deflection curves for both the exterior and interior girders were linear up to 55 kips per ram. The interior girder deflected 0.06 in. downward and the exterior girder, 0.05 in., after the tiedown force was applied. As the loads from the center rams increased, the downward deflection of the girder overhangs decreased linearly. At a load of 55 kips per ram, the overhang deflection of the interior girder was about 0.02 in. The ratio between the deflection of the interior and exterior girder varied from 1.2 at 5 kips per ram, to 1.36 at 55 kips per ram.

The linearity of all these curves suggests that deck cracking does not significantly affect the overall elastic behavior of the bridge. These experimental values of deflection of the girders were also compared with the analytical results to check the validity of the analytical model. This is discussed in Chapter 5.

4.3 Cracking of the Deck

According to the current Ontario Highway Bridge Design Code (OHBDC (1)), deck slabs should be designed for the ultimate limit state of strength, and also for the serviceability limit state of cracking. The requirement of the serviceability limit state of cracking need not be considered for slabs detailed in accordance with the empirical design. However, cracking of the deck was important in this study, because the thickness of the deck proposed by the Texas SDHPT is less than 9 in. minimum required by the revised OHBDC.

Fig. 4.1 includes all the cracks recorded after the fatigue test. As described in Sec. 4.1, two groups of transverse cracks were induced above the support at each end of the bridge from the preloading procedure. The width of these cracks varied from 0.002 in. to 0.005 in. at the CIP end, and from less than 0.002 to 0.003 in. at the panel end. No more cracking was recorded after the first static test. About 500,000 cycles after the fatigue test started, a few cracks, varying from 0.002 in. to 0.005 in. wide, were found at the bottom surface of the CIP deck under both loading points. These cracks stopped at the centerline of the bridge where the panel deck started. After the 5 million cycles of fatigue loading, these bottom cracks propagated to only about 3 ft away from the loading points. However, no cracking was observed around the loading points at the bottom surface of the panel deck. This demonstrates that the panel deck is stronger against cracking, due to its higher strength concrete and also to its prestressing. After the fatigue test, no widening of the top surface cracks induced by the preloading was observed. This indicated that the fatigue loading did not have a significant effect on the cracks of the section of this deck above the supports. However, two new cracks which ran transversely across the bridge and parallel to the

support line were found at the CIP deck. These two cracks were about 0.003 in. wide and located at 3.5 ft and 5.5 ft from the support. Also, two short, hairline cracks were found at the top surface around the interior girder at midspan, as shown in Fig. 4.1. They were caused by the high local stresses from the nearby loading plates.

4.4 Local Stress in Deck and Girders

4.4.1 General. Strain readings from the concrete, reinforcing steel, and girders were used to study typical local stresses in the deck and the girders. At a load of 26 kips per ram and a corresponding tiedown force of about 85 kips, the maximum concrete stress was about 0.6 ksi in the CIP deck, and 0.3 ksi at the panel deck. At that load level, the maximum stress in reinforcement was about 5.7 ksi at the CIP end and 9.8 ksi at the panel end. The fatigue loading generally lowered the top surface concrete tensile stresses in both types of deck. However, the fatigue test did not cause any significant change in the stresses in the reinforcement.

Stresses in the girders ranged from 0.3 ksi in tension to 5.3 ksi in compression. The stresses in the girders at the CIP deck and the panel deck were very similar. Once again, the fatigue loading had little effect on the stresses on the girders.

4.4.2 Local Stresses in the Deck Concrete. The readings from the bottom surface gage on both kinds of concrete decks were consistently very small. Therefore, only the top-surface concrete stresses will be discussed here. In both CIP deck and panel deck, the cracking had damaged a number of strain gages. This made it impossible to make complete stress distribution profiles at some locations on the deck. Figures 4.4 and 4.5 show the top-surface tensile concrete stress distribution along a line parallel to the axis of the bridge, and halfway between the interior and west exterior girder. In each figure, curves are plotted from experimental results of tests carried out at the pre-fatigue stage, after 2.2 million cycles, and after 5.0 million cycles of fatigue loading. For the CIP end, the three curves have a similar general trend: they increase almost linearly from the support to a distance of about 2.5 ft from the support, and then drop sharply. For the panel end, all three curves show that stresses decreased from the support to a distance of about 1 ft from the support; then they increased and peaked at about 2.5 ft from the support; and from then on, they decreased. The drop of stresses at 1 ft away from the support was believed due to the local effect of a crack passing nearby. However, in both CIP deck and panel deck, the stresses generally decreased as the fatigue test went on. The curves also indicate that the effect of the first 2.2 million cycles of fatigue loading had a more significant effect on lowering the concrete stresses than the last 2.8 million cycles of fatigue loading.

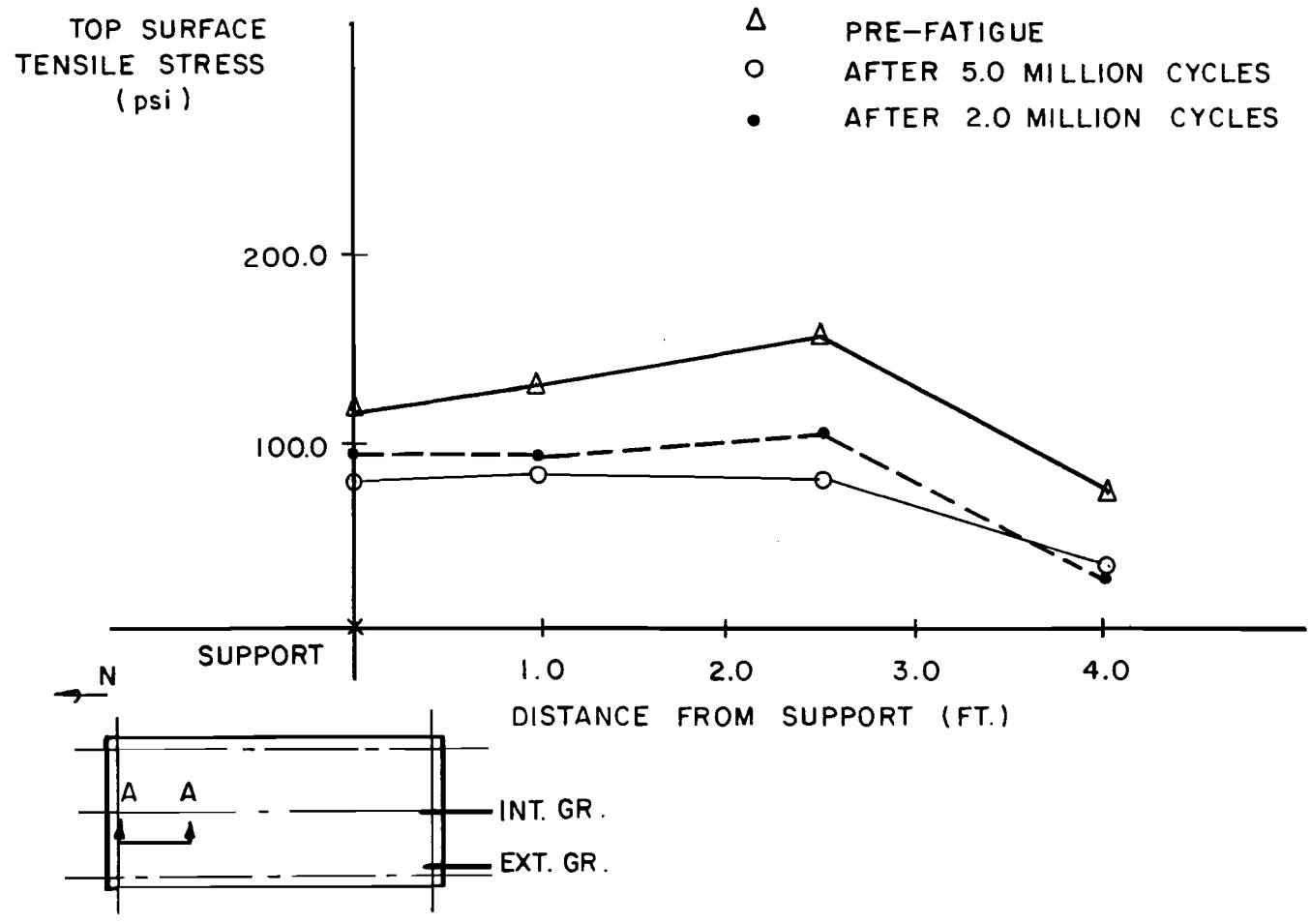

Fig. 4.4 Longitudinal concrete stress on CIP deck top surface

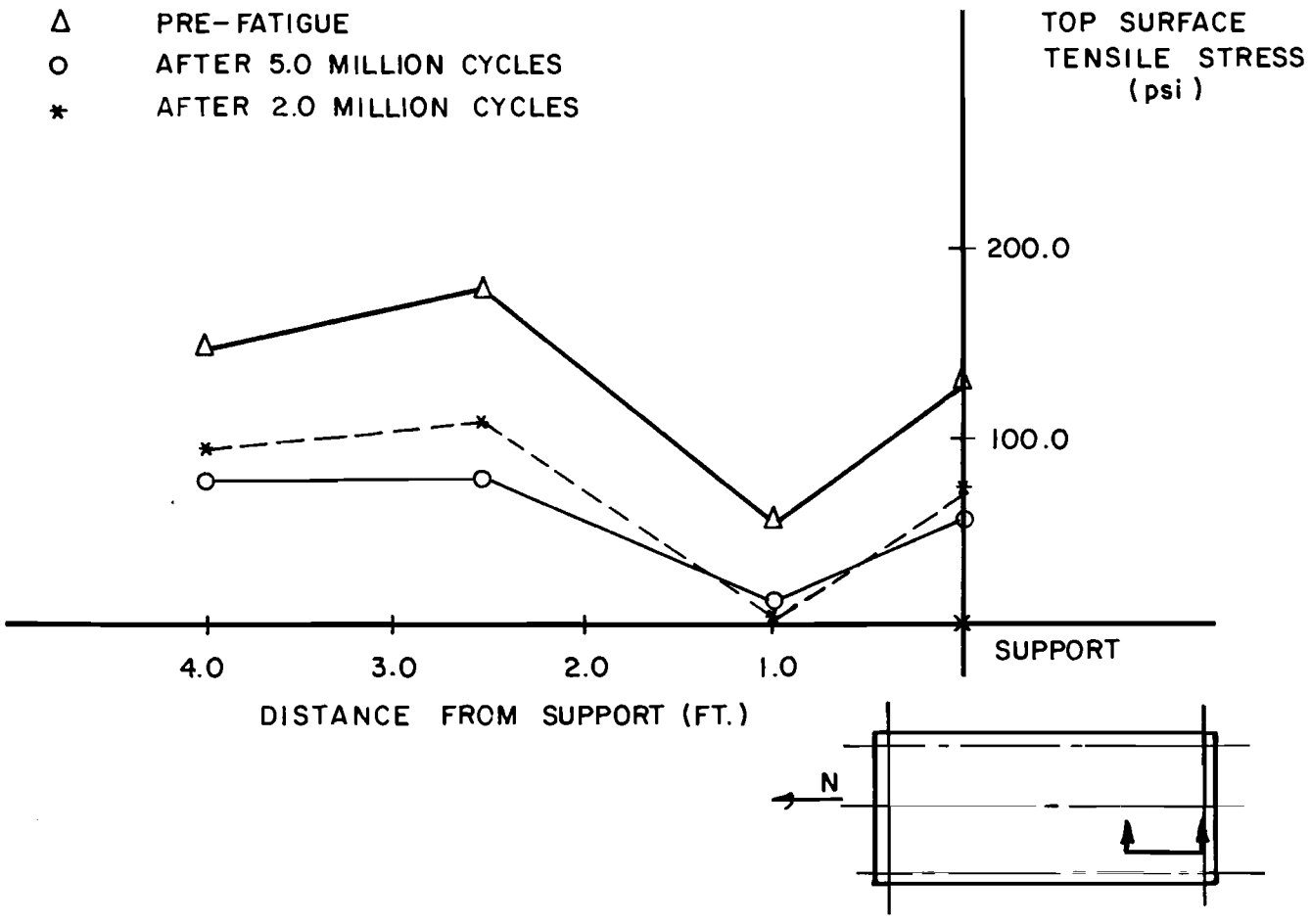

Fig. 4.5 Longitudinal concrete stress on the panel deck top surface

4.4.3 Local Stresses in Reinforcement. The experimental results illustrated that the stresses in the reinforcement before and after the fatigue test generally differed very slightly. However, the highest stress in the reinforcement in the panel deck was 9.8 ksi, which was almost 2 times the highest stress of reinforcement in the CIP deck. These highest stresses in reinforcement were detected at the two locations which were symmetrical to the centerline of the bridge. Cracks on the top surface of the deck were recorded at both locations. The presence of these cracks is believed to have increased these recorded stresses tremendously, since the stresses in the reinforcement at nearby locations where cracks were not detected were only about 1.0 ksi. The difference between the highest stress in the reinforcement at the panel end and the CIP end was due to the effect of a panel gap lying exactly underneath the reinforcement, where the highest reinforcement stress of the panel end was recorded.

4.4.4 Local Stresses on the Girders. Local stresses in the top and bottom flanges of the east exterior girder, and in the interior girder at the supports, under a load of 26 kips per ram, are summarized in Table 4.1. For the exterior girder, the change in either the tensile or compressive stresses was quite small.

For the interior girder, changes in the tensile stresses were small, but changes in the compressive stresses were comparatively large. This suggests that the reduction in deck stiffness caused by fatigue loading is more significant for the interior girder than for the exterior one. This is reasonable because the negative bending moment at the support was higher at the interior girder than the exterior one, because of the loading setup. Stresses at the top flange of the interior girder changed less as compared to the bottom flange, because the top flange was located closer to the neutral axis of the composite girder.

Using beam theory with cracked section and uncracked section properties from other studies (4), calculations were carried out for both the interior girder and exterior girder. All the experimental values were above the corresponding values for the uncracked section, and below the ones for the completely cracked section. This showed all the girders were behaving in the partially cracked mode at a load of 26 kips per ram.

The pre-fatigue and post-fatigue results at other locations showed that the changes were within 2-3 percent. This indicates the moments from the fatigue loading had very little effect on the deck-girder composite section at these locations.

Table 4.1 Stresses on Girders at Supports

		N, CIp End				S, Panel End			
		Calculated Stress (ksi)		Measured Stresses (ksi)		Calculated Stress (ksi)		Measured Stresses (ksi)	
		Uncracked Section	Cracked Section	Pre-Fatigue	Post-Fatigue	Uncracked Section	Cracked Section	Pre-Fatigue	Post-Fatigue
Interior Girder	Top Flange (Tensile)	0.33	5.17	----	----	0.32	6.67	1.722	1.828
	Bottom Flange (Comp.)	3.59	5.17	4.05	4.651	4.56	6.67	4.907[1]	5.344
Exterior Girder	Top Flange (Tensile)	0.15	2.29	0.76	0.84	0.11	2.42	0.38	0.52
	Bottom Flange (Comp.)	1.58	2.29	----	-----	1.66	2.42	1.44	1.46

CHAPTER 5

DISCUSSION OF RESULTS FOR NEGATIVE MOMENT TEST

5.1 Analysis of Test Specimens

5.1.1 General. Because of the time and expense needed to build a full-sized bridge, it was considered important, from the very beginning of this project, to develop analysis procedures for computing the response of the whole bridge. As a result, a computer model was developed for the SAP IV program (48) to simulate the bridge test specimen. This section is intended to discuss the comparison of the analytical prediction from the SAP IV output and the experimental results.

5.1.2 Analytical Procedure and Modeling: Original Mesh and Model

The details of the computational procedure and the original computer model are discussed and verified in a report for another investigation in the first phase of this project (3). Basically, the nonlinear response of the bridge was calculated as a sequence of linear elastic analyses.

The deck was modelled using two layers of 16-node thick shell elements to simulate the possible cracking of the deck. The composite action of the deck slab and girder was modelled by using a combination of the thick shell elements and three-dimensional beam elements, shown schematically in Fig 5.1. The beam elements were then connected to the thick shell elements at the corresponding nodal points using rigid links, satisfying the typical beam bending assumption of plane sections.

The real bridge, having one end cast-in-place and the other with precast panel, is not symmetrical in the north-south (longitudinal) direction. To model such a bridge specimen, different material properties, geometric configuration and prestressing force should be used for the northern and southern halves of the bridge. Even taking advantage of transverse symmetry, half of the bridge needs to be modelled. To reduce computational effort, two types of bridge model (CIP and precast panel) were developed individually. Because the idealized bridge was symmetric in both directions, each model could consist of only a quarter of the bridge, with appropriate boundary conditions. However, it was found that the results from analysis with these two models were quite close. Theefore, he simpler one of these two models, the CIP one, was adopted in this study (Fig. 5.2).

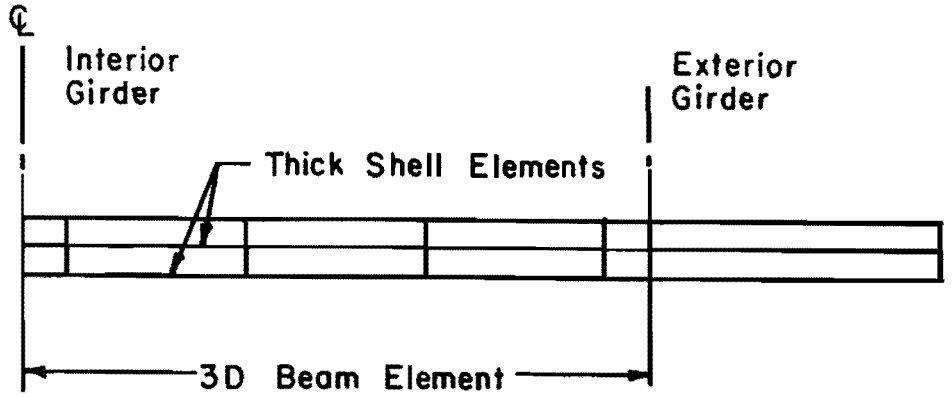

Fig. 5.1(a) Transverse section of bridge model

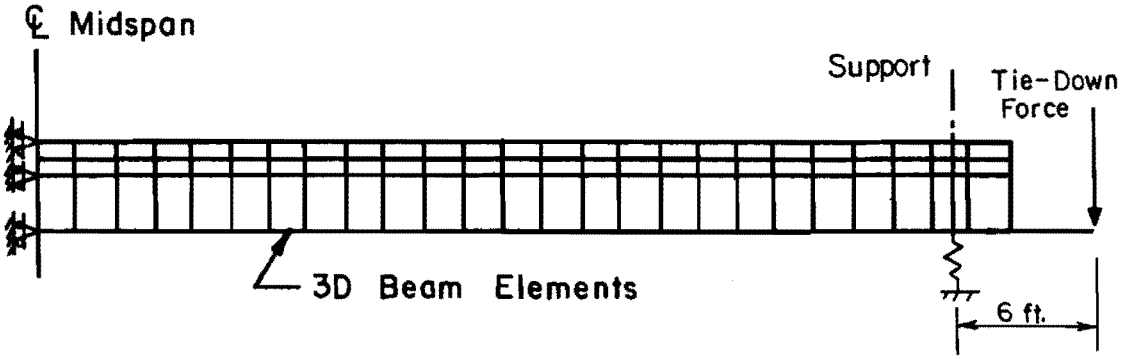

Fig. 5.1(b) Longitudinal section of bridge model

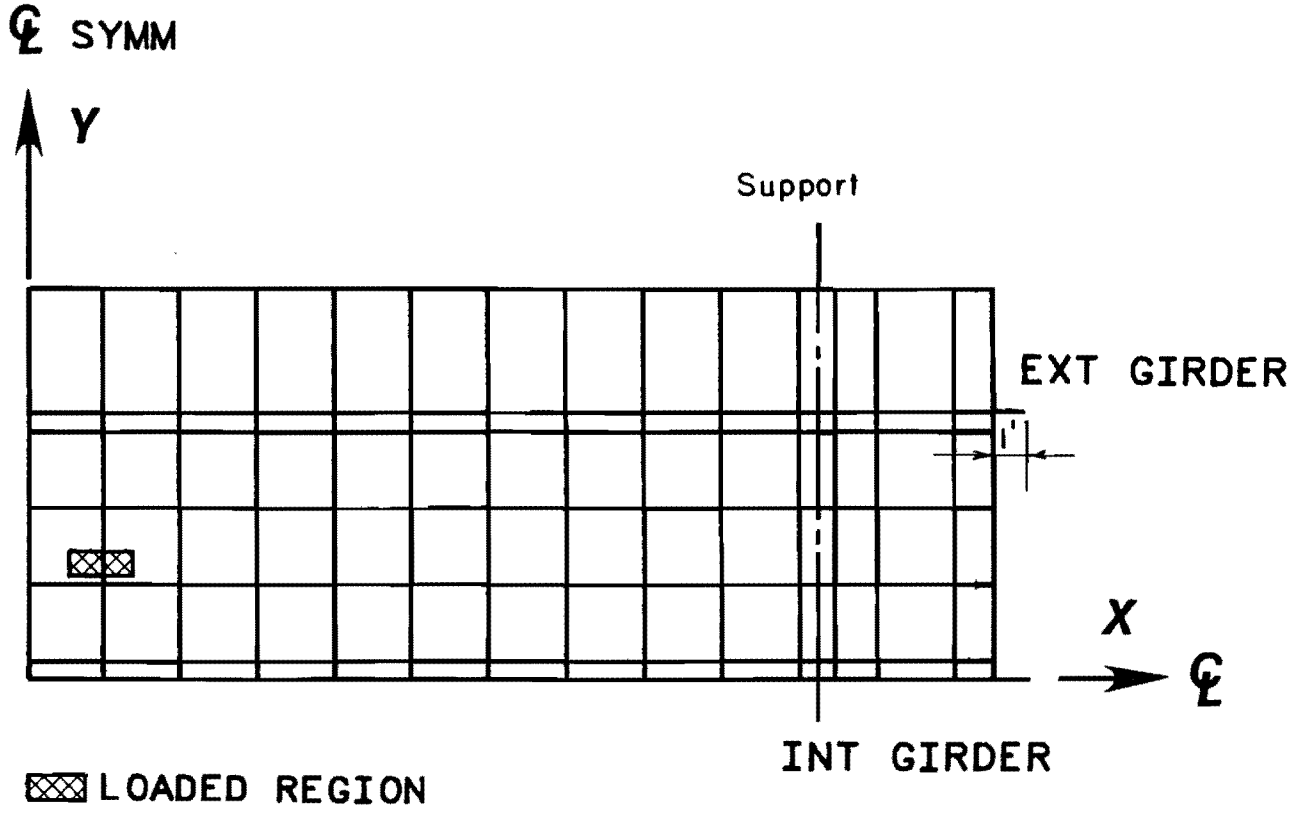

Fig. 5.2 Finite element mesh of quarter bridge specimen

The end and intermediate diaphragms were modelled using two three-dimensional beam elements. The neoprene pads at the supports were modelled using axial springs.

Modification of the Original Mesh and Model

Due to the differences in the loading setup, support location and the cracking condition between this test and the previous test in this project, some modifications were required to the original computer model and mesh.

1. One beam element was added at the end of each of the interior and exterior girders (Figs. 5.1 and 5.2), to simulate the real location of the tie-down loads;

2. A row of 6-in. wide thick shell elements was used for both the top and bottom layers of deck elements above the supports. The centerline of these elements was exactly above the support lines. The longitudinal dimensions of the elements at the overhang, and adjacent to the row of 6-in. elements at the interior span, were also adjusted;

3. All 6-in. elements on the top layer of the deck were treated as cracked when their properties were input. Because of the stress distribution on the concrete deck of a composite girder subjected to negative moment, two of the bottom layer elements lying above the interior and exterior girder were also assumed cracked. All cracks were defined to be parallel to the support line, consistent with the cracking orientation observed during the test;

4. The intermediate diaphragm was removed from the bridge model, since the corresponding real diaphragm broke early in the test; and

5. A new stiffness was adopted for the axial springs simulating the neoprene pad at each support. The spring stiffnesses were derived from the experimental data of previous tests in this project (3). These new stiffness values are closer to the real condition of the pads.

Load Input

Two kinds of loading were needed:

1. Ram Loading. Analyses were carried out using a combination of concentrated nodal loads to simulate the actual distributed load from the loading plate (Fig. 5.3); and

2. Tie-Down Loads. Two different tie-down forces were applied on the end of each of the additional beam elements. These

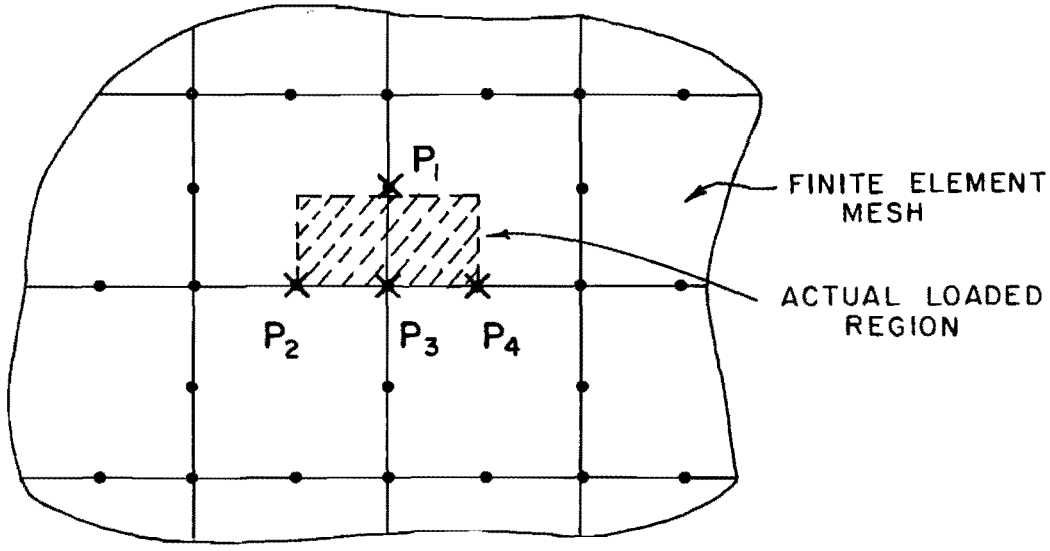

26 - Kip Total Load

X : Equivalent Concentrated Load

P_1 = 13 Kips ; P_3 = 6.5 Kips ; P_2 = 3.25 Kips ; P_4 = 3.25 Kips

Fig. 5.3 Equivalent concentrated loads for loaded region

two tie-down forces were derived from a static analysis of the tie-down channels which served as load spreaders across the overhangs at the end of the bridge. The loads on the channels were obtained from the readings of the load cell on each of the tie-down rods.

5.2 Comparison of Analytical and Experimental Results

5.2.1 Deflections. Table 5.1 compares the predicted and observed deflections of the girders at various locations. The experimental values were from the final static test, after the fatigue testing was completed. As shown in Table 5.1, the analysis predicted deflections to within 3 to 24 percent of the test results. The prediction was apparently better for the exterior than for the interior girder. The deflections were very small, and were therefore significantly affected by the stiffnesses assumed for the axial springs simulating the neoprene pads at supports. The analytical model generally overestimated the deflections of the girders except at the midspan section of the interior girder. However, considering the small magnitude of the deflections, the analytical results agreed quite well with the experimental values. The good agreement indicated that the SAP IV analytical model is a realistic model for simulation of the real structure in overall behavior.

5.2.2 Local Stresses on the Deck. Analytical and experimental stress distributions at various sections are compared in Figs. 5.4 through 5.9). Figs. 5.4 and 5.5 predicted stresses at the top surface of the deck, along the top of the exterior girder, are compared with the pre-fatigue and post-fatigue experimental values for CIP and panel decks. In both decks, the curve from analysis was closer to the pre-fatigue experimental curve than to the post-fatigue one. In Figures 5.6 and 5.7, predicted stresses on the top surface of the deck along the top of the interior girder are compared with the corresponding pre-fatigue and post-fatigue experimental results at the CIP and panel ends. These curves show the same trend observed for the exterior girder.

In Figs. 5.8 and 5.9, predicted stresses on the top surface of the deck, along the centerline between the interior and exterior girder, are plotted against the pre-fatigue and post-fatigue experimental results for the CIP deck and panel deck. For both the CIP and panel decks, the analytical curve was closer to the post-fatigue experimental curve than to the pre-fatigue one, a trend which is opposite to those previously noted for the top of the girders. This can be explained by the fact that in the composite action of a deck slab and girder under negative moment, the tensile stress on the deck is highest above the top flange of the girder, and decreases away from the flange. The degree of the cracking at any point on the deck depends on the magnitude of the tensile stress at that point. This implies that the deck at the middle between the 2 girders in this project

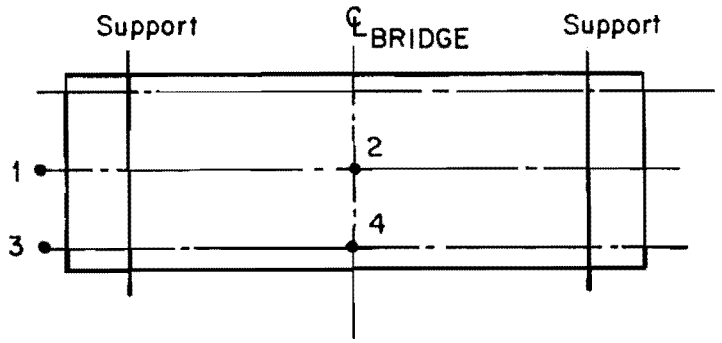

Location	Description	Deflection(in.)	
		Experimental	Analytical
1	overhang, interior girder	0.037	0.049
2	mid-span, interior girder	0.129	0.107
3	overhang exterior girder	0.025	0.029
4	mid-span, exterior girder	0.064	0.066

Table 5.1 Analytical and experimental deflection results of girders.

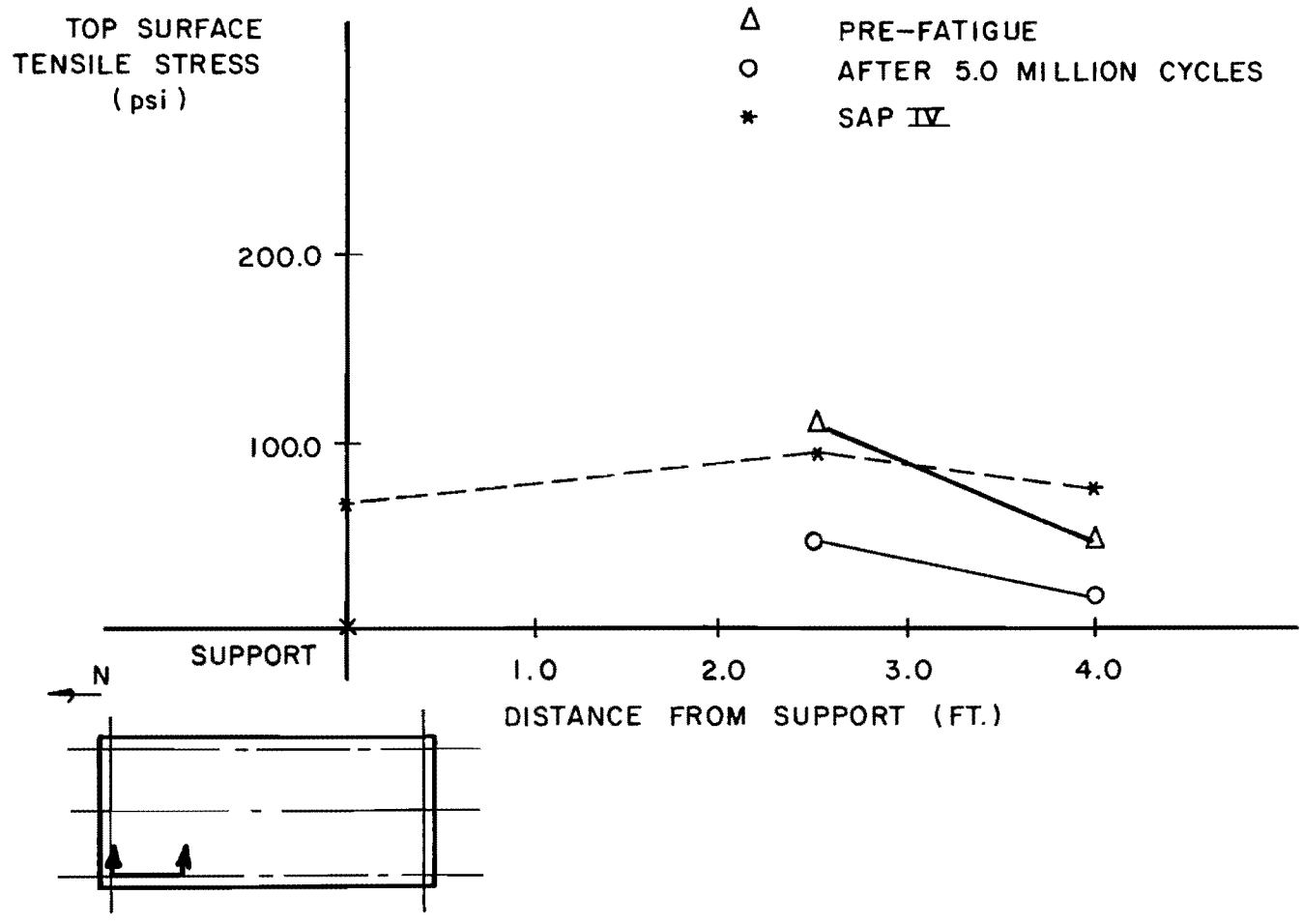

Fig. 5.4 Longitudinal concrete stress on deck top surface above exterior girder (CIP)

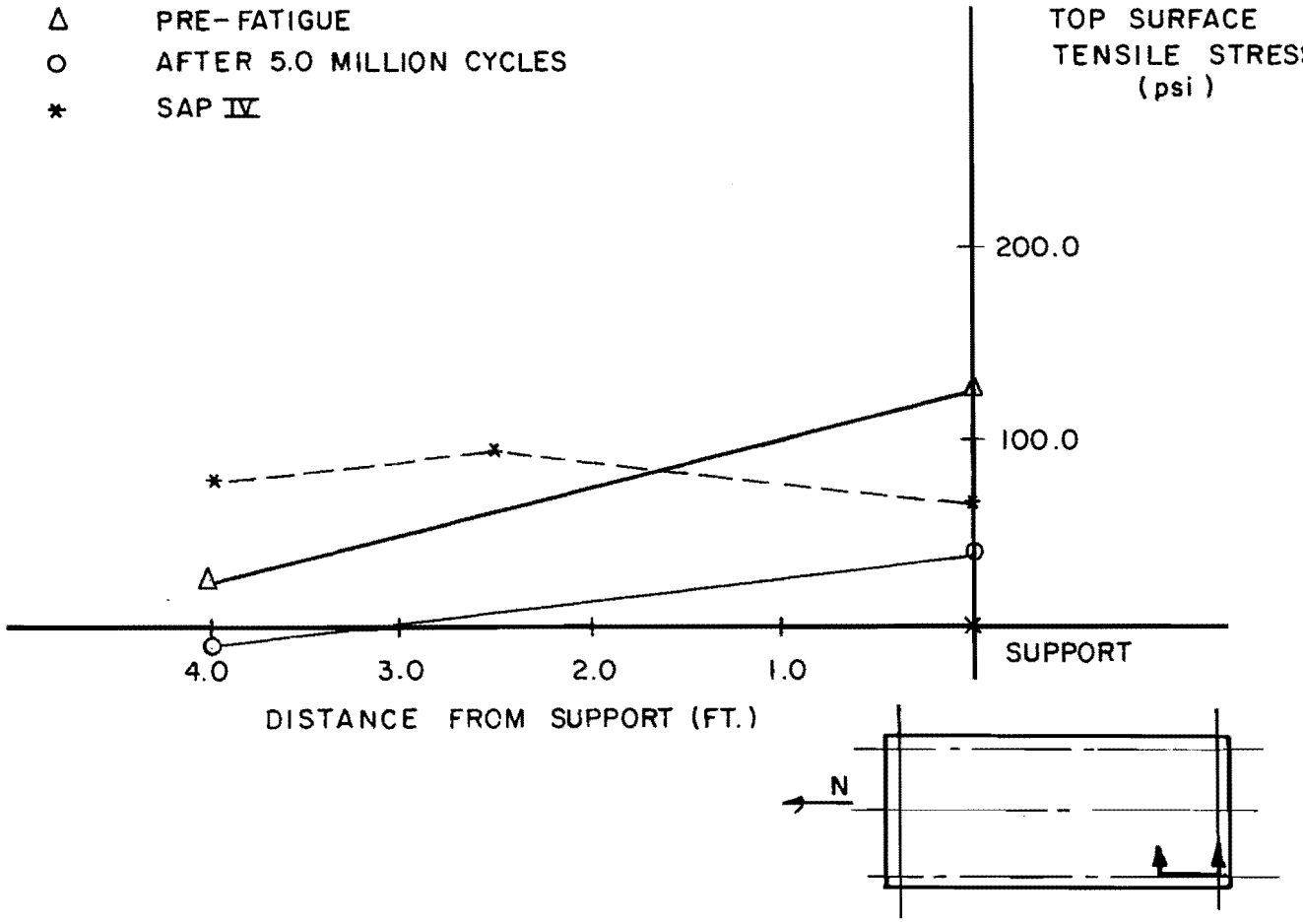

Fig. 5.5 Longitudinal concrete stress on deck top surface above exterior girder (panel)

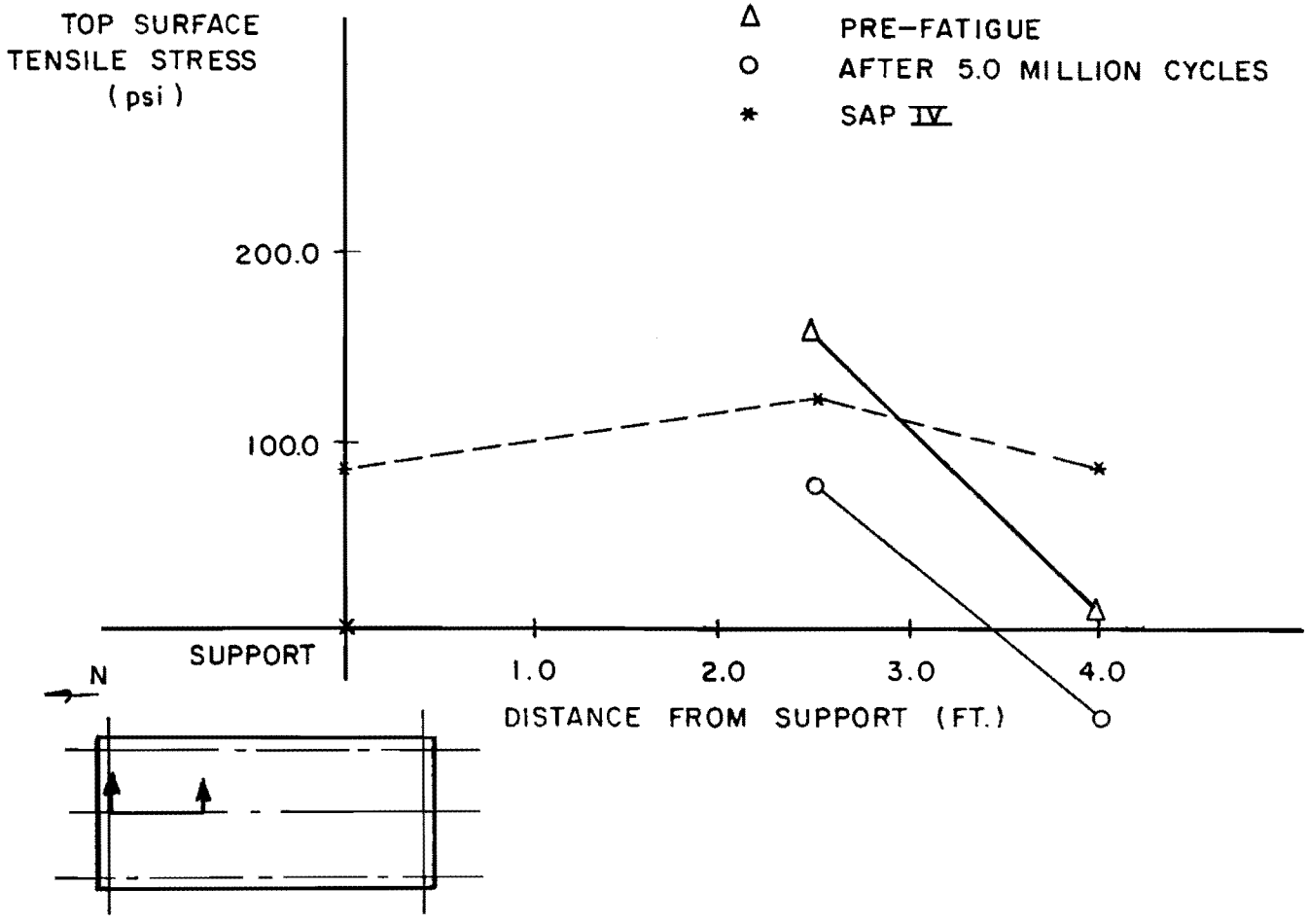

Fig. 5.6 Longitudinal concrete stress on deck top surface above interior girder (CIP)

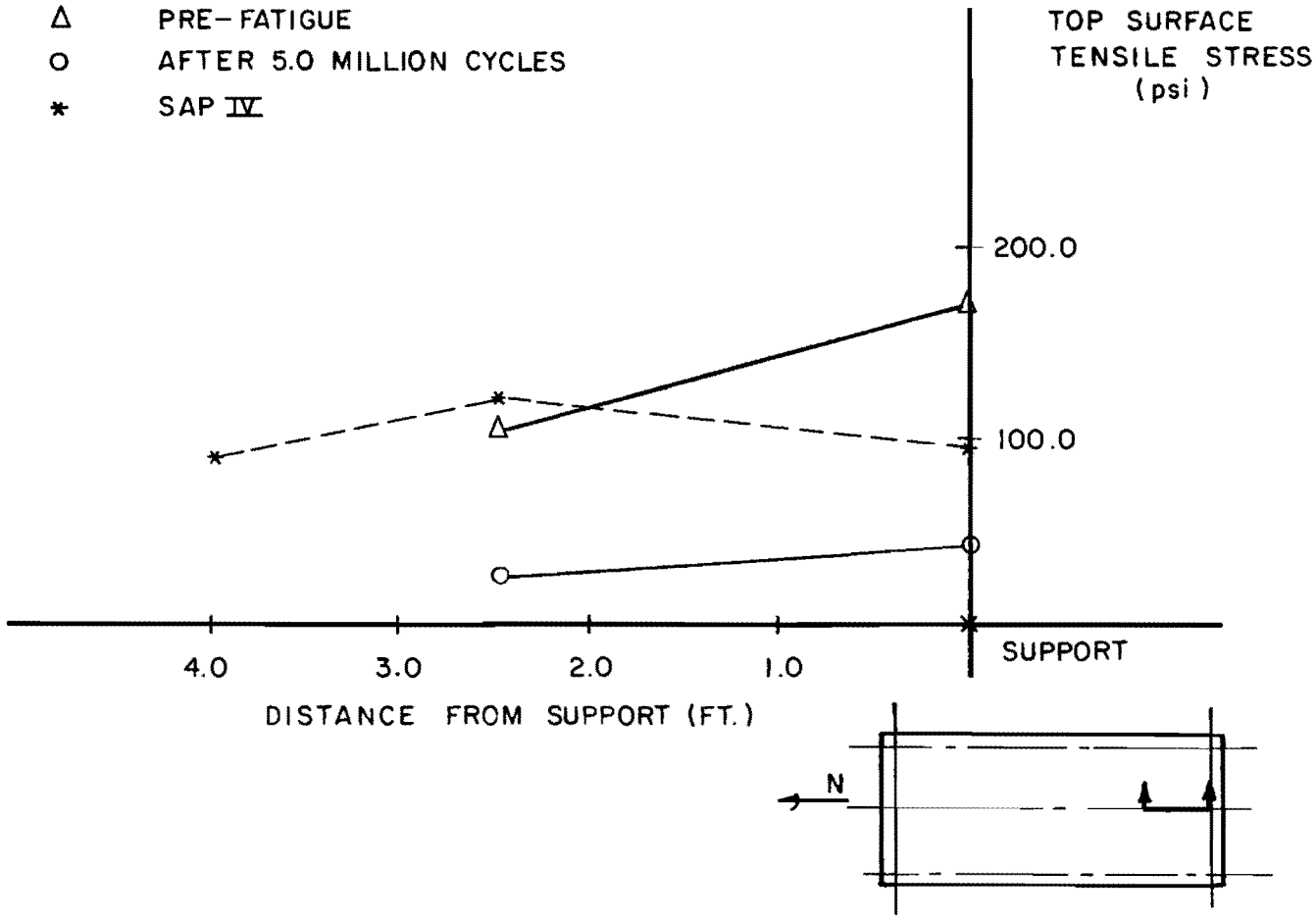

Fig. 5.7 Longitudinal concrete stress on deck top surface above interior girder (panel)

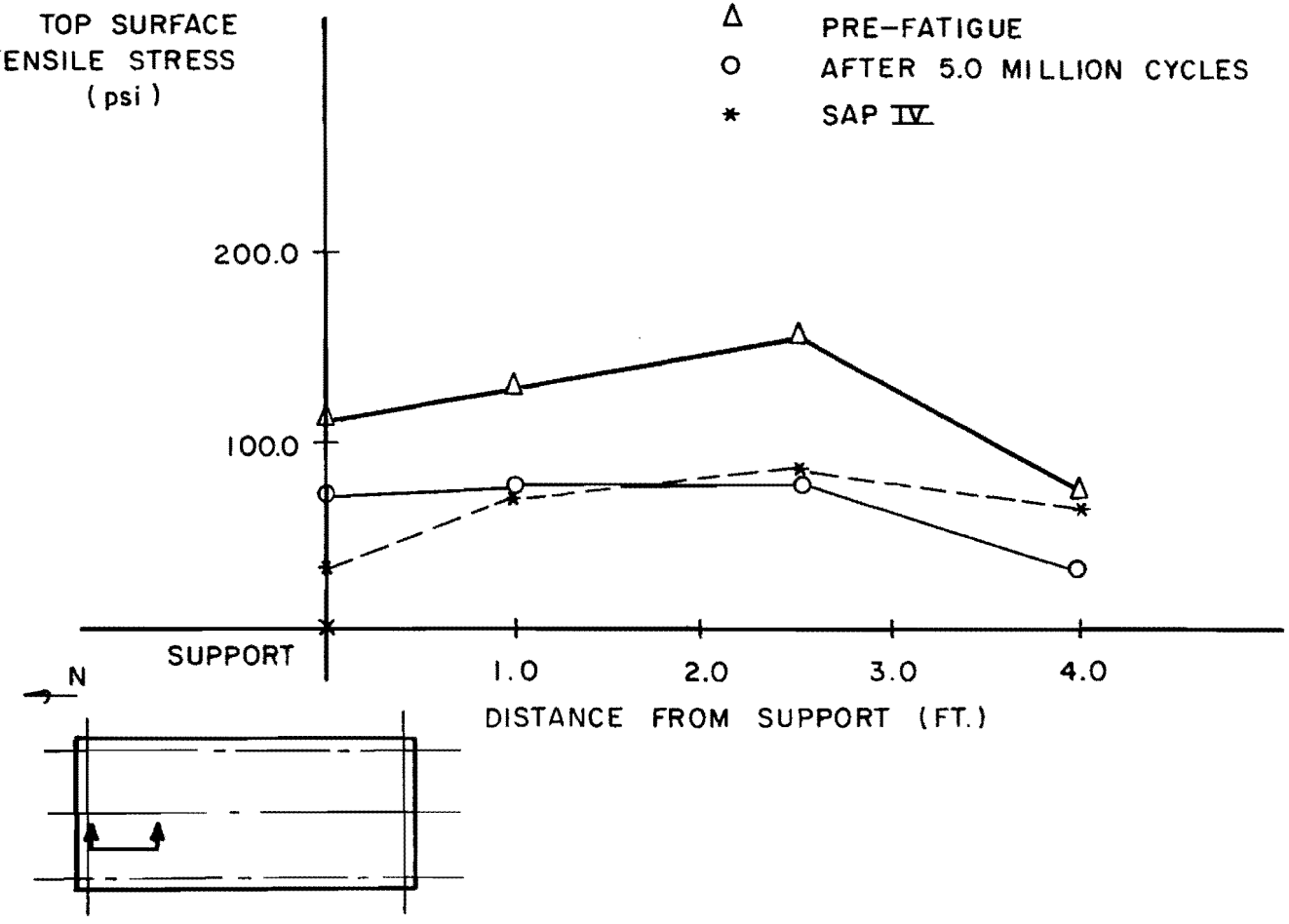

Fig. 5.8 Longitudinal concrete stress on deck top surface between girders (CIP)

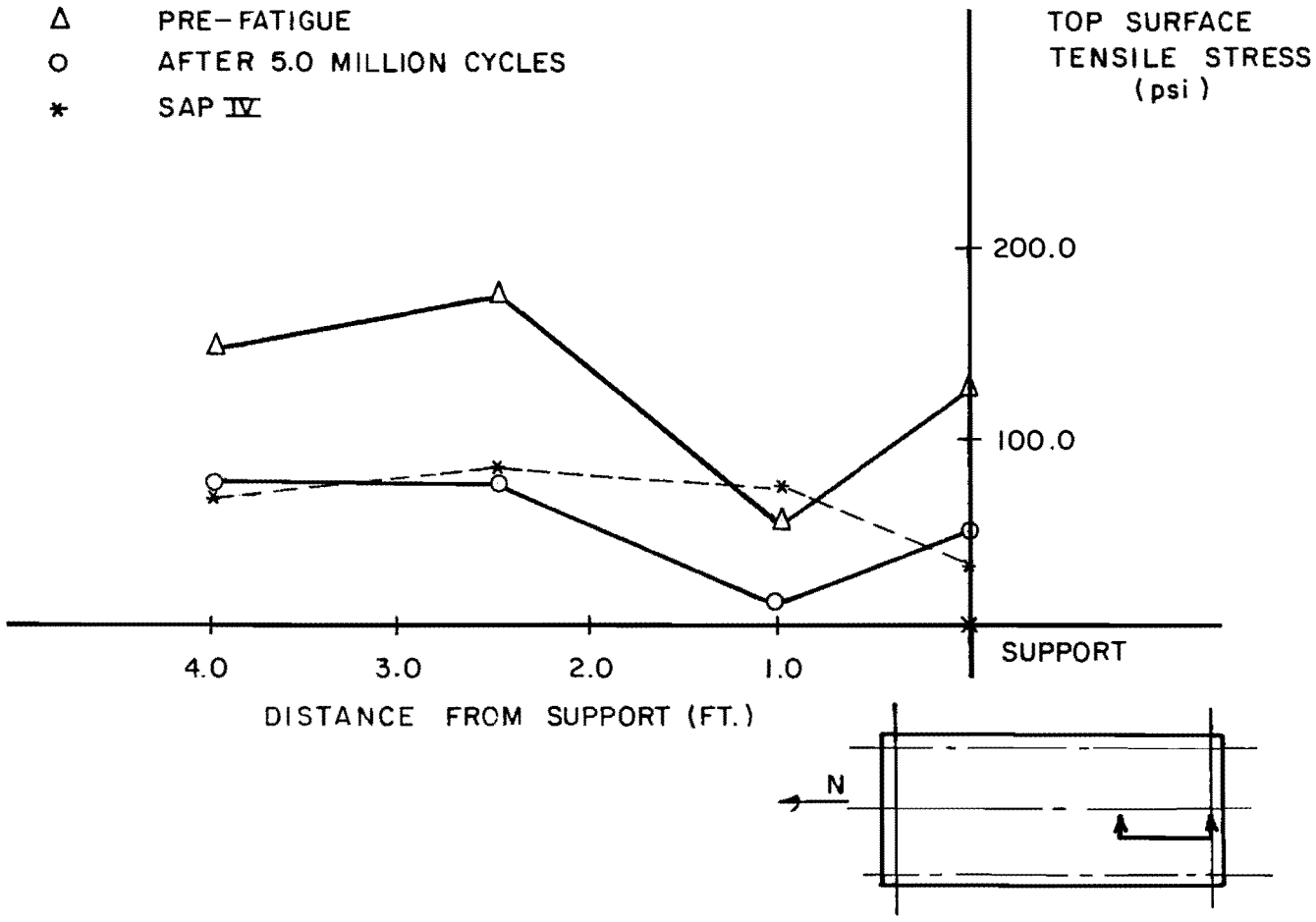

Fig. 5.9 Longitudinal concrete stress in deck top surface between girders (panel)

experienced less cracking than the part of deck exactly above the top flange of the girders. Therefore, after the preloading stage, which was intended to crack the deck along the support line, the cracks at the region of the deck above the girder were more fully developed than those on the deck halfway between the girders.

The analytical model assumed that all the top layer elements in the deck were fully cracked above the support lines. Consequently, for the pre-fatigue static test carried out shortly after preloading, the analytical model predicted better for the local stresses at the region of the deck above the girders, than at the region of the deck between the girders. However, for the static test after the fatigue test, the analytical model predicted quite well the stresses at the region of the deck between girders, because the cracks there were fully developed as a result of the fatigue loading. Taking into consideration the small magnitudes of all the deck stresses, the analytical model did give rather accurate predictions of the local behavior of the bridge.

CHAPTER 6

CONCENTRATED LOAD TESTS

6.1 Test Setup

The loading frame for the concentrated load is shown in Fig. 6.1. Two W8x67 beams were connected by 1-in thick plates bolted on top and bottom flanges at 4 ft apart to form the loading support. Holes were drilled in the top and bottom plates to allow the four Dywidag bars to go through and tie the loading reaction frame to the test floor. Two sets of double beams were placed 4 ft apart in parallel and transferred the reaction to a stiffened W21x67 beam. A hydraulic ram was placedn directly underneath the center of the frame for single load tests, as shown in Fig. 6.1. For the double-load tests, two rams were placed 4 ft apart under the loading frame. The four 1-in. Dywidag bars used to tie the loading frame to the laboratory structural floor slab are shown in Fig. 6.2. The ram reacted against the bridge deck; the loading frame, which was tied down to the floor, reacted against the 8"x20" steel plate footprint resting on the deck, as shown in Fig. 6.1. The oil pressure of the hydraulic ram was applied by a hydraulic hand pump. Locations for the tests are shown in Fig. 6.3.

6.2 Instrumentation

Loads. Because the effective ram area was known, the loads were monitored using a 100,000-psi pressure gage. For tests with double load points, the two rams were interconnected, and were assumed to apply equal loads.

Deflections at Loading Points. Defections were measured by a 6-in. linear potentiometer with accuracy to 0.001 in.

Cracking of the Deck. Deck cracks were color-marked at every load stage up to the failure point. Crack widths were compared with a pocket template whose smallest scale is 0.002 in. Photographs were taken to show the crack patterns and the failure surface.

6.3 Loading Procedure

In these tests, the deck was loaded to failure in about 10-kip increments. At each load stage, crack propagation and the deflections under the loading point were recorded. The loading frames were checked regularly by a carpenter's level during the test to ensure that the loads were applied vertically.

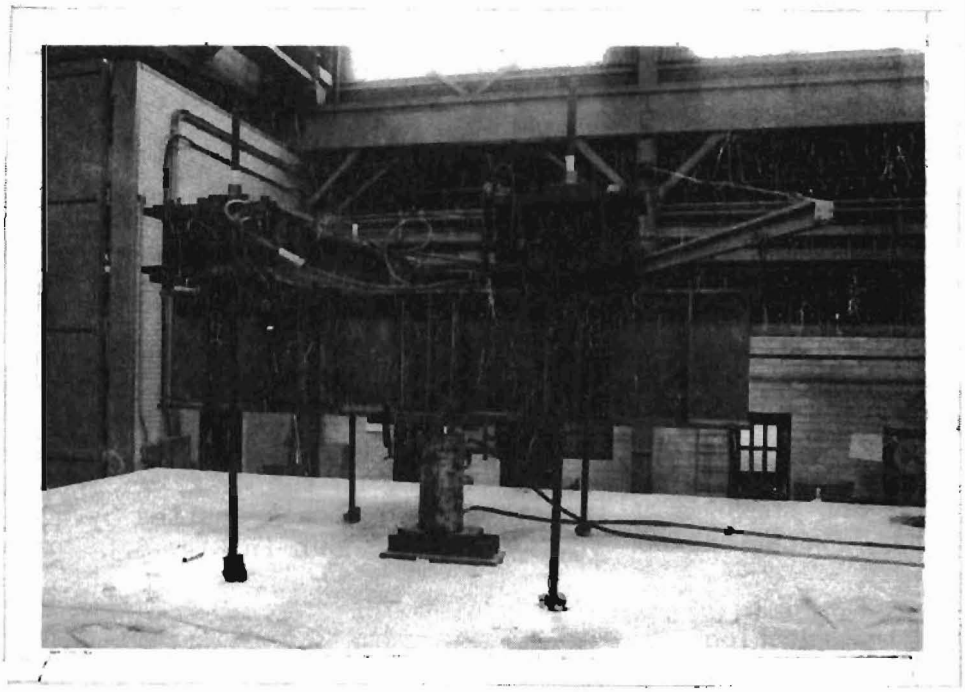

Fig. 6.1 Loading frame for concentrated load test

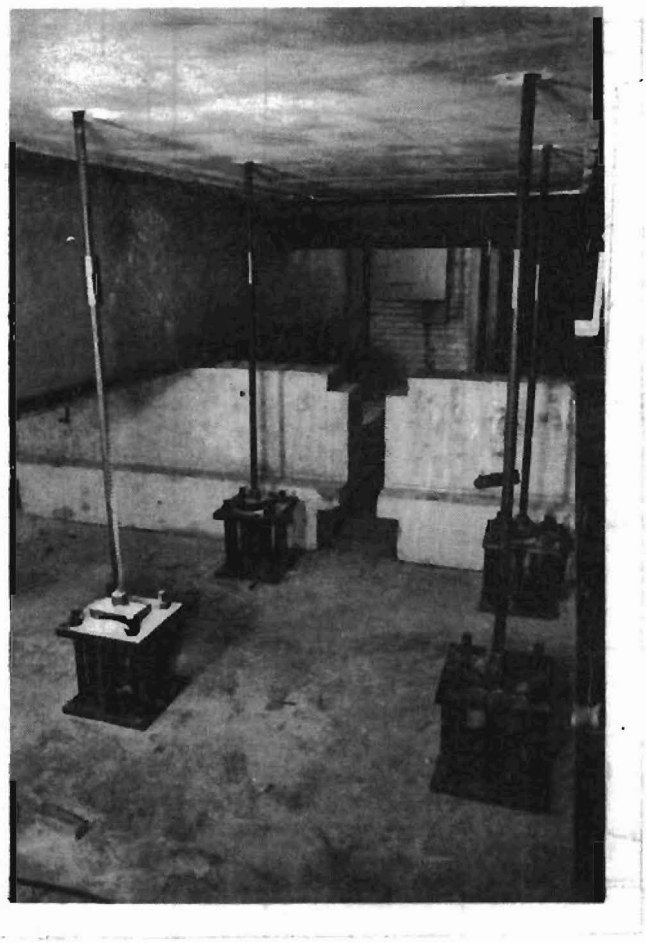

Fig. 6.2 Tiedown to test floor for loading frame

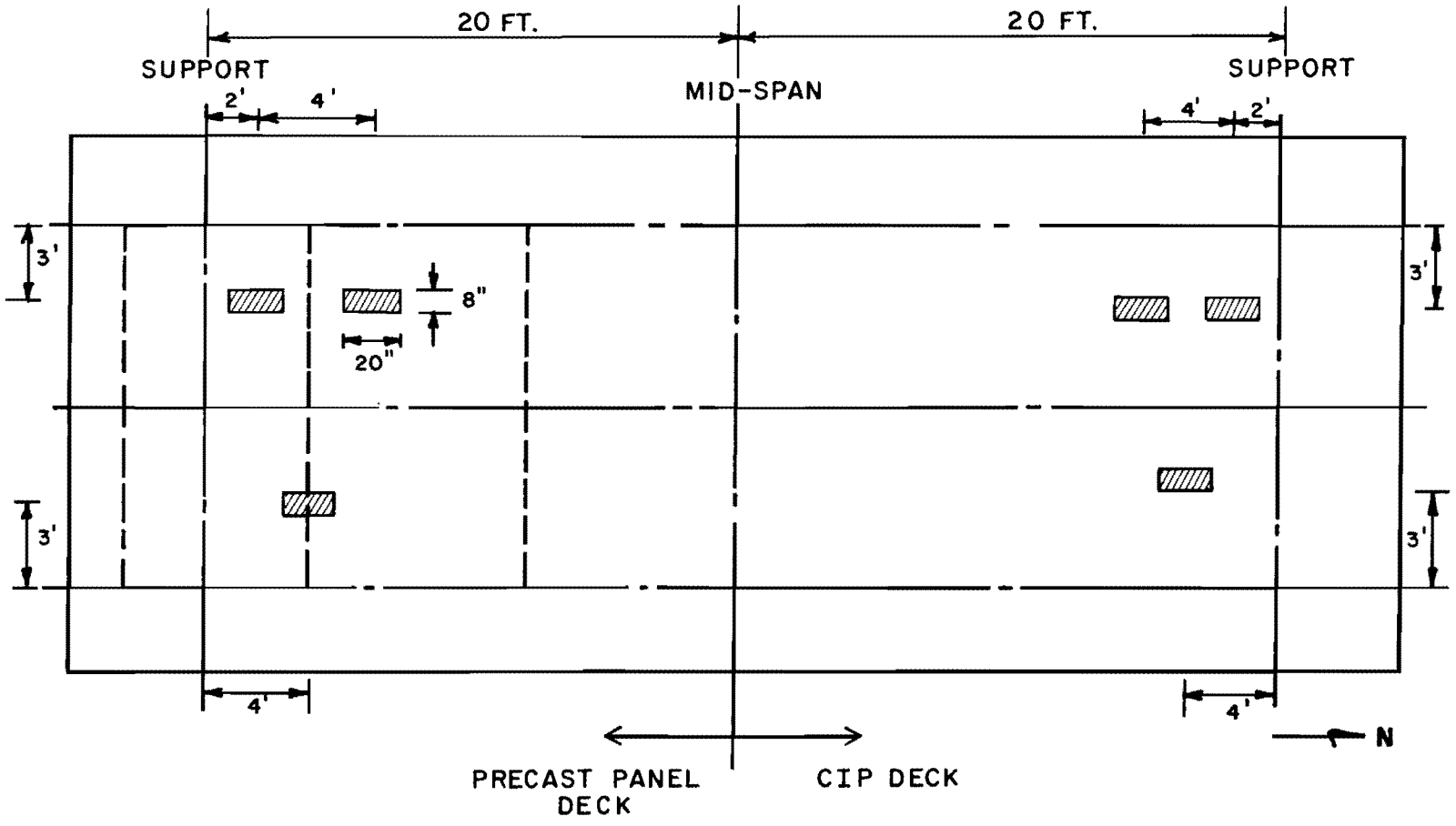

Fig. 6.3 Locations for concentrated load tests

CHAPTER 7

RESULTS OF CONCENTRATED LOAD TESTS

7.1 General

All tests were conducted in June 1985, after the test specimen had been subjected to 5 million cycles of fatigue loading and several more static tests. As discussed in Chapter 6 (Fig. 6.3), tests were carried out at 4 locations on the deck: NE, SE, NW and SW. Single-load tests were conducted at the first two locations, and double-load tests at the last two. Each test took less than two hours.

7.2 Load vs. Deflection

Figures 7.1 and 7.2 show the load vs deflection curves for the tests. All deflections were measured underneath the deck at the center point of the loading plate. Tests were designated as follows:

1. Test I-CIP: CIP deck, NE corner of the bridge, single load test, Fig. 7.1;

2. Test II-CIP: CIP deck, NW corner of the bridge, double load test, Fig. 7.1;

3. Test I-Panel: Panel deck, SE corner of the bridge, single load test, Fig. 7.2; and

4. Test II-Panel: Panel deck, SW corner of the bridge, double load test, Fig. 7.2

7.2.1 Single-Load Tests. For the CIP deck (Test I-CIP), the curve shows little nonlinearity until the load reaches 60 kips, about 3 times the service wheel load of 20.8 kips (including an impact factor). The slab failed at 142 kips, about 7 times the service wheel load. For the panel deck (Test I-Panel) the curve stays essentially linear up to a load of about 90 kips, about 4 times the service wheel load. The deck failed at 180 kips, about 9 times the service wheel load and 1.27 times the ultimate capacity of the CIP deck. The result correlated very well with similar tests by Bieschke and Klingner (47).

The load-deflection curve for the panel deck remains linear up to a higher load than that of the CIP deck, and also has a slope about 1.6 times greater. This implies that the panel deck was stiffer, due to the higher strength of concrete and the presence of prestressing strands in the precast, prestressed panel. The flexural cracking in test I-CIP was more extensive than for I-Panel, and the deflection at a

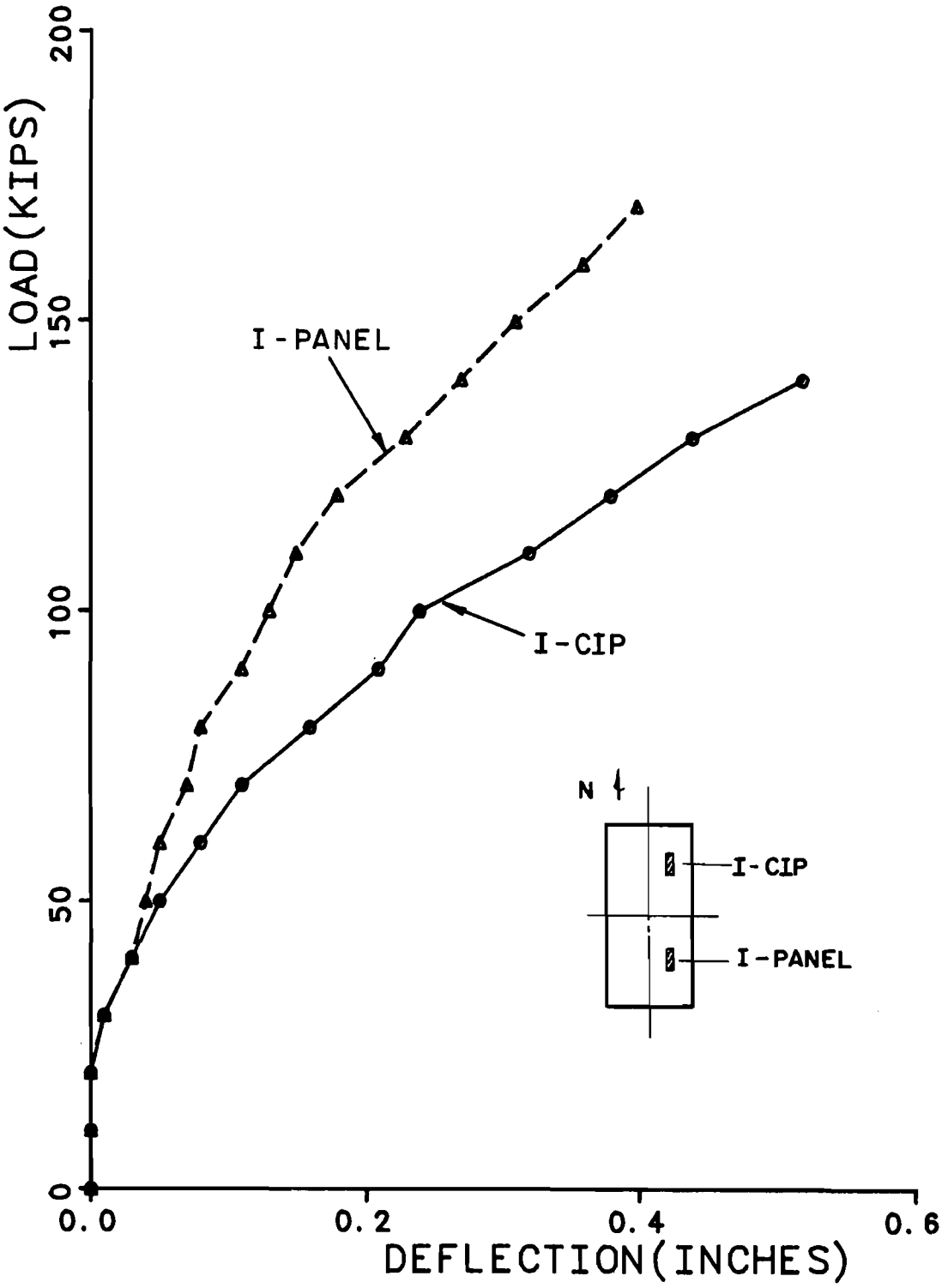

Fig. 7.1 Deflections from single load tests

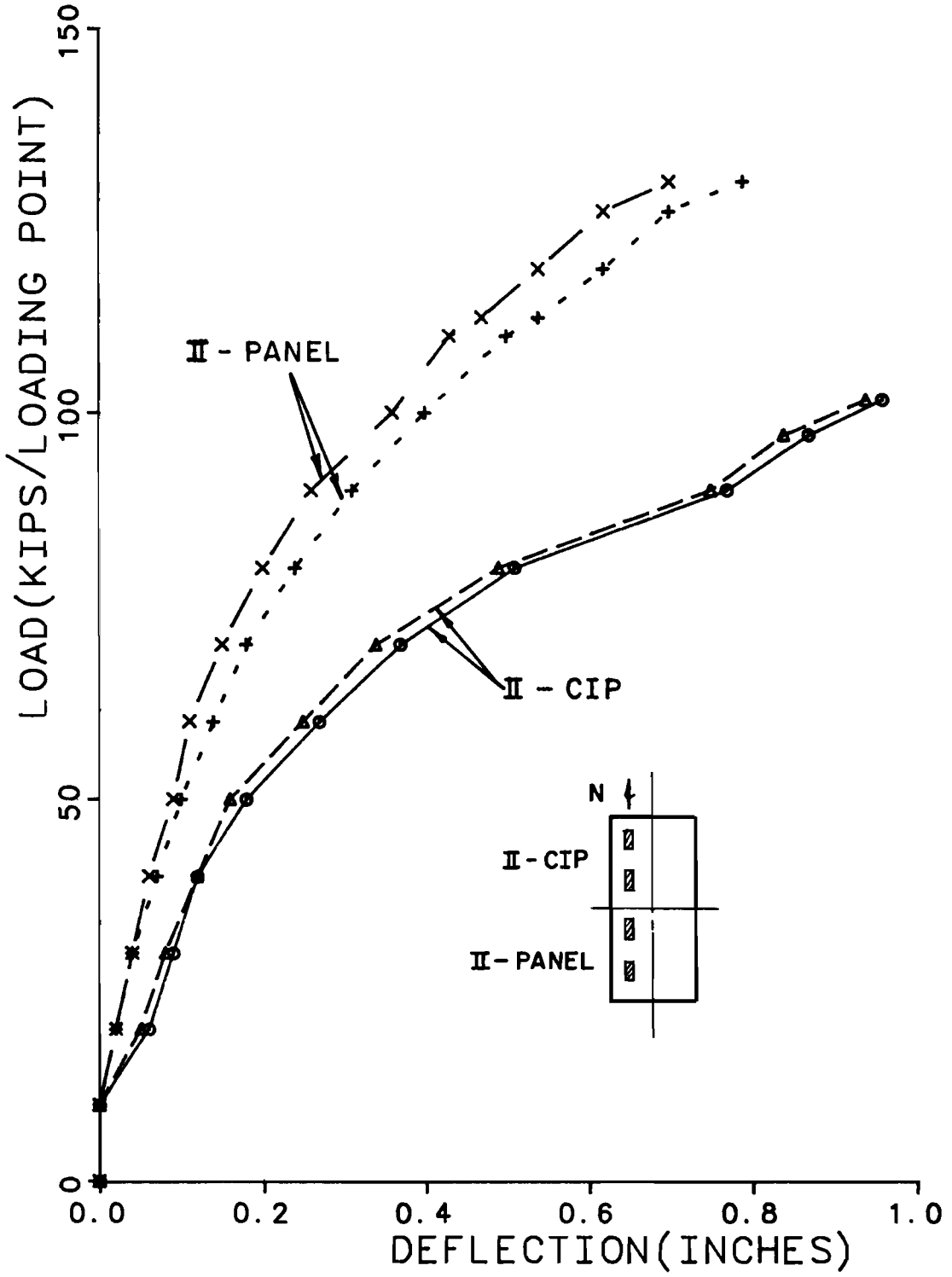

Fig. 7.2 Deflections from double load tests

given load level is thus greater for I-CIP than for I-Panel, as noted in Fig. 7.1.

7.2.2 Double-Load Tests. In both tests II-CIP and II-Panel, deflections under the two individual loading points were measured. As shown in Fig. 7.2, the load-deflection curves at the two points almost coincide. This implies that the loads from the two loading rams were almost equal, and that the orientation of the loading frame was maintained in both tests.

Once again, the curve for the panel deck (Test II-Panel) is steeper than the one for the CIP deck (Test II-Panel). The curves become nonlinear at a load of about 50 kips for the CIP deck, and about 70 kips for the panel deck. Both values are slightly lower than those for the corresponding single-load test. The CIP deck failed at a total load (both points) of about 204 kips, approximately 1.4 times the ultimate single-load capacity of the same CIP deck. The panel deck failed at a total load of 267 kips, approximately 1.5 times its ultimate single-load capacity. In both cases, the double-load capacity was less than twice the single-load capacity. This indicates that the areas affected by each loading point overlapped and interacted.

For both double-load cases, the ratio of the failure load for the panel deck (II-Panel) to that of the CIP-deck (II-CIP) is 1.28, very close to the corresponding ratio for the single-load case. This good correlation shows the homogeneity of the deck material and the consistency of the loading setup.

7.3 Cracking Patterns in Deck

Figures 7.3, 7.4, 7.5 and 7.6 show the crack patterns in the deck following all four concentrated load tests. Crack propagation was monitored carefully at each load stage during the tests.

7.3.1 Single Load Tests: I-CIP and I-Panel. The first crack at the bottom suface of the CIP deck (NE) was observed right at the loading point, at a load of 30 kips. As load increased, the cracks propagated longitudinally and reached the top flange of the girders, as shown in Fig. 7.3. The first top-surface crack, 3.5 ft away from the loading point, was recorded at a load of 90 kips. The top cracks propagated much more slowly than the bottom ones. Failure occurred by punching shear. The intersection of the failure surface with the top of the deck ws in the form of a rectangle around the perimeter of the loading plate. For the panel deck (Test I-Panel), the first crack was observed at the bottom surface right at the load point, at a load of 60 kips. The top surface crack, which first formed at 140 kips, was about 3.5 ft from the center of the loading ptate. These cracks propagated much more slowly and much less than those in the CIP deck, as shown in Fig. 7.4. Failure again occurred by punching shear, in a very similar manner to the CIP deck (Test I-CIP). In both cases, the

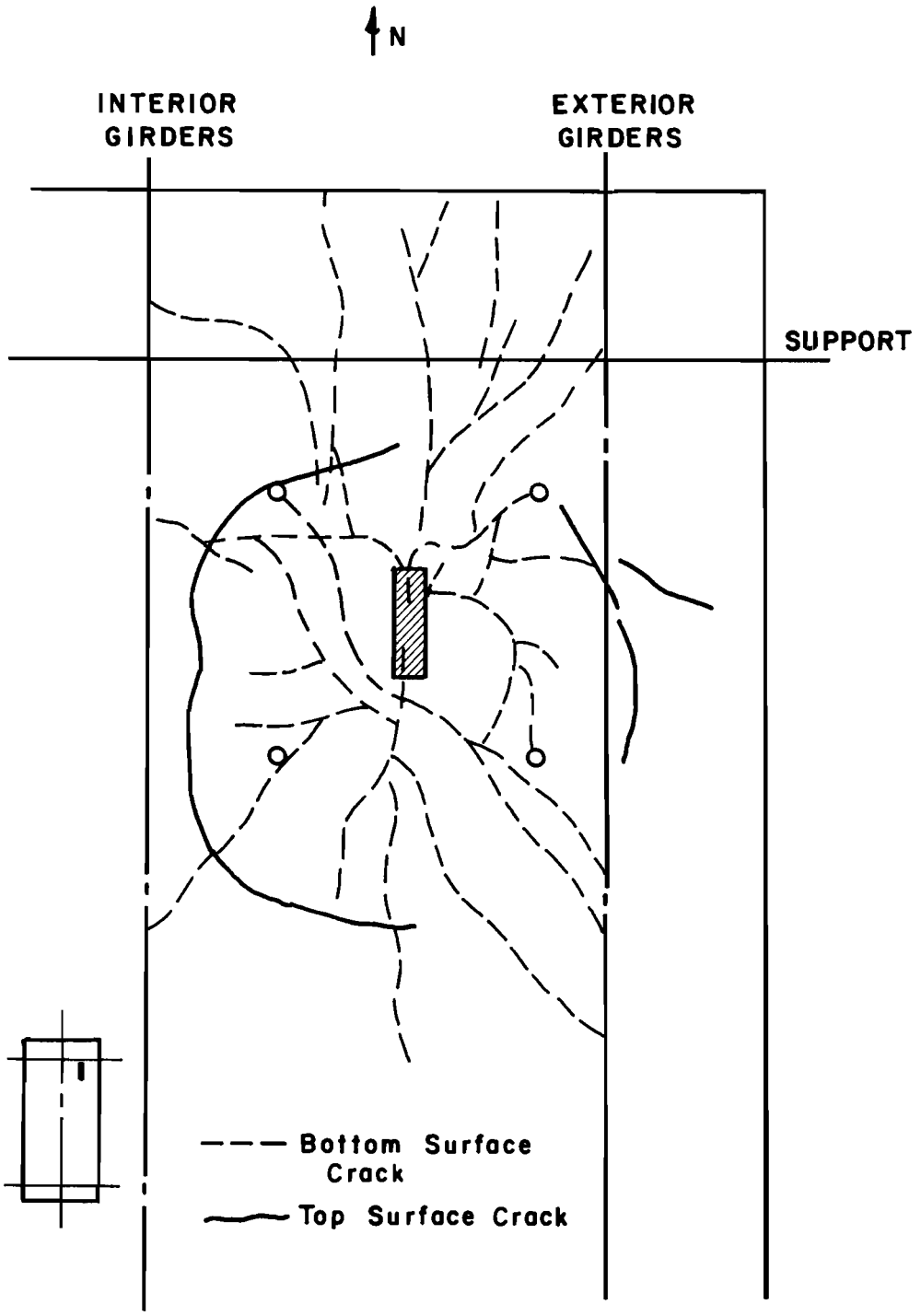

Fig. 7.3 Deck cracking from single load test I-CIP

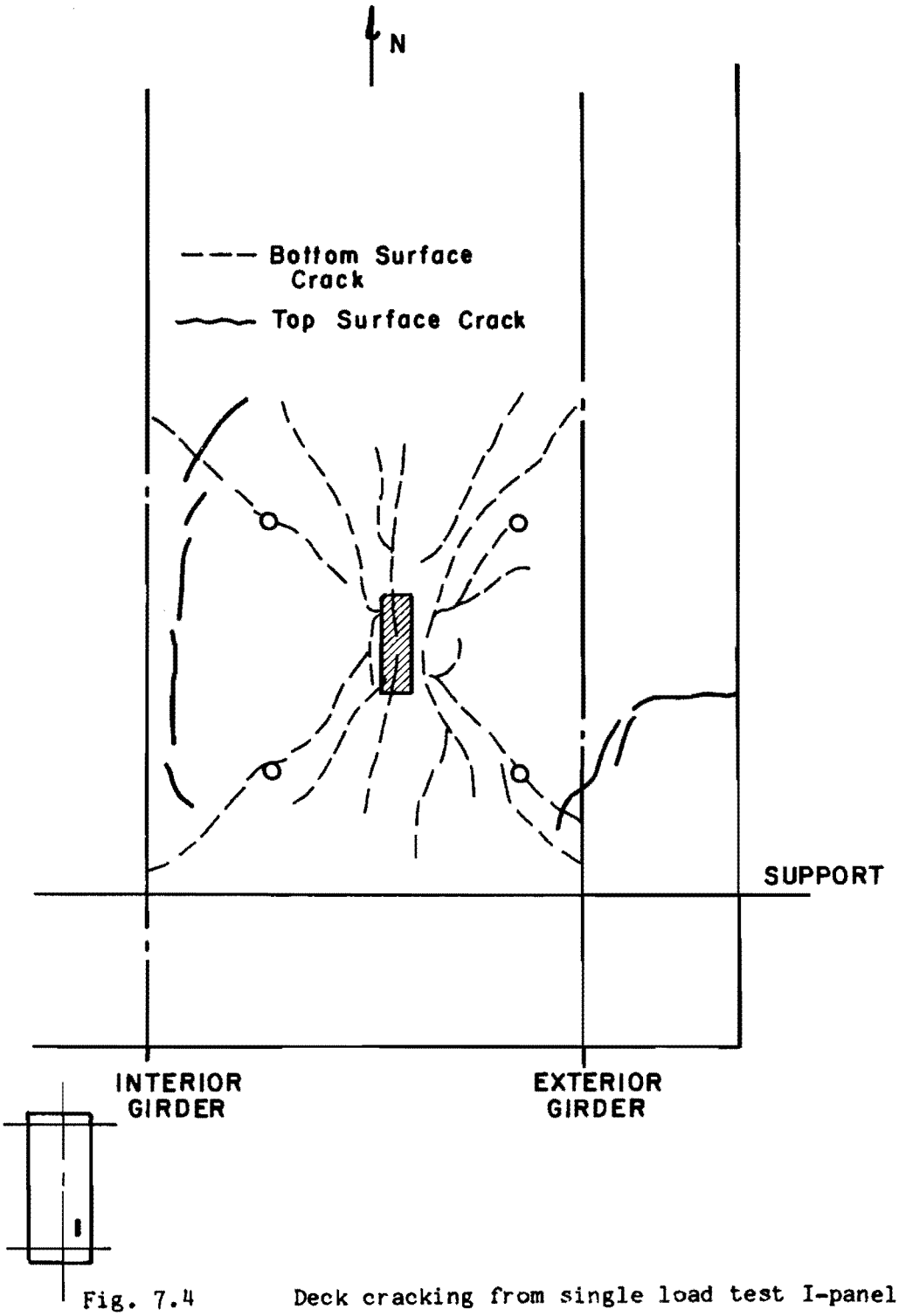

Fig. 7.4 Deck cracking from single load test I-panel

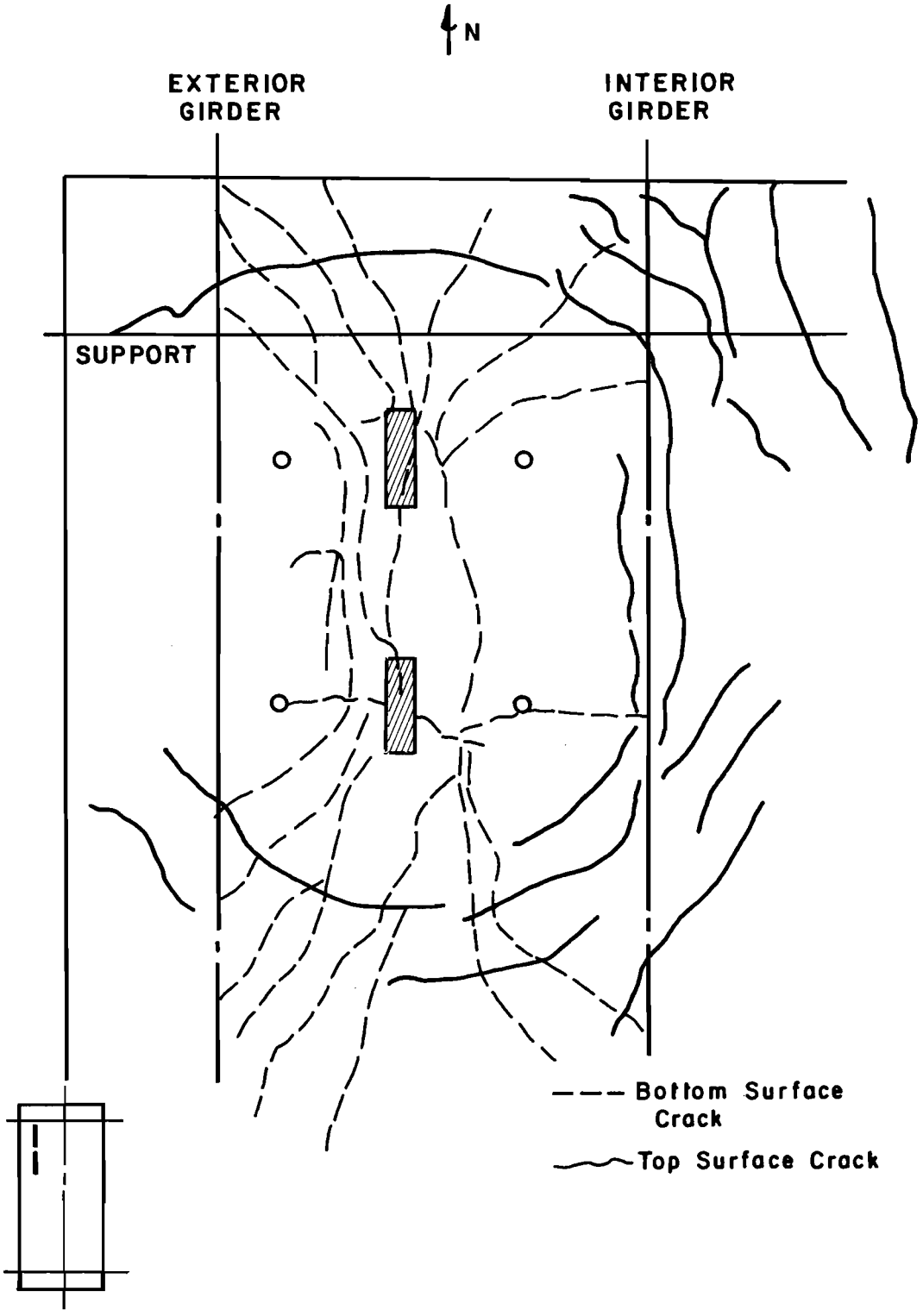

Fig. 7.5 Deck cracking from double load test II-CIP

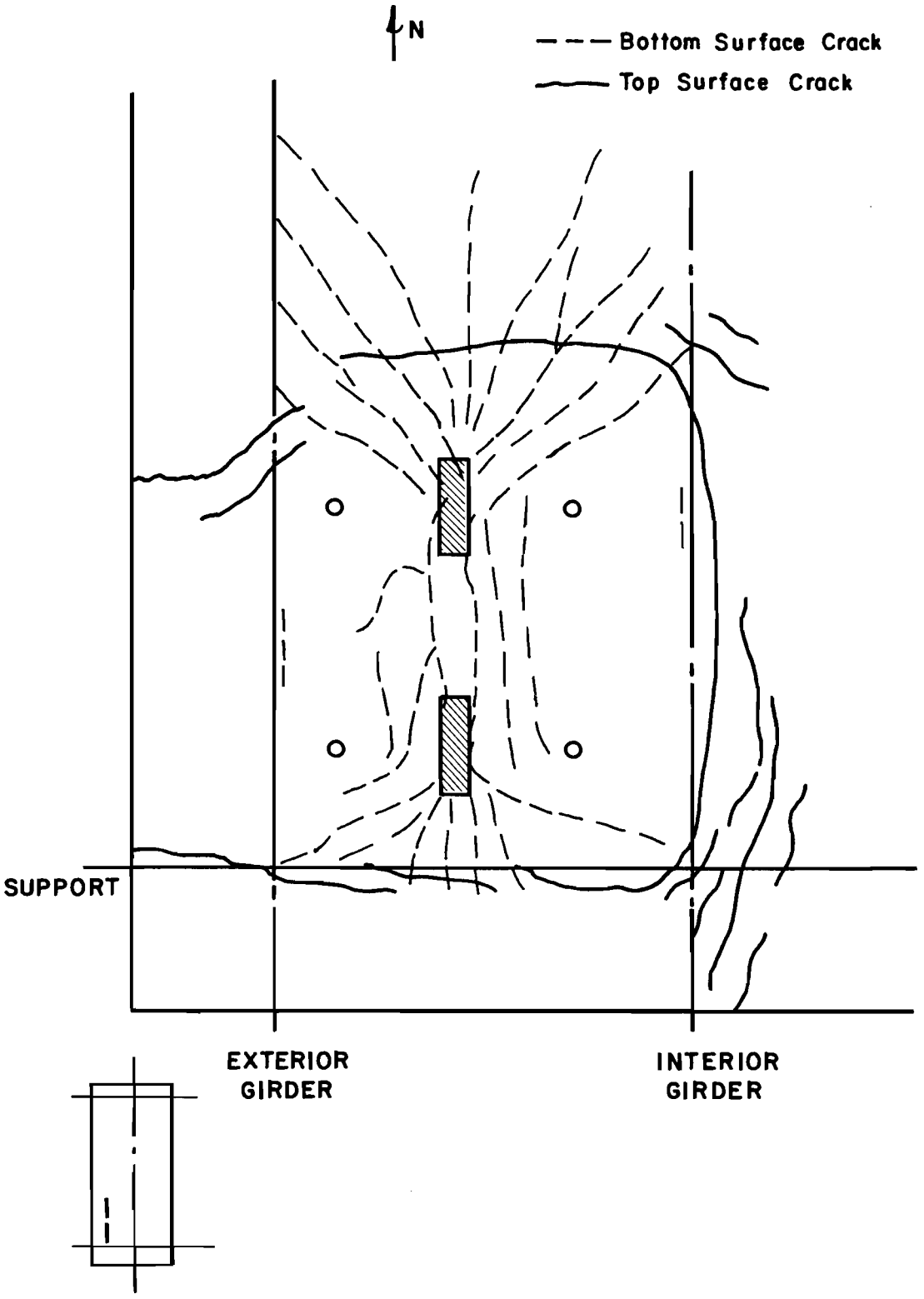

Fig. 7.6 Deck cracking from double load test II-panel

top cracks propagated past the web of the exterior girder at high load. As shown from the results of both tests, the prestressing strands in the panels, which produced compression in the bottom 4 in. of the deck, delayed the crack formation much more than did the reinforcing bars in the CIP deck.

7.3.2 Double Load Tests: II-CIP and II-Panel. In Test II-CIP, the first bottom-surface crack formed, at 20 kips per ram, between the two loading points in the CIP deck (Fig. 7.5). The first top-surface crack was observed at a load of 50 kips per actuator, at a distance of 3.75 ft away from the south loading point. Both the top and bottom cracks propagated faster and more extensively than did those in the corresponding single-load test. Some of the top cracks, shown in Fig. 7.5, extended 5 ft past the web of the interior girder. Only the top surface under the north loading plate was punched in shear. At failure, a wide crack developed on the top surface between the loads. At failure the largest crack was about 0.05 in. wide.

In Test II-Panel, the first crack formed at 50 kips per ram on the bottom surface, and at 90 kips per ram on the top surface. Similar to the companion single-load test, the cracks in the panel deck did not propagate as rapidly nor as far as did those in CIP deck. The top cracks (Fig. 7.6) formed about 4 to 5 ft from the perimeter of the loading zone. Once again, only the south loading plate caused a punching shear failure on the deck. At failure, a top surface crack formed between the loads, and was almost about 0.05 in. wide.

CHAPTER 8

DISCUSSION OF RESULTS FROM CONCENTRATED LOAD TESTS

8.1 Theoretical Punching Shear Capacity

8.1.1 General Model. A general punching shear model for a load applied on a rectangular footprint is shown in Figs. 8.1 and 8.2. In this model, the failure surface on each of the four sides is assumed to have the same angle of inclination, (Fig. 8.1). The failure surface is assumed to propagate downward to $\bar{d}$, the average effective depth of the section under consideration. From equilibrium principles, the punching shear capacity equals the sum of the vertical components of the ultimate tensile forces acting on the 4 inclined failure surfaces, as shown in Fig. 8.2. In other words:

$$V_c = 2\bar{d}\tan\theta \ (b_1 + b_2 + 2\bar{d}/\tan\theta) \ f_t \qquad (8.1)$$

where:

V_c = nominal shear strength from concrete

b_1, b_2 = short and long sides of the concentrated load footprint (Fig. 8.1)

f_t = ultimate tensile capacity of concrete

In carrying out this calculation, f_t was estimated using Equation 11-356 of ACI 318-83 (49): f_t equals $(2 + 4/\beta_c)\sqrt{f_c}$ but not more than $4\sqrt{f_c}$, where β_c is the ratio of b_2 to b_1.

Results of the punching shear calculations are summarized in Figs. 8.3 through 8.6. For the single-load tests, the actual values of b_1 and b_2 were used. The slab was never actually punched through in any of the four tests. It was therefore impossible to measure the real failure angles. However, in the single-load tests, judging from the distance between the failure surfaces at top and bottom of the deck in each test, a failure angle of about 39 degrees appeared to be quite reasonable. That an angle of 39 degrees in the equation for punching shear also gave an extremely good correlation between experimental and calculated results for both the CIP and panel decks.

As shown in Fig. 8.1, the actual crack patterns suggested that the two loads were actually acting like a line load of length b_2. For the double-load case, therefore, b_2 was taken as the distance between the outside edges of the two loading plates (Fig. 8.7). An angle of 38 degrees gave a reasonable correlation between the experimental and calculated results for both CIP and panel deck.

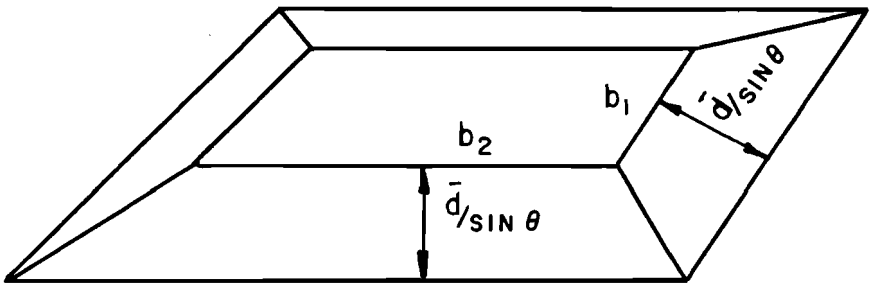

Fig. 8.1 Assumed failure surface of general punching shear model.

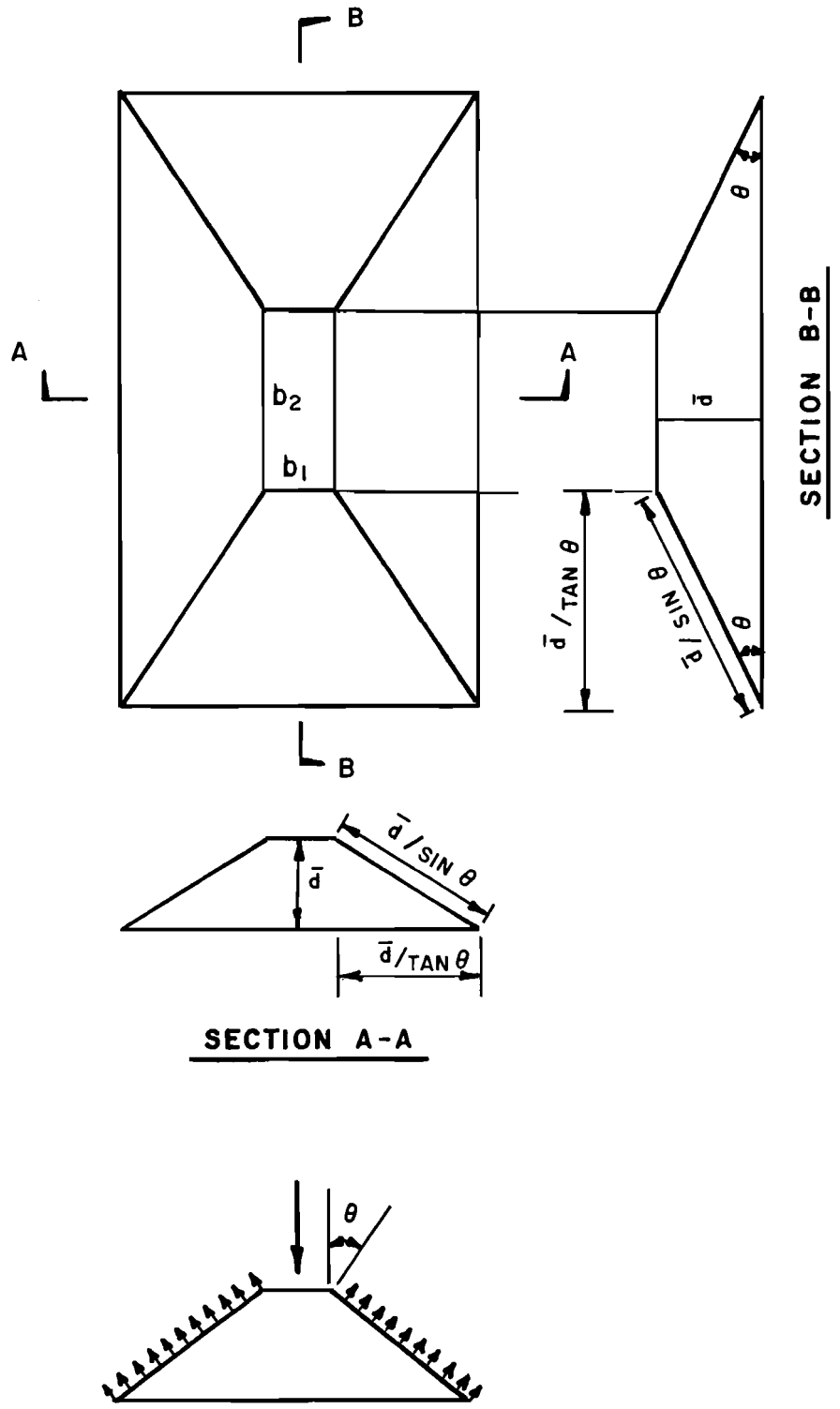

Fig. 8.2 Plan and sectional views of failure surface, general punching shear model.

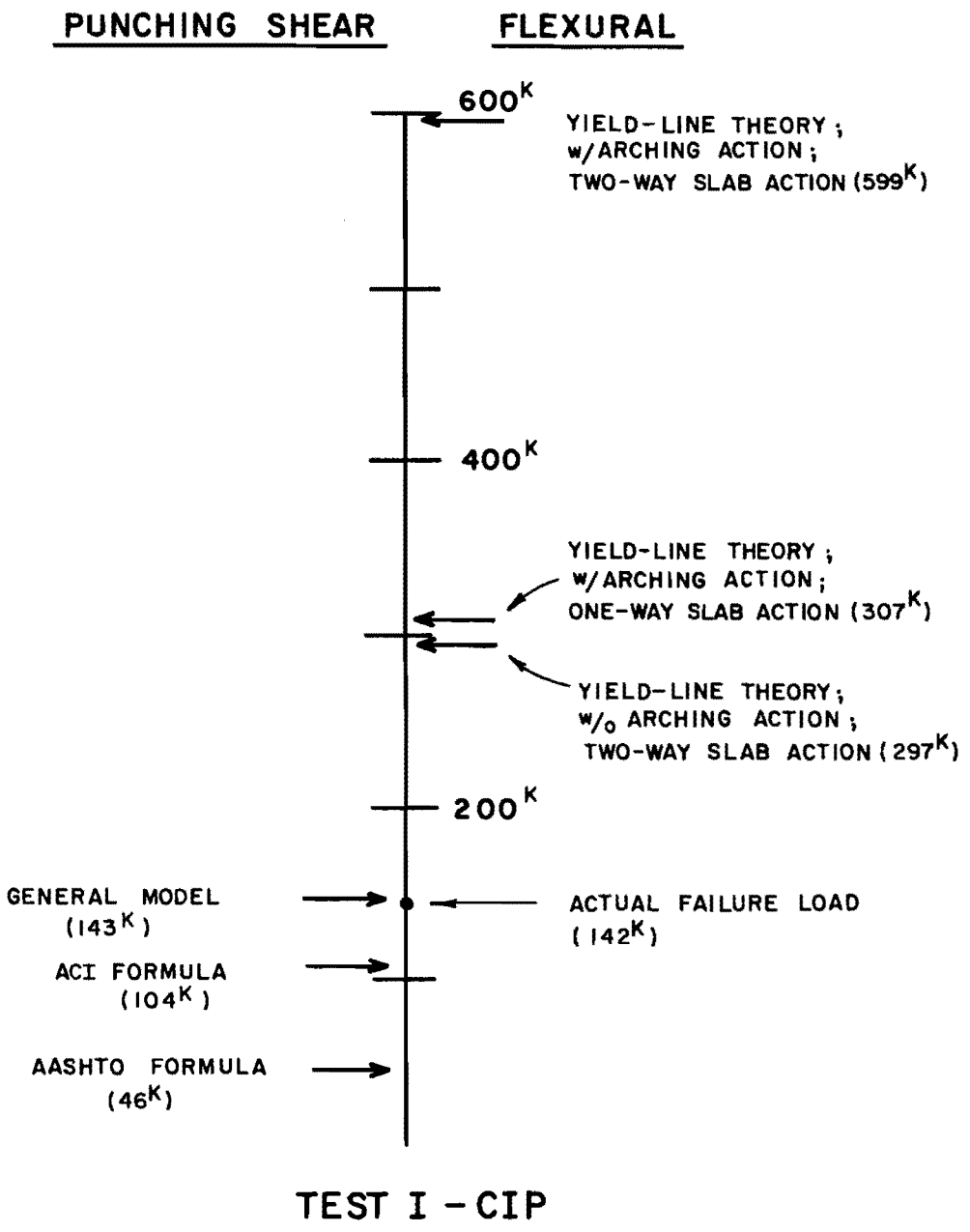

Fig. 8.3 Analytical and experimental results from test I-CIP

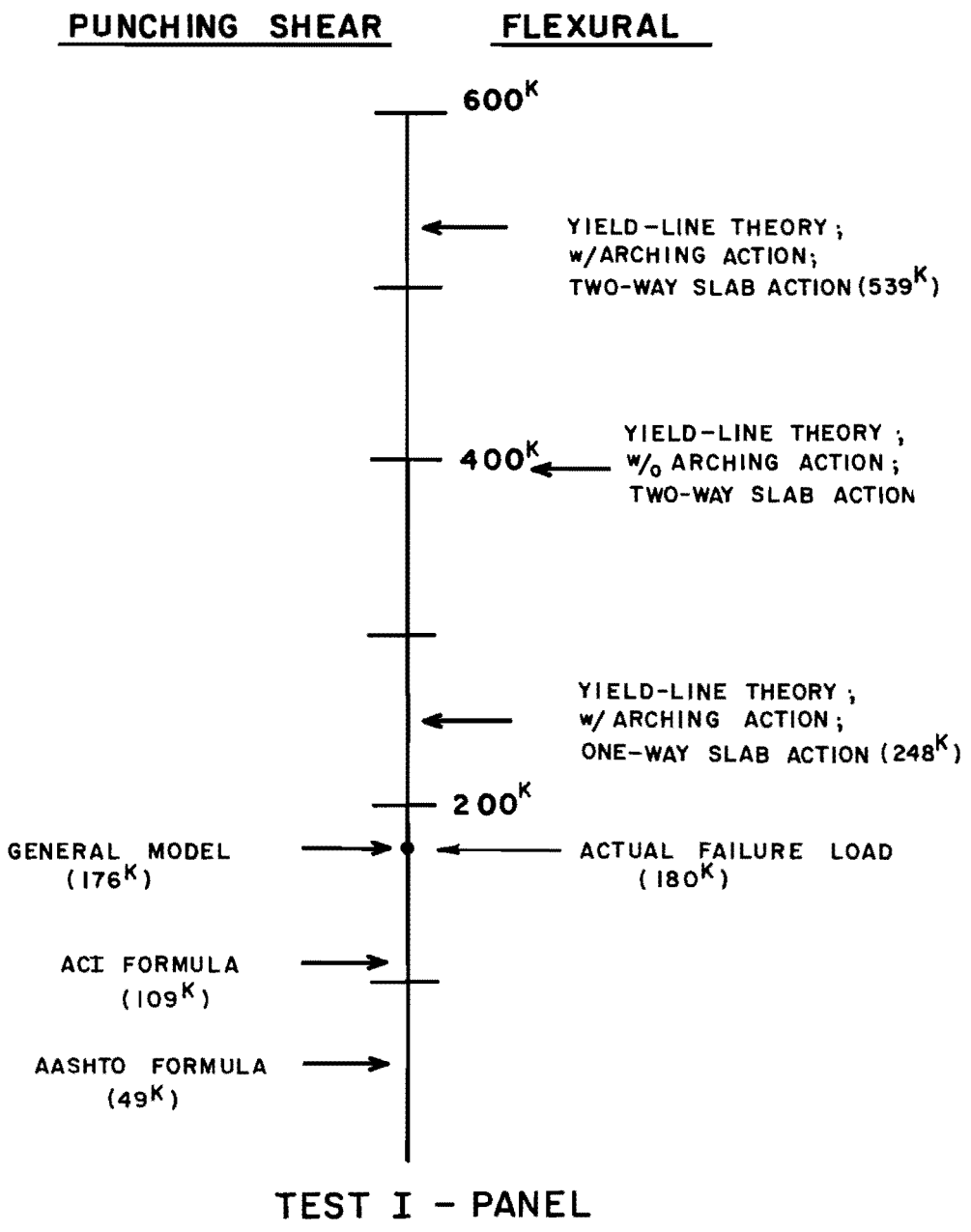

Fig. 8.4 Analytical and experimental results from test I-panel

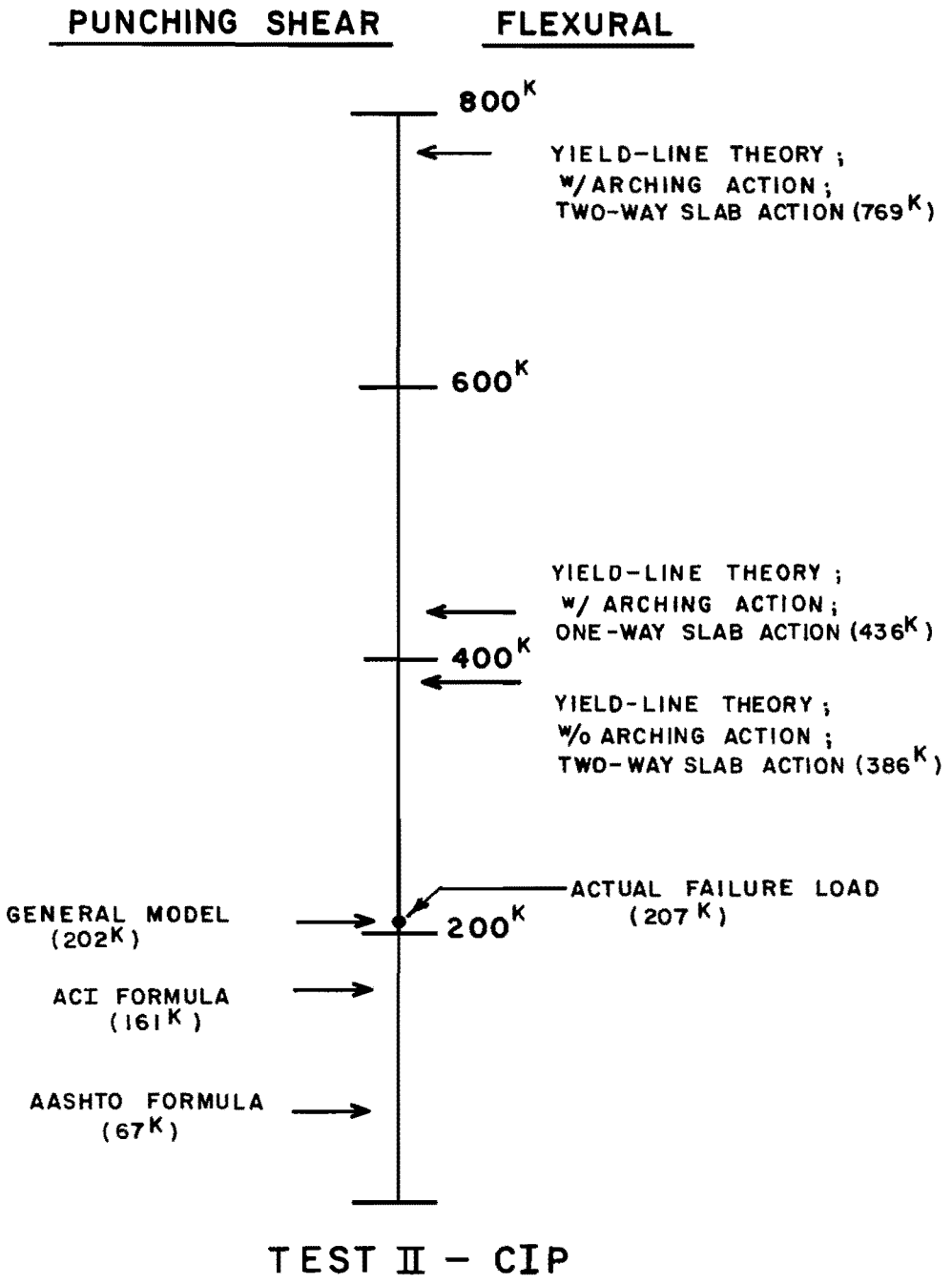

Fig. 8.5 Analytical and experimental results from test II-CIP

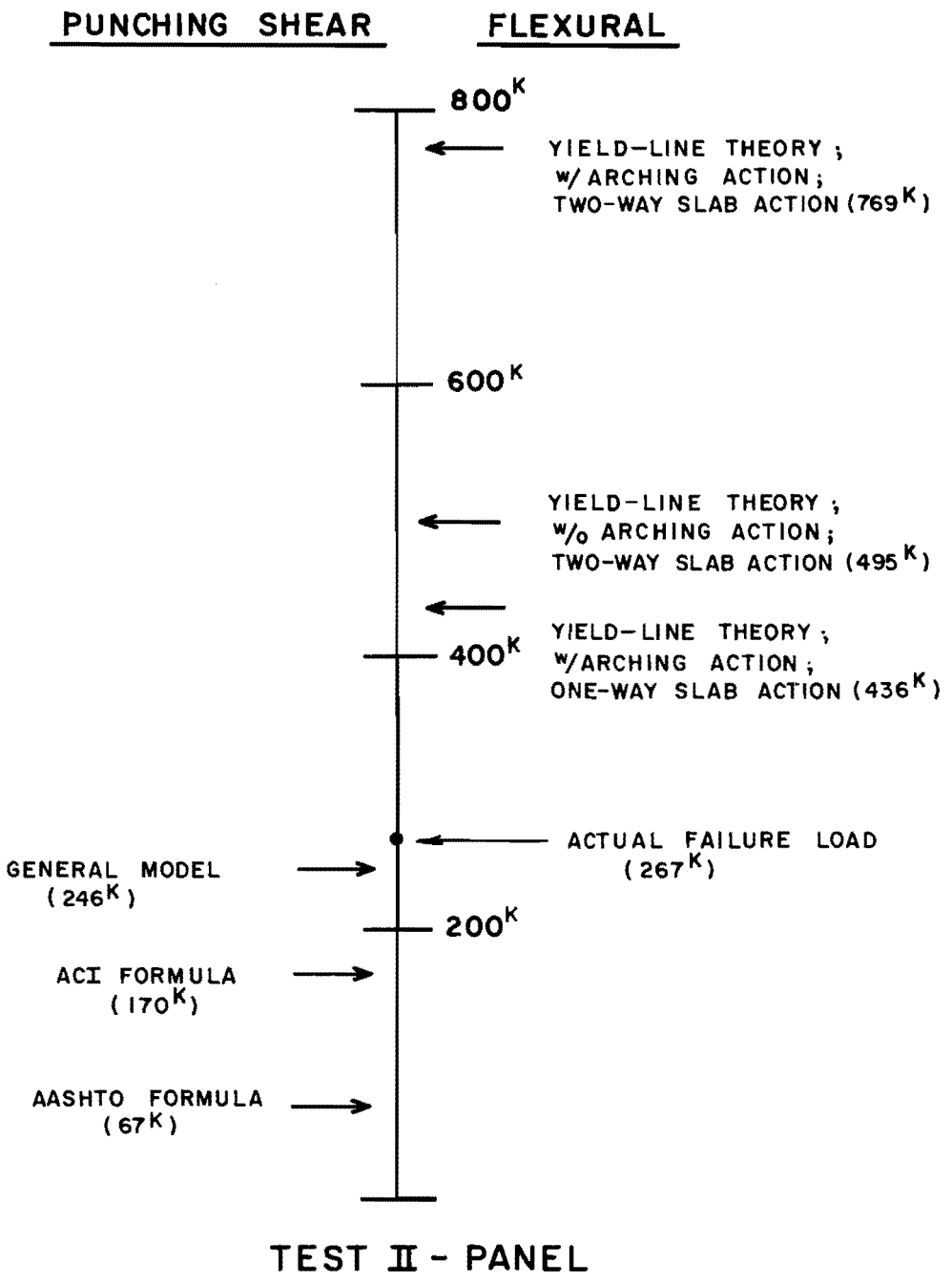

Fig. 8.6 Analytical and experimental results from test II-panel

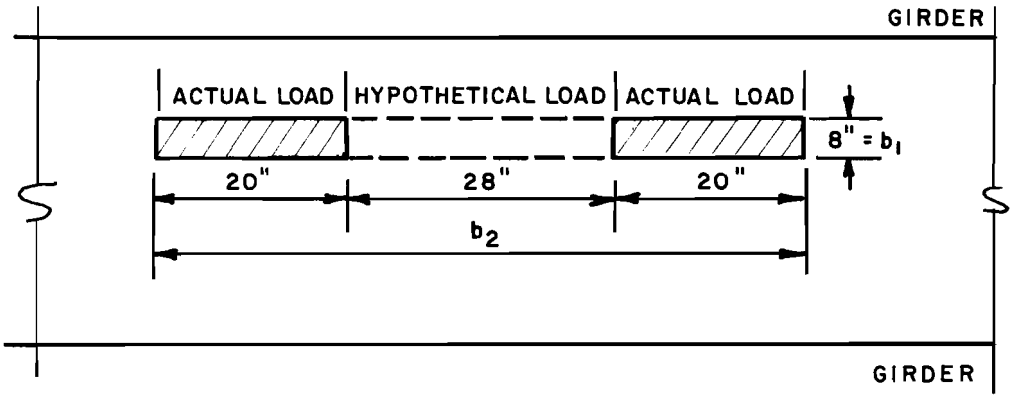

Fig. 8.7 Idealized loading length for double-load case

8.1.2 ACI Formula (49). The ACI formula was applied using exactly the same model as described in Subsec. 8.1.1, except that the angle was assumed to be 45 degrees. The equation assumes the critical section as being located at $\bar{d}/2$ from the edge of the loaded area, and can be expressed as:

$$V_c = 2(2+4/\beta_c)(b_1+b_2+2\bar{d})\sqrt{f'_c}\,\bar{d} < 8(b_1+b_2+2\bar{d})\sqrt{f'_c}\,\bar{d} \qquad (8.2)$$

(Eq. 11-36 of Ref. 49)

All notations are the same as described in Subsec. 8.1.1.

The results are summarized in Figs. 8.3 through 8.6. Actual values of b_1 and b_2 were used for the single-load cases. As before, b_2 was taken as 68 in. All calculated values were lower than the experimental ones, indicating the conservatism of the ACI formula for punching shear. The ACI formula estimated the punching shear capacity better for the CIP deck than for the panel deck. The actual failure angles in the tests were flatter than the value of 45 degrees assumed by ACI.

8.1.3 AASHTO Punching Shear Formula. The AASHTO formula can be expressed as:

$$V_c = 2(0.8+2/\beta_c)(b_1+b_2+2\bar{d})\bar{d}\sqrt{f'_c}$$

but less than

$$d = 1.8\sqrt{f'_c}(b_1+b_2+2\bar{d})\bar{d} \qquad (8.3)$$

(Eq. 8-13 of Ref. 2)

The AASHTO formula is very similar to the ACI formula. The calculations were carried out with the same values for all the parameters as in Subsec. 8.1.2. The results are also presented in Figs. 8.3 and 8.4. The AASHTO formula underestimates the capacity of the deck even more than does the ACI formula. In all four loading conditions tested, the AASHTO formula underestimated the capacity of the deck by a factor of at least 3.

8.2 Yield-Line Theory

8.2.1 Yield-Line Theory without Arching Action: Two-Way Slab Action Assumed. Yield-line theory is an accepted method for computing an upper bound to the ultimate load capacity in flexure for a slab. Assumed yield-line patterns are shown in Figs. 8.8 and 8.9. Distances a and b are the distances between the points of intersection of the girders and the closest longitudinal cracks observed in the actual

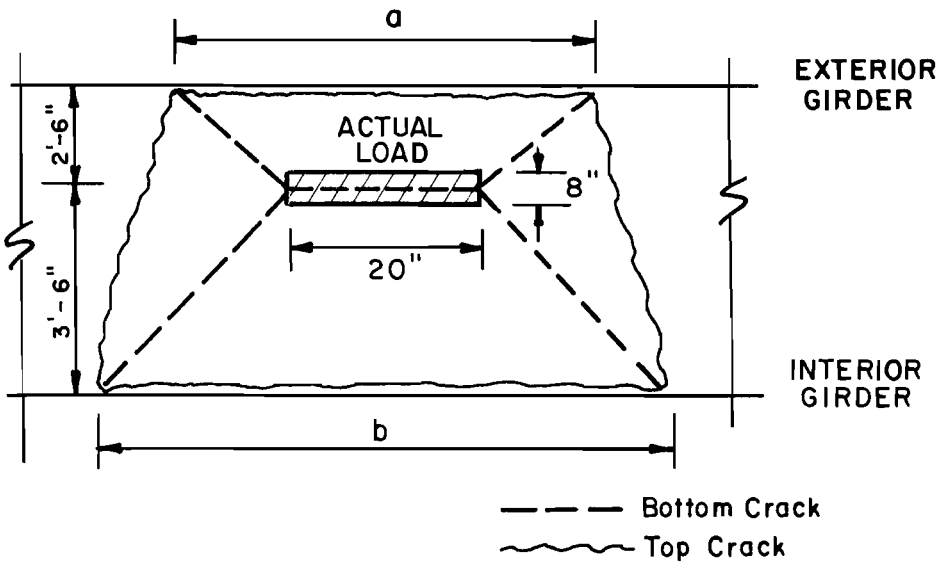

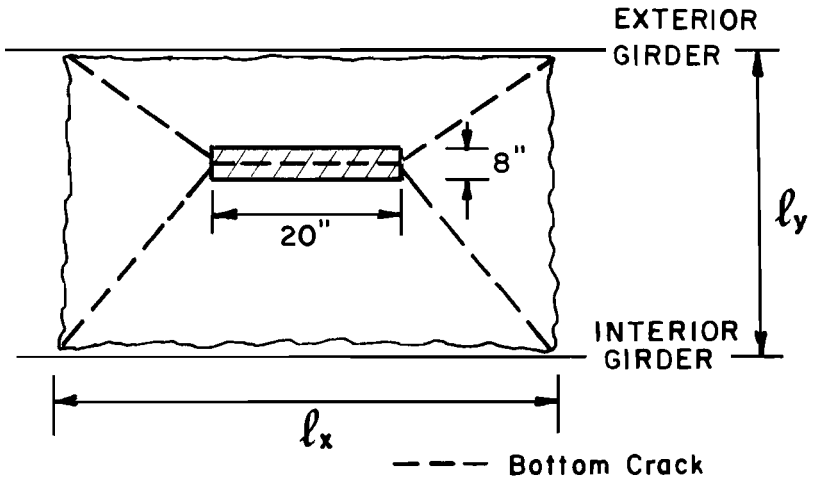

$$\ell_x = \frac{a+b}{2}$$

Fig. 8.8 Assumed yield-line patterns for single-load case

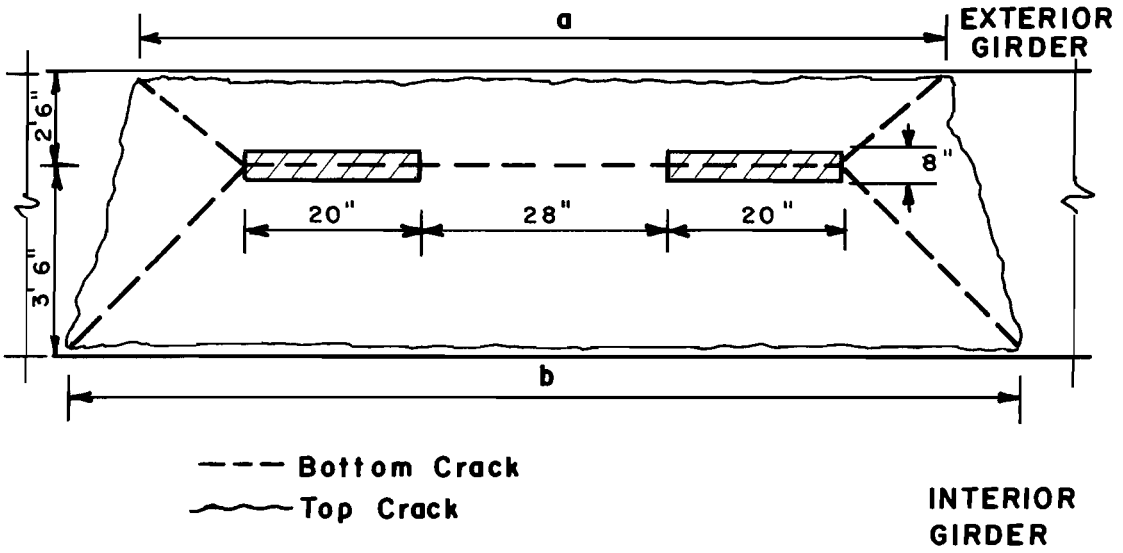

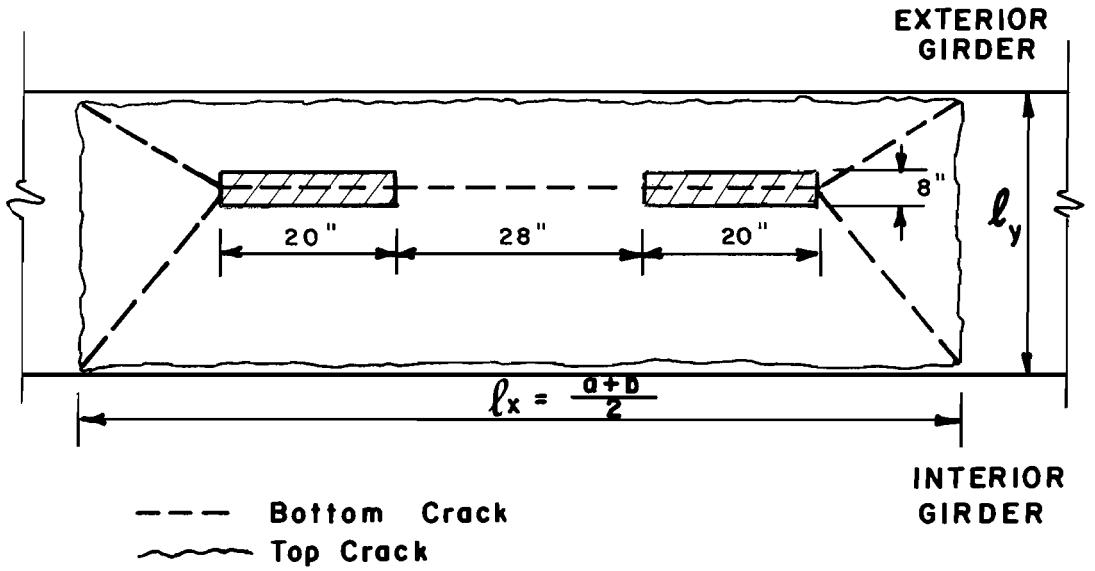

Fig. 8.9 Assumed yield-line patterns for double-load case

tests. The actual crack pattern was then idealized as shown in Figs. 8.8 and 8.9:

1. The longitudinal dimension ℓ_x was taken as the average of the measured longitudinal distances a and b.

2. The transverse dimension ℓ_y was measured between the inside edges of the top flanges of the girders.

In addition, the effects of both positive and negative moment resistances of the deck in each direction are considered in determining yield-line capacity. The flexural resistances per unit width were calculated using the actual material properties (Appendix A). No capacity reduction factor was applied in making the analyses. Small displacements were assumed, and internal work due to membrane stresses (arching action) was neglected. Each yield-line pattern corresponds to an equilibrium relationship between the external concentrated load and the internal resisting moments. Sample calculations are shown in Appendix B.

The results predicted by this analysis method are also included in Figs. 8.3 through 8.6. The predicted values for the single-load tests were about twice the test values. For the double-load tests, the predicted values were about 1.8 times the experimental values. This analysis assumed that the slab exhibited two-way action. However, in all of the actual tests, the crack pattern on the top surface never developed enough to show complete formation of crack as on a two-way slab. This suggests that a two-way action was not entirely an accurate description of the slabs behavior in these tests.

8.2.2 Yield-Line Theory with Arching Action Included: One-Way Slab Action Assumed. As discussed in the report for Phase 1 of this project (1), the flexural strength of a slab can be much higher than the values predicted by yield-line theory due to the effect of arching action. Assuming one-way action in the transverse direction, an axial force-moment interaction diagram (Fig. 8.10) was developed (1). Using this interaction diagram and assuming that the transverse membrane force increased linearly with applied load, a modified ultimate flexural capacity m_n^* of the slab was obtained including the effect of arching action. As shown in Figs. 8.11 and 8.12, the observed cracking pattern corresponded to a one-way slab with the length of the crack taken as ℓ_x (Subsec. 8.2.1). With m_n^* and the crack pattern shown in Figs. 8.11 and 8.12, calculations were carried out to obtain the ultimate flexural capacity of the deck in each test. The results were also presented in Figs. 8.3 through 8.6. Notice that only $1/4\ m_n^*$ was used for the crack adjacent to the exterior girder. This is due to the smaller arching forces acting on the deck above the exterior girder because of lower restraint. The predicted values from this analysis were from 1.4 to 2.1 times the failure loads.

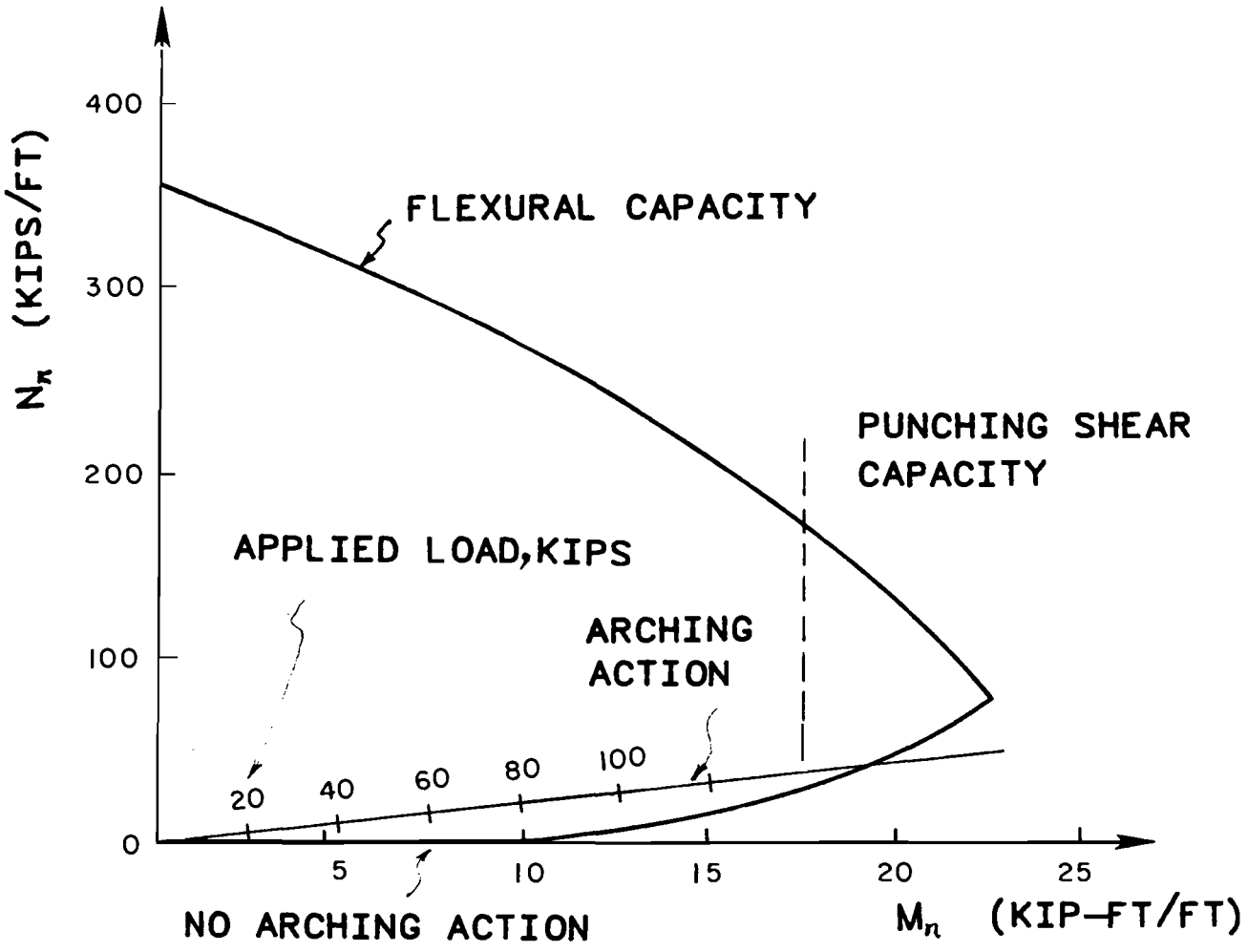

Fig. 8.10 Increase in flexural capacity of underreinforced slab due to compressive membrane force

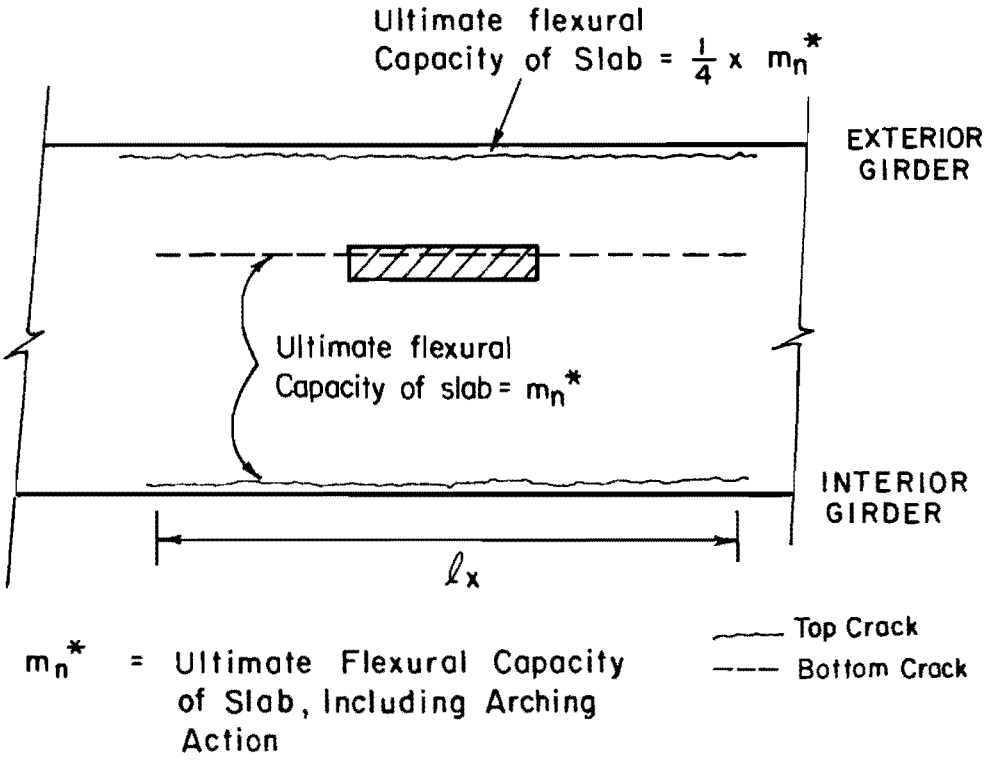

Fig. 8.11 Assumed yield-line pattern for flexural capacity from one-way slab action, with arching action included (single-load case)

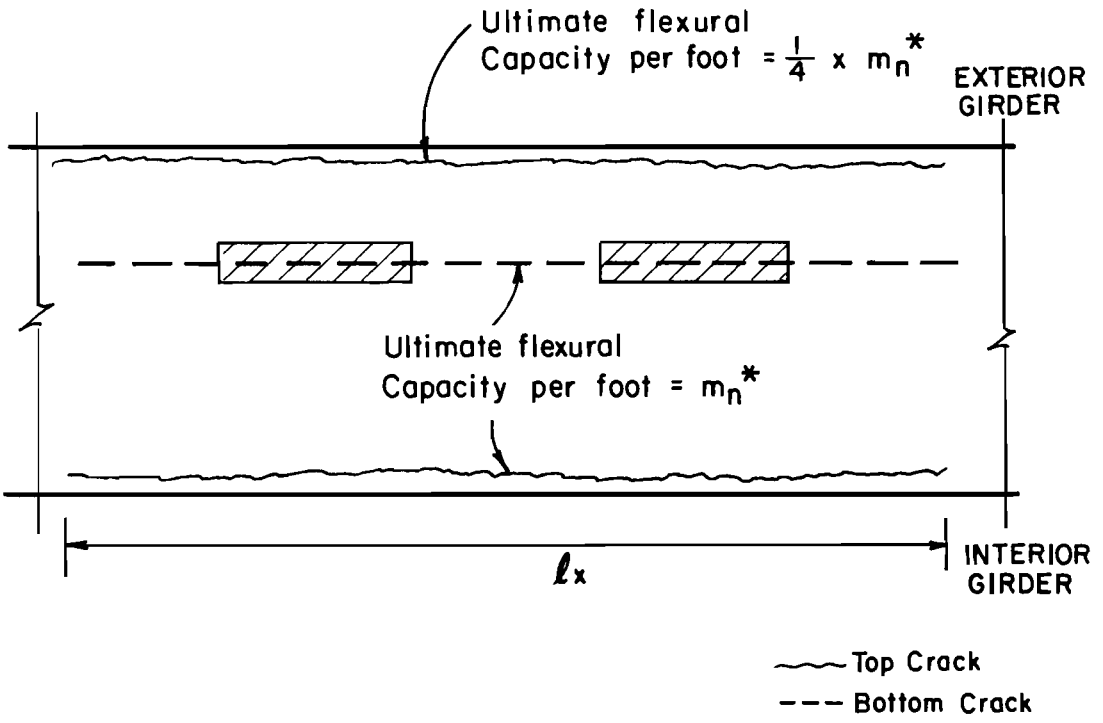

Fig. 8.12 Assumed yield-line pattern for flexural capacity from one-way slab action, with arching action included (double-load case).

8.2.3 Yield-Line Theory with Arching Action Included: Two-Way Slab Action Assumed. Using the crack pattern adopted in Subsec. 8.2.1 which corresponds to a two-way slab action and m_n^* (Subsec. 8.2.2), calculations for the ultimate capacity of the slab for each test were carried out. Once again only 1/4 m_n^* was used for the top crack adjacent to the top flange of the exterior girder. The results were included in Figs. 8.3 through 8.6. The predicted values were about three to four times the failure loads.

8.2.4 Yield-Line Theory Including Effect of Axial Flexibility. This approach is probably the best available theory for treating slabs similar to the decks studied in this investigation. Because satisfactory results were obtained using simpler approaches, it was not considered necessary to discuss this technique further in this report. If further study is desired, the reader is referred to technical papers such as Ref. 54.

8.3 Comparison of Results

As summarized in Figs. 8.3 through 8.6, the general punching shear model gives the closest prediction to the experimental results in all four tests. The flexural capacities of the slab as predicted by yield-line theory, with or without arching action, were higher than the actual failure loads. On the other hand, the values predicted by the ACI and AASHTO formulas based on punching shear model other than the general model, were lower than the test values. All experimental observations indicated that the failure mode in all four tests was punching shear. Also, as mentioned in Subsec. 8.1.1, the failure angle assumed for the general punching shearing model was reasonable when compared to the available test data.

For each test, three analyses were done using the concept of yield-line theory with different assumptions. The basic differences among the three analyses can be summarized as follows:

1. one-way vs. two-way slab action; and
2. neglect (m_n) vs. consideration (m_n^*) of arching action.

By using the same assumed lengths of yield lines, the one-way slab yield line pattern gave a smaller predicted capacity than did the two-way slab pattern, since the one-way mechanism did not include any transverse yield lines. As shown in Fig. 8.10, m_n^* was about two times m_n. As a result, either the two-way yield line patter with m_n or the one-way crack pattern with m_n^*, gives a low estimate to the actual flexural capacity of the deck, while the two-way yield line pattern with m_n^* gives a higher estimate. However, the slab failed in punching shear long before it reached even the lowest of the calculated flexural capacities. Both the ACI and the AASHTO punching shear formula were

shear formula were shown to be very conservative. The capacities predicted by the ACI formula were about 0.7 times the actual ones, while the values predicted by the AASHTO formula were about 0.3 times the actual ones.

In summary, even in an Ontario-type bridge deck, which has less reinforcement than a conventional AASHTO bridge deck, punching shear is still the critical failure mode under concentrated load. The deck flexural capacity predicted using yield-line theory is not likely to control in a conventionally designed deck. Both ACI and AASHTO formulas gave very conservative estimates of the deck's punching shear capacity. Punching shear capacity was predicted very closely by a punching shear model based on a failure surface inclined at an angle shallower than 45 degrees.

CHAPTER 9

SUMMARY, CONCLUSIONS AND RECOMMENDATIONS

9.1 Summary

The test specimen was a full-size composite bridge with 7 1/2-in thick concrete deck on three 36-in deep, W-shape steel girders, spaced at 7 ft. Half the deck had two layers of reinforcement, designed in accordance with the provisions of the Ontario Bridge Design Code. The other half had 4-in thick precast, prestressed panels which replaced the lower grid of reinforcement in the cast-in-place deck. The test specimen was supported at a 40-ft span.

Tie-down forces were applied at the overhang at each end of the bridge, and two tandem loads were applied at midspan using hydraulic actuators. To induce negative moments at supports, static loads up to 30 kips per actuator were first applied to the bridge with its overhangs tied down. Then a fatigue test consisting of 5 million cycles (load range from 5 kips to 26 kips per actuator) was carried out, followed by another static test. Finally, the test specimen was subjected to concentrated load tests involving single and tandem loads.

Analytical predictions using a finite element model were compared with the experimental results from the negative moment test. Analytical predictions of deck capacity were compared with the experimental results of the concentrated load tests.

9.2 Conclusions

1) The northern half of the bridge deck, which was full-scale, cast-in-place reinforced concrete on steel girders, and was detailed in accordance with the provisions of the Ontario Highway Bridge Design Code, performed satisfactorily at the support region when subjected to negative moment levels consistent with current AASHTO design loads.

2) The southern half of the bridge deck, which used precast, prestressed panels, also performed satisfactorily in the negative moment region.

3) Both the cast-in-place deck and the precast, prestressed panel deck gave satisfactory behavior at the midspan region, under static tandem loads which were approximately 2.5 times the current AASHTO design level, and which were placed 4 ft apart.

4) Fatigue loading (5 million cycles with a range of 5 to 26 kips) did not significantly change the behavior of the deck, as observed in static tests before and after fatigue loading.

5) Analytical predictions were carried out using a finite element model which included revised stiffness in cracked regions. Analytical and experimental results agreed quite well, showing that the analytical model is satisfactory and may be extended to other bridge configurations.

6) Under single concentrated loads, the deck failed in punching shear. Results of the concentrated single load test in this study correlated very will with similar tests by Bieschke and Klingner (47). Tests with tandem loads were also carried out, and the deck again failed by punching shear.

7) A general model of the punching shear mechanism for both single and tandem loads closely predicted the ultimate strength of the deck. However, for the deck tested in this project (as with most conventional bridge decks), the punching shear failure mode controlled the load capacity.

8) Both the ACI and AASHTO formulas for punching shear capacity were very conservative in estimating the load capacity of the deck.

9) Overall, the experimental program showed that the precast, prestressed panel deck was stronger, stiffer and more crack-resistant than the cast-in-place deck.

9.3 Recommendations

Cast-in-place and precast, prestressed panel bridge decks similar to the one tested in this study, and detailed with Ontario-type reinforcement, can be built in the field. Their field performance should be evaluated by the Texas SDHPT.

9.4 Further Research

This study is part of a series of investigations conducted in the Ferguson Structural Engineering Laboratory at The University of Texas at Austin. In this study, the service and overload behavior of two types of bridge deck were investigated, under static and fatigue loads. While both cast-in-place and precast, prestressed panel decks were studied, a relatively narrow range of geometries was considered. To obtain a broader understanding of the behavior of bridge decks at the negative moment region before the new deck design is completely incorporated in Texas SDHPT design provisions, parametric studies should be conducted involving variables such as the span to thickness

ratio of the deck, the effects of line loads, skew bridge behavior, the range of the applied fatigue loads producing negative moment, and the stiffness of integral barriers.

APPENDIX A

MATERIAL PROPERTIES

TABLE A.1 Concrete Mix Design for Cast-in-Place Deck

Design Strength:	3600 psi
Water-Cement Ratio:	0.485
Slump:	3 in.
Type I Cement:	0.36%
Water:	0.42%
Aggregate:	0.22%
Added Water:	0%
Admixture:	6% air entrained

TABLE A.2 Mechanical Characteristics of Cast-in-Place Deck

Concrete	
Casting Date:	2/28/84
f'_c: 14 day:	3510 psi
28 day:	4240 psi
180 day:	5160 psi
Slump:	3 in.
Steel	
Size:	#4
Grade:	60
Tested yield strength:	73 ksi

TABLE A.3 Seven-Day Modulus of Rupture Data,

Cast-in-Place Deck

1	3465	433
2	3470	434
3	4050	506
4	3890	486
5	2880	360
6	2080	385
7	3040	380
8	3580	448
9	3700	463

Average:	433 psi
Standard Deviation	49.6 psi

$ft = My/I = ((18P/4)3/(6^4/12) = P/8$ (psi)

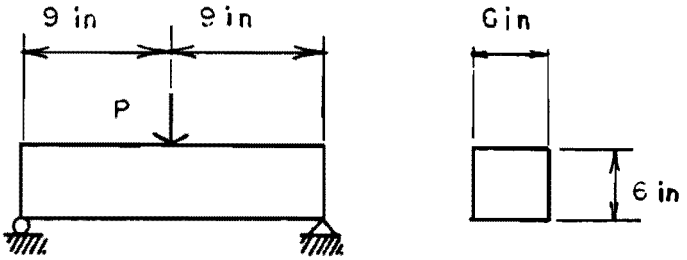

TABLE A.4 Mechanical Characteristics of Precast, Prestressed Panels

Concrete	
Release Strength:	4000 psi
Design Strength:	6000 psi
Type:	Texas Class H, Type III (high early strength) cement, 6-1/2 sacks/cu. yd.)
Casting date:	2/2/84
f'_c 48 hr:	5104 psi
7 day:	6593 psi
Slump:	4 in.
Prestressing Steel	
Size of strand:	3/8-in. diameter
Type:	7-wire
Grade:	270, stressed-relieved
Prestress force per strand:	16.1 kips

APPENDIX B

SAMPLE CALCULATIONS

FOR

DECK CAPACITY

Yield-Line Tneory (Two-way Slab Action, Not Including Arching Action)

Using the material properties of the deck in App.A and data from test I-CIP; we can get the flexural capacities of the deck per linear foot:

M^-_{xx} = 101.30 K-in./ft

M^+_{xx} = 91.29 K-in./ft

M^-_{yy} = 91.29 K-in./ft

M^+_{yy} = 101.30 K-in./ft

External Work

w = Pressure(K/in^2) at the deck surface under the loading plate

δ = Deflection(in.) of the deck under the loading plate

$W_{ext.} = (w \times 20 \times 4 \times \delta/2)\ 2 = P/2$

P = Total Load

Internal Work(Refer to Fig.8.8a)

$$W_{int.} = (M_{yy} L_x \theta_x + M_{xx} L_y \theta_y)$$

$$= (91.29+101.3)(7.75)(\delta/30 + \delta/42) + (2)(6)(\delta/36.5)(101.3+91.29)$$

$$= 148.64\ \delta$$

Internal Work = External Work

$$148.64\,\delta = P\delta/2$$

$$P = 297.26 \text{ Kips}$$

REFERENCES

1. Ontario Highway Bridge Design Code, Ontario Ministry of Transportation and Communications, 2nd Edition, 1983.

2. Standard Specifications for Highway Bridges, 13th Edition, American Association of State Highway and Transportation Officials, 1983.

3. Fang, I.-K., "Behavior of Ontario-Type Bridge Deck on Steel Girders," Dissertation presented to The University of Texas at Austin, in partial fulfillment of the requirements for the degree of Doctor of Philosophy, December 1985.E

4. Elling, C.W., "Distribution of Girder Loads in a Composite Highway Bridge," Thesis presented to The University of Texas at Austin, Texas, in partial fulfillment of the requirements for the degree of Master of Science in Engineering, May, 1985.

5. Ockleston, A. J., "Load Tests on a Three Story Concrete Building in Johannesburg," The Structural Engineer, Vol. 33, No. 10, October 1955, pp. 304-322.

6. Ockleston, A.J., "Arching Action in Reinforced Concrete Slabs," The Structural Engineer, Vol. 36, No. 6, June 1958, pp. 197-201.

7. Leibenberg, A.C., "Arching Action in Concrete Slabs," National Building Research Institute, Council for Scientific and Industrial Research, Report 234, South Africa, 1966.

8. Guyon, Y., Prestressed Concrete, Vol. 2, New York, John Wiley & Sons, 1962.

9. Christiansen, K. P., "The Effect of Membrane Stresses on the Ultimate Strength of the Internal Panel in a Reinforced Concrete Slab," The Structural Engineer, Vol. 41, No. 8, August 1963, pp. 261-265.

10. Christiansen, K. P., "Experimental Investigation of Rectangular Concrete Slabs with Horizontal Restraints," Materials and Structures, Vol. 16, No. 93, May-June 1982, pp. 178-192.

11. Park, R., "The Lateral Stiffness and Strength Required to Ensure Membrane Action at the Ultimate Load of a Reinforced Concrete Slab-and-Beam Floor," Magazine of Concrete Research, Vol. 17, No. 50, March 1965, pp. 29-38.

12. Park, R., "Tensile Membrane Behaviour of Uniformly Loaded Rectangular Reinforced Concrete Slabs with Fully Restrained Edges," Magazine of Concrete Research, Vol. 16, No. 46, March 1964, pp. 39-44.

13. Park, R., "The Ultimate Strength and Long-Term Behavior of Uniformly Loaded, Two-Way Concrete Slabs with Partial Lateral Restraint at All Edges," Magazine of Concrete Research, Vol. 16, No. 48, September 1964, pp. 139-152.

14. Park, R., "Ultimate Strength of Rectangular Concrete Slabs Under Short-term Uniform Loading with Edges Restrained Against Lateral Movement," Proceeding of the Institute of Civil Engineers, Vol. 28, No. 6705, 1964, pp. 125-145.

15. Park, R., Gamble, W. L., Reinfored Concrete Slabs, 1980.

16. Girolami, A. G., Sozen, M. A., and Gamble, W. L., "Flexural Strength of Reinforced Concrete Slabs with Externally Applied In-Plane Forces," Report to the Defense Office of the Secretary of the Army and Office of Civil Defense, October 1970.

17. Gamble, W. L., Flug, H., and Sozen, M. A., "Strength of Slabs Subjected to Multiaxial Bending and Compression," Report to the Defense Office of the Secretary of the Army and Office of Civil Defense, October 1970.

18. Hopkins, David C., and Park, R., "Test on a Reinforced Concrete Slab and Beam Floor Designed with Allowance for Membrane Action," and "Cracking, Deflection and Ultimate Load of Concrete Slab Systems," Special Publication SP-30, American Concrete Institute, 1971, pp. 223-250.

19. Tong, P. Y., and Batchelor, B., deV., "Compressive Membrane Enhancement in Two-Way Bridge Slabs," Special Publication SP-30, American Concrete Institute, 1971, pp. 271-286.

20. Brotchie, J. F. and Holley, M. J., "Membrane Action in Slabs", Special Publication SP-30, American Concrete Institute, 191, pp. 345-377.

21. Csagoly, P. F. and Dorton, R. A., "The Development of the Ontario Highway Design Bridge Code," Transportation Research Record, No. 665, 1978, pp. 1-12.

22. Buckland, P. G. and Sexsmith, R. G., "A Comparison of Design Loads for Highway Bridges," Canadian Journal of Civil Engineering, Vol. 8, No. 1, 1981, pp. 16-21.

23. Bakht, B., Cheung, M. S., Dorton, R., "A Comparison of Design Loads for Highway Bridges: Discussion," Canadian Journal of Civil Engineering, Vol. 9, No. 1, 1982, pp. 138-140.

24. Bakht, G. and Csagoly, P> F., "Bridge Testing," Research Report No. 79-SSR-10, Ministry of Transportation and Communications of Ontario, Downsview, August 1979, pp. 127.

25. Batchelor, B. deV., Hewitt, B. E., Csagoly, P., and Holowka, M., "Investigation of the Ultimate Strength of Deck Slabs of Composite Steel/Concrete Bridges," Transportation Research Record, No. 664, 1978, pp. 162-170.

26. Batchelor, B. deV., Hewitt, B.E., and Csagoly, P., "Investigation of the Fatigue Strength of Dek Slabs of Composite Steel/Concrete Bridges," Transportation Research Record, No. 664, 1978, pp. 153-161.

27. Hewitt, B. E. and Batchelor, B. deV., "Punching Shear Strength of Restrained Slabs," Proceedings, ASCE, ST9, September 1975, pp. 1827-1853.

28. Hewitt, B. E., "An Investigation of the Punching Strength of Restrained Slabs with Particular Reference to the Deck Slabs of Composite I-Beam Bridges," Thesis presented to Queen's University of Kingston, Canada, in 1972, in partial fulfillment of the requirements for the degree of Doctor of Philosophy.

29. Csagoly, P., Holowka, M., and Dorton, R. A., "The True Behavior of Thin Concrete Bridge Slabs," Transportation Researach Record, No. 664, 1978, pp. 171-179.

30. Dorton, R. A., and Holowka, M., "The Conestogo River Bridge -- Design and Testing," Canadian Journal of Civil Engineering, Vol. 4, No. 1, 1977, pp. 18-39.

31. Bakht, B., "Testing of the Manitou Bridge to Determine Its Safe Load Carrying Capacity," Canadian Journal of Civil Engineering, Vol. 8, No. 1, 1981, pp. 218-229.

32. Holowka, M., "Testing of a Trapezoidal Box Girder Bridge," Structural Research Report RR221, Ontario Ministry of Transportation and Communications, November 1979.

33. Holowka, M. and Csagoly, P., "A Composite Prestressed Concrete AASHTO Girder Bridge," Research Report RR222, Ontario Ministry of Transportation and Communications, July 1980.

34. Beal, D. B., "Strength of Concrete Bridge Deck," Research Report 89, New York State Department of Transportation, July 1981.

35. Ontario Highway Bridge Design Code, Ontario Ministry of Transportation and Communications, Ontario, Canada, 1983, 357 pp. (with Commentary).

36. Drawings for "Proposed Bridge Deck Details (Ontario 1977 Bridge Code)," File No. 1284, Texas SDHPT, October 1981 (2 sheets).

37. Texas Highway Department, "Summary Report on Investigation to Determine Feasibility of Using In-Place Precast Prestressed Form Panels for Highway Bridge Decks," PCI Journal, Vol. 20, No. 3, May-June 1975, pp. 62-67.

38. Kluge, R. W. and Sawyer, H. A., "Interacting Pretensioned Concrete Form Panels for Bridge Decks," PCI Journal, Vol. 20, No. 3, May-June 1975, pp. 34-61.

39. Barnoff, R. M. and Orndorff, J. A., "Construction and Testing of an Experimental Prestressed Concrete Bridge," Report No. 1, The Pennsylvania State Univesity, University Park, Pennsylvania, 1974.

40. Barnoff, R. M. and Rainey, D. L., "Laboratory Tests of Prestressed Concrete Deck Planks and Deck Plank Assemblies," Report No. 2, The Pennsylvania Transportation Institute, The Pennsylvania State University, University Park, Pennsylvania, 1974.

41. Jones, H. L. and Furr, H. L. "Study of In-Service Bridges Constructed with Prestressed Panel Subdecks," Research Report 145-1, Texas Transportation Institute, Texas A & M University, College Station, Texas, 1970.

42. Jones, H. L. and Furr, H. L., "Development of Length of Strands in Prestressed Panel Subdecks," Research Report 145-2, Texas Transportation Institute, Texas A & M University, College Station, Texas, 1970.

43. Buth, E., Furr, H. L., Jones, H. L., and Toprac, A. A., "Evaluation of a Prestressed Panel, Cast-in-Place Concrete Bridge," Research Report 145-3, Texas Transportation Institute, Texas A & M University, College Station, Texas, 1972.

44. Furr, H. L. and Ingram, Leonard L., "Cyclic Load Tests of Composite Prestressed-Reinforced Concrete Panels," Research Report 145-4, Texas Transportation Institute, Texas A & M University, College Station, Texas, 1972.

45. Barker, J. M., "Research, Adaptation and Experience with Precast Prestressed Bridge Deck Panels," PCI Journal, Vol. 20, No. 6, November-December, 1975, pp. 67-82.

46. Reed, R. L., "Application and Design of Prestressed Deck Panels," Transportation Research Record, No. 665, 1978, pp. 164-171.

47. Bieschke, L. A. and Klingner, R. E., "The Effect of Transverse Strand Extensions on the Behavior of Precast Prestressed Panel Bridges," Research Report No. 303-1F, Center for Transportation Research, The University of Texas at Austin, June 1982.

48. Bathe, K.J., Wilson, E.L., and Peterson, F.E., "SAPIV: A Structural Analysis Program for Static and Dynamic Response of Linear Systems,: Report No. EERC 73-11, Earthquake Engineering Research Center, University of California at Berkeley, 1973.

49. Building Code Requirements for Reinforced Concrete, American Concrete Institute 318-83.

50. Copa, R. J. and Clark, L. A., Concrete Slab, Analysis and Design, Elsevier Applied Science Publishers, London, 1984.

51. Johnson, R. P., Structural Concrete, McGraw-Hill Publishing Company Limited, London, 1965.

52. Jones, L. L. and Wood, R. H., Yield-Line Analysis of Slabs, Chatto and Windus Ltd., London, 1967.

53. Morrell, Patrick J. B., Design of Reinforced Concrete Elements, Crosby Lockwood Staples, London, 1977.

54. Gesund, H. F., "Limit Design opf Slabs for Concentrated Loads," Journal of the Structural Division, ASCE, Vol. 107, No. ST9, September 1981.